

Characterising the Contribution of Hrd1 Complex Components to the UPR: Implications for Cancer Cell Survival

Grace Tara Evans

Wolfson College

Nuffield Department of Orthopaedics, Rheumatology and Musculoskeletal Sciences

University of Oxford

2023

A thesis submitted in fulfilment of the requirements for the degree of:

MSc(Res) in Molecular and Cellular Medicine

Supervised by Professor John Christianson and Professor Udo Opperman

Declaration

I declare that this thesis has never been submitted, either in the same or a different form, to this or another University for a degree or other qualification. All the work presented in this thesis is the result of my own work unless otherwise stated and does not constitute parts of any other thesis. The work herein described was carried out whilst I was an MRes student at the Botnar Research Centre, under the supervision of Professor John Christianson and Professor Udo Opperman.

Acknowledgments

I would like to express my sincere thanks to Professor John Christianson for his supervision on this project and his expert knowledge in the field. It has been a privilege to work alongside him and all members of the Christianson lab: Giorgia Gaeta, Sarah Picaud, Chian Yang, Richard Little and Matt Jackson. I would like to thank them for all their generous help and guidance over the past year. This is especially true for DPhil student Giorgia for all her advice and lab training, from cell culture to my first western blot of many, for which I am extremely grateful.

Thank you all!

Abstract

The Hrd1 complex is a large multiprotein complex that spans the endoplasmic reticulum (ER) membrane with Hrd1 itself functioning as an E3 ligase in the endoplasmic reticulum associate degradation (ERAD) pathway in which unfolded and misfolded proteins are cleared from the ER in order to maintain protein homeostasis. Various components of the complex are transcriptionally regulated by the unfolded protein response (UPR), a protein quality control mechanism activated upon the detection of stress, meaning the complex itself can adapt to fluctuations in levels of cellular stress.

Proteotoxic stress is often upregulated in cancer cells with this capable of manifesting as ER stress. Therefore, some cancer cells are particularly reliant on the UPR and ERAD in order to maintain the fidelity of the proteome and manage basal stress levels below a threshold that allows for survival. Much of the direct contribution of the Hrd1 complex, and specifically the role of each of its components, in this phenomenon remains unknown. This study aimed to systemically reduce the bioavailability of individual Hrd1 components to determine the resulting effect on cancer cell survival and proliferation.

Table of contents:

Introduction.....6

Cancer and proteotoxic stress.....6

The unfolded protein response.....7

Endoplasmic reticulum associated degradation (ERAD): ties to the UPR and its implications in cancer.....9

The composition of the Hrd1 complex.....10

Features of triple-negative breast cancer.....15

Project aims and its relevance.....15

Materials and methods.....17

Results.....26

Modelling ER stress in breast cancer.....26

The effect of UPR activation in TNBCs at the protein level.....32

Demonstration of synthetic lethality in TNBC cells.....34

Knockdown of Hrd1 complex components.....36

Validating knockdowns of the Hrd1 complex components.....37

An inducible shRNA system.....39

Visualising Dox-induced depletion of Hrd1.....44

Inducible depletion of HERPUD1.....49

Generation of Hrd1 knockout cells.....50

Splicing assay for Hrd1 depleted cells.....51

Reducing Hrd1 abundance disrupts cell viability and reduces tolerance to stress when grown in 2D.....51

Furth assessing viability of Hrd1 depleted cells in 2D cultures.....55

Using Spheroids as a 3D growth assay.....57

Culturing MDA-MB-231 spheroids.....59

Determining the effects of knockdown method on TNBC spheroid formation.....61

Effects of synthetic stress on growth of TNBC spheroids.....62

Effects of UPR inhibitors on TNBC spheroid growth.....63

Lysing spheroids for western blot.....64

Assessing Ki-67 expression in TNBC cells depleted of Hrd1.....65

Assessing autophagy dependence in Hrd1 depleted TNBC cells.....66

The impact of Hrd1 depletion on apoptosis.....68

Discussion.....71

The impact of Hrd1 depletion in TNBC Cells.....71

The impact of loss of other Hrd1 complex components on TNBC cells.....72

Knockdowns vs. knockouts.....74

Conclusions from spheroid experiments.....75

Options for expanding the study.....76

The relevance of this data from a therapeutic perspective.....78

References.....79

Introduction

Cancer Cells and Proteotoxic Stress

Cancer cells are often hallmarked by proteotoxic stress (Figure 1) – arising from an increased frequency of protein misfolding and the accumulation of misfolded forms. Protein folding becomes more error prone due to the high metabolic demands of these cancer cells and the cytotoxic consequences this creates (Figure 2, (Chen & Cubillos-Ruiz, 2020)) as well as being caused by interaction with the tumour microenvironment (Nagaraj et al., 2010).

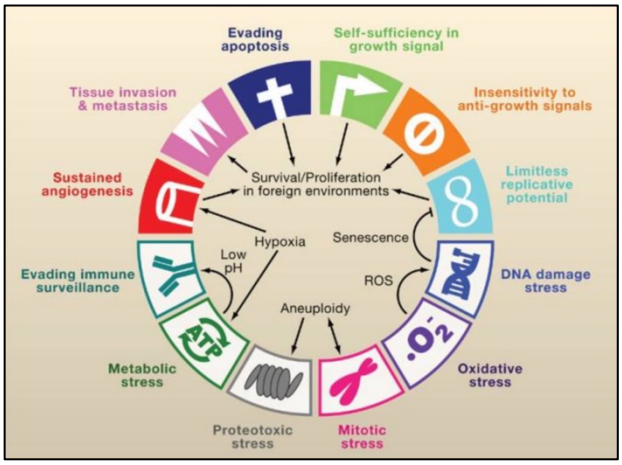


Figure 1: *'the hallmarks of cancers' – various factors that characterise cells as being cancerous, one of which is proteotoxic stress* (Luo et al., 2009).

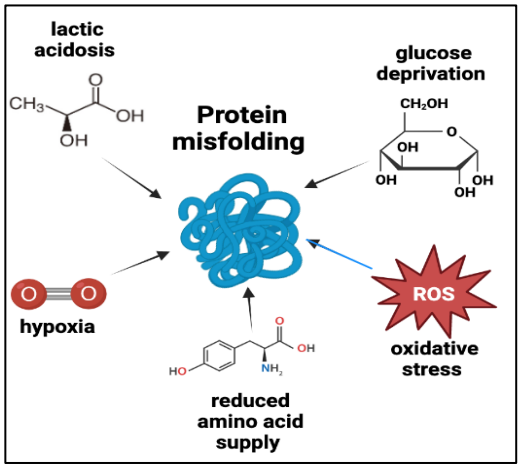


Figure 2: *factors contributing to increased protein misfolding, with these processes being upregulated in cancer cells (created with Biorender.com)*

Proteotoxic stress can manifest in the form of endoplasmic reticulum (ER stress) in which unfolded and misfolded protein accumulate within the ER and disrupt the secretory pathway. A range of cancers are said to exhibit chronic ER stress, with examples including multiple myeloma as well as prostate cancer and breast cancer (Chen & Cubillos-Ruiz, 2020). Focusing on breast cancer, specifically triple-negative breast cancer (TNBC) cells display upregulated basal ER stress levels (Chen et al., 2014). This cancer subtype is a particularly aggressive form of breast cancer, typically

affecting a younger population as well as having a typically poor prognosis and fewer treatment options. As breast cancer and TNBC form a solid malignancy, their ER stress is in a large part accounted for by the hypoxic conditions found within the tumour (Chipurupalli et al., 2019).

The Unfolded Protein Response

Cancer cells adapt to this stress to sustain viability and ensure fidelity of the proteome by maintaining protein homeostasis- accomplished by taking advantage of typically non-cancerous cellular pathways through what is envisioned to be a form of 'non-oncogenic addiction' (Nagel et al., 2016). In the ER, proteotoxic stress is sensed and mitigated by the as the unfolded protein response (UPR) - a multi-armed protein quality control mechanism that brings about stress resolution through eliciting transcriptional programmes (Figure 3). Each branch of the UPR is named after its key signalling molecule, including: Inositol Requiring Enzyme 1 (IRE1), Activating Transcription Factor 6 (ATF6) and (PKR-like ER Kinase (PERK). In response to the detection of ER stress, the cell will initially adopt a pro-survival response phase through actions predominantly mediated by both the IRE1 and ATF6 pathways, but also to some extent the PERK pathway. If these efforts to restore proteostasis are unsuccessful, cells will then initiate and transition to a pro-apoptotic response mediated predominantly by the PERK branch.

Binding-immunoglobulin protein (BIP), also known as GRP78, is an ER chaperone protein with a principle role in protein folding but there is strong evidence that it also functions as a sensor of activation of the UPR (Bertolotti et al., 2000). BIP is thought to influence all three branches of the UPR by binding each transducer and supressing their action. In conditions of ER stress, BIP is released from these bound UPR components allowing for the subsequent activation of the UPR pathways (Bakunts et al., 2017). The amplitude of the resulting UPR response is determined in a

ratiometric manner by which the UPR senses levels of BIP itself and the levels of BIP sequestering proteins (Bakunts et al., 2017).

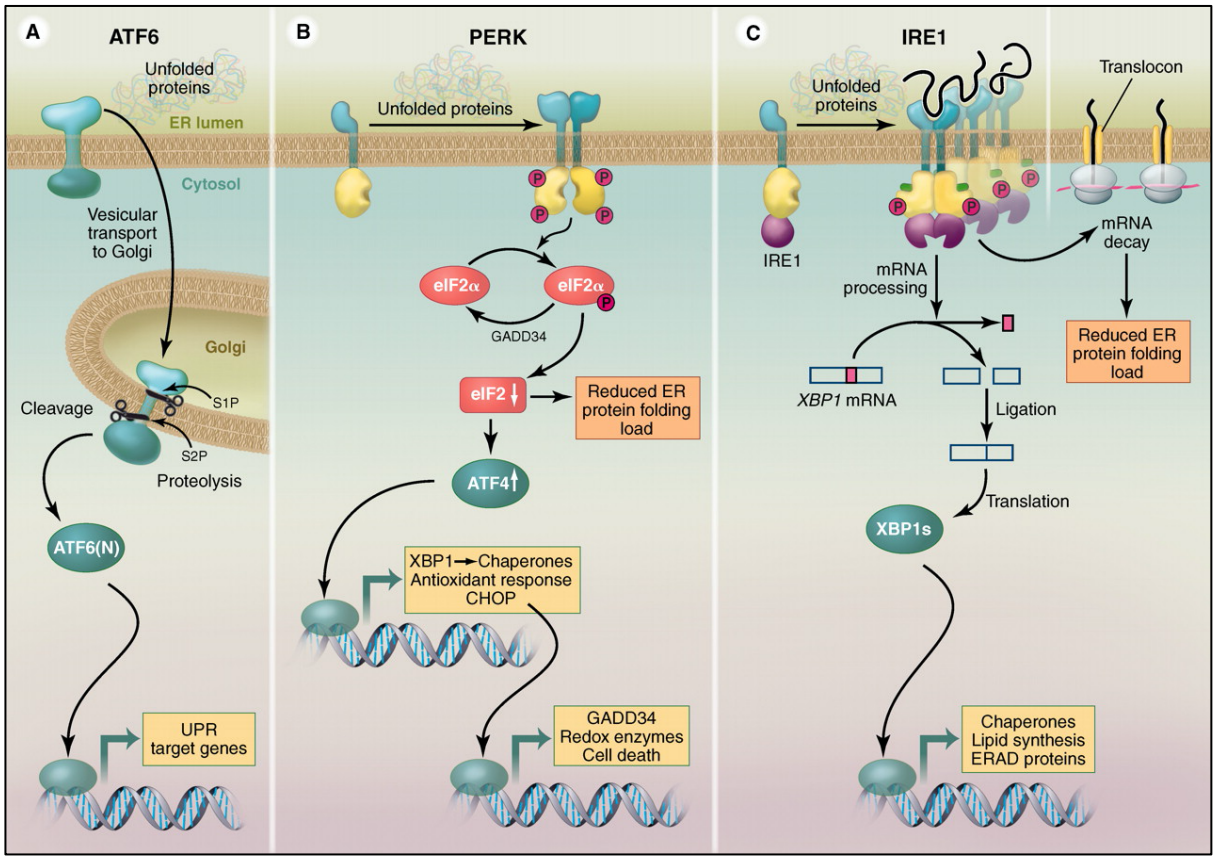


Figure 3: The unfolded protein response (UPR) with three of the main branches identified (ATF6, PERK and IRE1) (Walter & Ron, 2011).

The IRE1 branch is the most evolutionarily conserved arm of the UPR (Zhang et al., 2016). IRE1 is a transmembrane protein that contains both a kinase and a ribonuclease (RNase) domain in its cytoplasmically exposed region. Upon activation by BIP, IRE1 forms a dimer/oligomer that then is capable of splicing x-box binding protein 1 (XBP1) transcription factor to activate it.

ATF6 is a type II ER transmembrane protein and, upon detection of ER stress, is translocated to the Golgi. Once in the Golgi, ATF6 is then cleaved by site 1 protease (S1P) and site 2 protease (S2P) with resulting N-terminal cytosolic fragment of ATF6 translocating to the nucleus where it acts as a transcription factor (Metcalf et al., 2020).

Like IRE1, upon activation PERK oligomerises, triggering the phosphorylation of eIf2α and in turn causing a global reduction in translation initiation (Metcalf et al., 2020) and so reducing levels of protein synthesis. One transcript that avoids this effect, and instead is upregulated in ER stress, is of activation of transcription factor 4 (ATF4). ATF4 has also been shown to activate C/EBP homologous protein (CHOP) (Metcalf et al., 2020). Like BIP, CHOP is another protein allied with all three branches of the UPR (Hu et al., 2019). CHOP functions as a transcription factor, functioning downstream of the outlined arms. CHOP has been implicated in the transcriptional regulation of both pro and anti-apoptotic genes including genes associated with proliferation. However, it is the CHOP activated apoptosis pathway that is associated with ER stress.

The XBP1 and ATF6 transcription factors, within the UPR, regulate constituents of the ubiquitin-proteasome dependent quality control pathway known as ER-associated degradation (ERAD).

Endoplasmic Reticulum Associated Degradation (ERAD): Ties to the UPR and its Implications in Cancer

ERAD uses ubiquitin ligase complexes to clear misfolded proteins from the ER- recognising, retrotranslocating and ubiquitylating substrates to target them for degrading by proteasomes (Figure 4). The ability to clear unwanted proteins allows for the ER to maintain normal function, maintain protein homeostasis, and prevent cells from entering apoptosis. One hypothesis is that some cancer cells may take advantage of the ERAD pathway and its activity through the previously outlined strategy on non-oncogenic addiction. Cancer cells experiencing ER stress may become reliant on this pathway as a way of clearing the large quantity of aberrant proteins they produce, relative to non-cancerous cells, to allow for cell

survival by increasing the threshold for apoptosis. Therefore, what happens when this dependency is interrupted is of great interest.

A key player in the ERAD process is the Hrd1 complex – a large multi-protein complex that spans the ER membrane and is organised around the E3 ubiquitin ligase Hrd1. As an E3 ligase, Hrd1 is responsible for mediating the transfer of ubiquitin from the E2 ubiquitin conjugating enzyme to substrates for proteasome-mediated degradation. To carry this process out, many other factors co-assemble with Hrd1 to enable substrate recognition, retrotranslocation and ubiquitylation. As mentioned previously, activation of the UPR transcriptionally regulate various ERAD factors - particularly those that comprise the Hrd1 complex (Figure 4). This indicates that ERAD is responsive to changes in ER stress levels. As well as Hrd1 components being transcriptionally regulated by the IRE1 and ATF6 branches, recent studies have also identified a feedback role for Hrd1 in regulating the abundance of the cellular IRE1 (Sun et al., 2015). Loss of the Hrd1 cofactor SEL1L was shown to dramatically increase IRE1 levels in various tissues, with no change in IRE1 mRNA levels. However, the effect of these increased levels on XBP1 splicing, and therefore UPR activation, is not known (Sun et al., 2015).

Although other mammalian E3 ligases have been implicated in ERAD, its diverse client range (Kanehara et al., 2010), intimate ties to the UPR, and essentiality for viability (Hrd1 knockout in murine models displaying embryonic lethality (Doroudgar et al., 2015)) suggest that Hrd1 could be a valuable therapeutic target.

The Composition of the Hrd1 Complex:

Hrd1 forms the core of the Hrd1 complex, with various co-factors, accessory proteins and lectins forming a large multi-subunit complex that can execute the crucial steps in the ERAD process. Functional studies characterising

eukaryotic ERAD components in yeast has provided a strong foundation for our understanding of the mammalian Hrd1 complex with the first mutagenesis studies identifying these genes haven taken place more than 25 years ago (Bordallo et al., 1998; Hampton et al., 1996; Knop et al., 1996). It was also around this time that yeast microsomes were used to reconstitute the process of ERAD *in vitro* – with this being the first study in which ERAD was given its name (McCracken & Brodsky, 1996). As this process is highly conserved, many of the discovered components in yeast have mammalian orthologues. The interaction of the UPR with ERAD was also demonstrated first using yeast, specifically by producing Hrd1 mutants (Friedlander et al., 2000). Additionally in yeast, overexpressing Hrd1 has been shown to rescue knockouts of other Hrd1 components with unaffected ERAD processing as a result (Carvalho et al., 2010), although this has not yet been proven true in mammalian cells.

Table 1: the structural components of the mammalian Hrd1 complex

Accepted abbreviation	Full name	Function
Hrd1	HMG-CoA reductase degradation 1	E3 ubiquitin ligase
SEL1L	Suppressor Of Lin-12-Like Protein 1	Adaptor protein
FAM8A1	Family With Sequence Similarity 8	Complex organisation, encourages HERPUD1 recruitment
HERPUD1	Homocysteine-responsive endoplasmic reticulum-resident ubiquitin-like domain member 1	Adaptor protein, Stabilises the complex, strongly upregulated by the UPR

HERPUD2	Homocysteine-responsive endoplasmic reticulum-resident ubiquitin-like domain member 1	Adaptor protein
XTP3-B	XTP3-Transactivated Protein B	Lectin
OS-9	Osteosarcoma amplified 9	Lectin, substrate of HRD1
Ube2g2	Ubiquitin-conjugating enzyme E2 G2	ubiquitin-conjugating enzyme (E2), assembles and transfers K48-linked polyubiquitin chains to substrates, known to interact with several E3s
Ube2j1	Ubiquitin-conjugating enzyme E2 J1	ubiquitin-conjugating enzyme (E2), phosphorylated during ER stress
UbxD8	UBX Domain-Containing Protein 8	Complex organisation and p97 recruitment
Derlin-1	Degradation in endoplasmic reticulum protein 1	CDC48 recruitment
Derlin-2	Degradation in endoplasmic reticulum protein 2	CDC48 recruitment, dislocation and retrotranslocation
Derlin 3	Degradation in endoplasmic reticulum protein 3	dislocation and retrotranslocation

AUP1	Ancient Ubiquitous Protein 1	Role in organisation of the complex

Previous work in our lab has investigated the interaction of HRD1 with its various cofactors (Christianson et al., 2011; Schulz et al., 2017), while others have used quantitative LC-MS/MS to estimate the composition and abundance of components within HRD1-containing complexes (Hwang et al., 2017). This supported SEL1L, FAM8A1, OS-9, XTP3-B and Ube2j1 as some of the most significant interactors of HRD1, as well as HERPUD1 and HERPUD2 but with these two proteins in relatively low abundance thought to be attributed to their rapid turnover rates. Although both SEL1L and HERPUD1 are deemed to be important components within the Hrd1 complex, direct interaction of these two components has not been reported.

The roles of OS-9 and XTP3-B roles in ERAD were once thought to be redundant, but subsequent studies first implicated Yos9, the yeast homologue of OS-9, in the recognition of both glycosylated and non-glycosylated substrates. This was then also discovered to be true for OS-9 (Bernasconi et al., 2008; Christianson et al., 2008). More recent findings state both OS-9 and XTP3-B as responsible in the determination of state for newly synthesised proteins, making the decision based on the distribution of glycan and non-glycan degrons (van der Goot et al., 2018). Mutations in the lectin domains of either protein prevent their binding to SEL1L suggesting this is how they are recruited to the complex (Christianson et al., 2008).

The exact contribution of HERPUD1 vs HERPUD2 to ERAD is largely unknown but the ability of these two components to form hetero oligomers has been observed (Huang et al., 2014), suggesting the possibility they may coexist in the complex despite their roles being partially redundant. The observation that HERPUD1, but not HERPUD2, is stress regulated led to the preferential pursuit of HERPUD1 in this study.

Both Ube2j1 and Ube2g2 are ubiquitin-conjugating enzymes (E2) with roles in ERAD and are transcriptionally regulated by the UPR. Polyubiquitin signatures on ERAD substrates can largely be attributed to the action of these two enzymes (Christianson et al., 2023). Additionally, Ube2g2 is a known binding partner of AUP1, a protein primarily known for its role in lipid droplet formation but also thought to be responsible for the recruitment of Ube2g2 to the Hrd1 complex (Spandl et al., 2011).

All three outlined members of the Derlin family have been shown to interact with ERAD substrates with Derlin-1 required for the degradation of Class I membrane proteins (Lilley & Ploegh, 2004) and Derlin-2 and 3 involved in the degradation of misfolded glycosylated proteins - but not non-glycosylated proteins (Oda et al., 2006). This Derlin-substrate interaction occurs prior to an interaction with p97 ATPase (Ye et al., 2005), the enzyme responsible for extraction of polypeptides from the ER membrane for degradation suggesting the importance of Derlins in the retrotranslocation step of ERAD, with these three Derlins all associating with p97 (Lilley & Ploegh, 2004; Oda et al., 2006). Previous work has implicated both Derlin-2 and Derlin-3 in the UPR (Oda et al., 2006). However, it is believed that UPR upregulation has more of an effect on Derlin-3, with transcriptomic studies indicating the DERL3 gene as massively upregulated in conditions of ER stress (Eura et al., 2020).

FAM8A1 has shown to be crucial in the organisation of the Hrd1 complex, interacting with both SEL1L and HRD1 (Christianson et al., 2011) and with its loss in HEK-293 cells resulting in the subsequent loss of HRD1, SEL1L, Ube2j1 and HERPUD1 from the complex (*Schulz et al., 2017).*

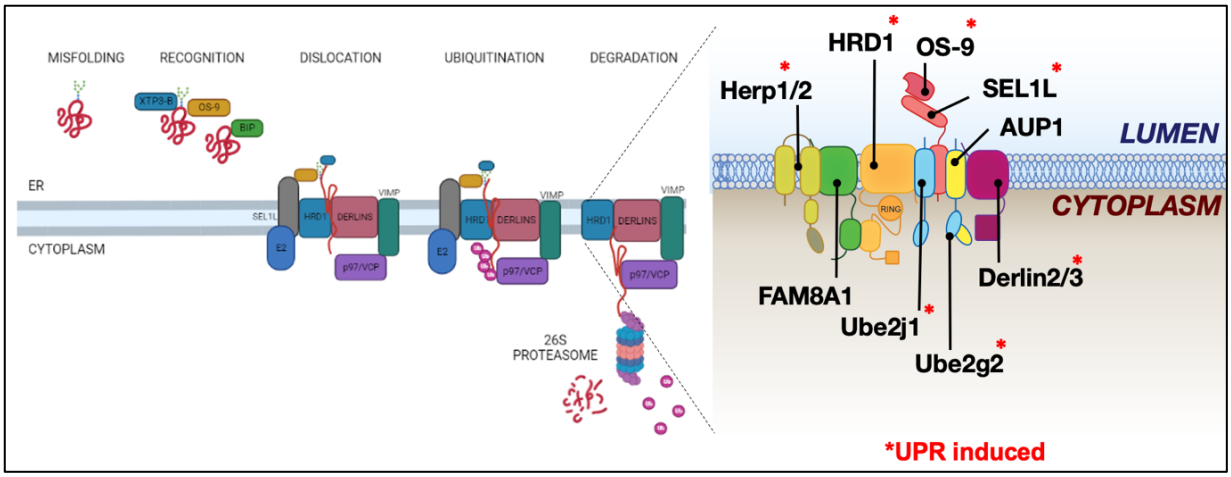


Figure 4: an overview of the ERAD pathway and the Hrd1 ubiquitin ligase complex. The components of the complex that are transcriptionally regulated by the UPR, in the presence of ER stress, have been highlighted (Schulz et al., 2017).

Features of Triple-Negative Breast Cancer:

Cells designated as TNBC lack receptors for progesterone, oestrogen as well as Human Epidermal Growth Factor Receptor 2 (HER2). TNBC classified cells are also associated with mutations in the BRCA tumour suppressor genes (Chen et al., 2018). Due to these receptors' absence, hormonal therapy is not a viable option for these patients with treatment then defaulting to surgical removal where possible as well as chemotherapy. TNBC patients are said to respond positively to current chemotherapy options initially but with a high rate of recurrence (American Cancer Society, 2022).

The role of the UPR in breast cancer has gained clinical interest as its function and contribution to cancer prognosis and outcome are better understood. Specifically, the IRE1 pathway has been widely implicated in breast cancer with the IRE1 gene shown to be upregulated in breast cancer, more so than in any other cancer (Zhang et al., 2020) and this upregulation correlating with lower patient survival rates. XBP1 is also highly upregulated in breast cancer in particular (Oakes, 2020) as well as being shown to promote survival in the hypoxic conditions within solid tumours (Romero-Ramirez et al., 2004). There is also increasing evidence that the

majority of available chemotherapeutics cause an induction of stress responses, with this activation associated with a subsequent resistance to chemotherapy (Holohan et al., 2013).

Project Aims and its Relevance:

There have been numerous studies on characterising the mammalian Hrd1 complex, but questions remain about the stoichiometry and what each component contributes to ERAD processing. Not all Hrd1 complex components are stress-regulated or targets of the UPR, so a Hrd1 complex assembled during ER stress could differ from one formed with no/low basal stress. Moreover, there is not an extensive understanding of the Hrd1 complex in the context of cancer and its intrinsic stress so how the Hrd1 complexes may vary both structurally and in terms of reliance upon the various complex components for survival to non-malignant populations is of great interest.

This project aims to determine how components comprising the Hrd1 ubiquitin ligase complex contribute to survival of TNBC model cell lines experiencing ER stress. These studies are carried out under basal stress levels as well as under further ER stress induction.

Reliance of cancer cells on stress resolution pathways to prevent apoptosis, has led to a hypothesis that this dependence can be exploited therapeutically to produce anti-cancer therapeutics. Under this premiss, cancer cells could either be treated with an additional stressor to drive cells into apoptosis or alternatively, the stress resolution pathways could be inhibited to lower the threshold at which apoptotic induction can be reached.

To date, the range of inhibitors of these pathways has been limited, with few proven to have long term efficacy. Bortezomib is a proteasome inhibitor that works by preventing degradation of the protein at the last stage of the

ERAD pathway. However, there is adaptation to the absence of proteolytic activity and after a few years, patients typically have to switch to an alternative treatment due to ineffectiveness (Zaal et al., 2017). Moreover, bortezomib has had limited clinical success in the treatment of breast cancer specifically, showing poor results at clinical trial (Yang et al., 2006). As there appears to be no direct functional redundancy with Hrd1 and its contribution to the UPR (Fenech et al., 2020), ERAD (via Hrd1) represents an appealing upstream target that may prove more successful.

Currently only one inhibitor of Hrd1 has been reported. CP26 was identified in a small molecule screen for retrotranslocation but it appears to have low potency as well as binding to a range of Hrd1 components (Ruan et al., 2019), likely increasing the risk of off target effects. Thus, there are no viable compounds available that directly inhibit ERAD at the level of the Hrd1 complex. As there are fewer treatment options for those with TNBC, and breast cancer itself being said to be the most common form of cancer in the UK, accounting for 15% of all new cancer cases (Cancer Research UK, 2023), there is a need for improvement in the options of therapeutics available.

Collectively, this supports developing a strategy for modulating ERAD activity of the Hrd1 complex during the UPR with the ultimate goal of applying this as a targeted cancer therapeutic. Perturbations in ERAD are not just associated with cancer but also a range of other disease types such as cystic fibrosis and Parkinson's (Guerriero & Brodsky, 2012). This means increasing our understanding of ERAD and Hrd1 may also have further applications in the treatment of non-cancerous diseases.

This study supplements work performed by others in the Christianson lab, namely multiple myeloma research and working to characterise the 'stressed' Hrd1 complex.

Materials and Methods

Cell culture

MDA-MB-436 cells were grown in Dulbecco's modified eagle medium (DMEM) (Gibco) supplemented with 10% foetal bovine serum (FBS) (Sigma-Aldrich). ATCC suggests Leibovitz (L15) media for the culture of MDA-MB-436 cells, but without access to a CO_2 free incubator, this was not possible for this project. DMEM supplemented with FBS has been used extensively in the literature to culture this cell type (Pirsko et al., 2018) and therefore was suitable for this project. MDA-MB-231 cells were kindly provided by Professor Ester Hammond's lab and were also grown in DMEM supplemented with 10% FBS upon their recommendation. Both lines were consistently tested for mycoplasma throughout this project with negative detection each time. Cells were passaged with 0.25% Trypsin-EDTA (Gibco).

Freezing cells

Cells were frozen in a solution of 9:1 FBS to DMSO and placed Mr Frosty cell freezers at -80°C before being moved to liquid nitrogen the following day for long term storage.

Lentiviral transduction using shRNAs

500 µl of viral solution (unknown concentration) were applied to cells in 2 cm dishes with the media changed to virus free media the following morning. Lentiblast premium (OZ Biosciences) was used at 1 µl/ml of media to enhance transduction efficiency. Selection media was only added 48 hours after transduction to allow times for the cell population to recover.

RNA extraction

Cells were first lysed in Trizol (Sigma-Aldrich) with the resulting RNA extraction then being performed using the Direct-zol RNA kit (Zymo). Samples were eluted in nuclease free water before storing at -80°C.

Nucleic acid purity and concentration:
Absorbance values were calculated using a NanoPhotometer (Implen).

cDNA synthesis
cDNA was produced either using the high-capacity RT kit (Invitrogen) or RT synthesis kits (Primer design).

qPCR
qPCRs were performed on triplicate cDNA samples using SYBR Taq (Thermo Fisher) and analysed using the CFX Maestro software (Bio-Rad). Actin was used as a housekeeping gene.

XBP1 splicing assay
A PCR was set up using cDNA My Taq red mix (Meridian) and XBP1 primers (Table 5) that are able to detect unspliced, spliced and hybrid variants. PCR products were run on 3% agarose gel with added SYBR™ safe (Invitrogen) as a gel stain. These were run using TAE buffer (Thermo Fisher) and the Mupid™ electrophoresis system (Geneflow). The quality of RNA used in this assay was assessed beforehand by separation on 1.5% agarose gels to eliminate any samples that produce smears. A low molecular weight range ladder was used (Thermo Fisher).

Protein sample preparation
Cells were lysed in RIPA (50 mM Tris-HCl pH 7.5, 150 mM NaCl, 1% NP-40, 0.5% Sodium Deoxycholate, 0.1% SDS, 5 mM EDTA) or TritonX -100 (50 mM Tris-HCl pH 7.5, 150 mM NaCl, 1% TritonX-100, 5 mM EDTA). Lysis buffers were supplemented with both N-ethylmaleimide (NEM, 2 nM) and protease inhibitors (cOmplete tablets, Roche). Lysis took place or 30 minutes on ice followed by a 10,000 RPM centrifugation at 4°C for 30 minutes. Total protein concentration was quantified using the Pierce™ BCA assay (Thermo Fisher) and a Clariostar machine. Bovine serum albumin

(Thermo Fisher) was used for protein standards. The samples were then normalised to the sample with the lowest total protein concentration, typically ~1 µg/µl . Using the previously chosen lysis buffer. Samples were then supplemented with laemmli buffer (1 M Tris HCl pH 6.8, 2% SDS, 10% glycerol and 0.004% bromophenol blue) with DTT (0.85 µg final concentration). Samples were then heated at 60°C for 10 minutes before storage at -20°C.

SDS-PAGE and western blotting

Samples were separated on 4-12% SDS-PAGE gels (Invitrogen) in MES, 2-(N-morpholino)ethanesulfonic acid, buffer (Invitrogen) and for 1 hour at 150 V. The ladder used was Precision Plus Protein All Blue Standards (BIO-RAD). The resulting gels were then transferred to a 0.45 µM PVDF membrane (Amersham) using Tris-glycine buffer (110 V for 75 minutes).

Membranes were then blocked using phosphate buffered saline with Tween (Sigma-Aldrich) (PBST) containing 5% milk for 1 hour, then incubated with each primary antibody overnight at 4°C or for 1 hour at RT. Membranes were then washed in PBST (3 x 5 minutes) followed by secondary antibody incubation (RT, 1 hour). Post incubation, membranes were washed in PBST (3 x 10 minutes). Membranes were then probed with SuperSignal™ West Pico Plus (ECL, Thermo Fisher) and the resulting chemiluminescence imaged using a UVITEC imager. Detection with Anti-tubulin was included each time as a loading control. Restore™ Stripping buffer (Thermo Fisher) was occasionally used to allow for reblotting membranes.

Alamar Blue assay

Cells were seeded in 96-well plates at 10,000 cells per well. Cells were treated with the chosen drugs the day after seeding and incubated for five days. On the fifth day Alamar Blue dye (1 mg/ml resazurin powder (Sigma-Aldrich) in PBS) was added to each well at a ratio of 1:10 reagent to media followed by a 6-hour incubation. Absorbance readouts were then given

using a Clariostar plate reader with wells containing solely media being used as a blank. On the graphs produced the lowest concentration plotted is representative of untreated cells, this was done to allow plotting on a logarithmic scale. If an error bar is missing for a plotted point, this is because the marker symbol, used when plotting the graph, is larger than the error bar.

Crystal violet assay

Cells were plated at a gradient of concentrations on either 24 or 12-well plates and drug treated after the cells had reattached. The resulting colonies are fixed using a 1:1 solution of methanol/acetone for 10 minutes at 4°C. The fixative was then removed, and crystal violet staining solution was applied to each well, left at room temperature for 30 minutes before aspirating the stain and removing any residual dye by washing with distilled water. These plates were then imaged using a plate imager with integrated density values (correlated with cell number) computed using ImageJ.

Doxycycline induction of shRNAs

Doxycycline (DOX, Sigma-Aldrich) was used at a concentration of 100 ng/ml the day after plating puromycin selected transduced cells.

Celigo imaging

Cells were transduced with lentiviral shRNAs following the procedure described above. One day after transduction these cells were transferred to 96 well plates and subsequently imaged every day, for 7 consecutive days, post-transduction. Propidium iodide (Thermo Fisher) was added at 5 µm and left to incubate for 20 minutes in the dark prior to imaging.

Spheroid growth assay

Ultra-low attachment plates (ULT, PerkinElmer) were used with 2.5% Matrigel (Corning) and a seeding concentration of 3000 cells/well. After plating, spheroids were left to grow for 20 days in ULT plates with media

being replaced/replenished throughout. In some cases, the culture time was cut short a few days due to time restraints, this has been noted where relevant with comparisons only being made between spheroids that have been cultured in the same plate and therefore grown for the same amount of time. Images were then taken on a Nikon TE300 (inverted) microscope using the 4x objective lens. Area of the spheroids were then measured using ImageJ.

Fixing spheroids

Spheroids were lifted from their culture plates using a p100 pipette with a wide bore tip and transferred to 1x PBS, washed 3 times with this solution and then covered in 4% paraformaldehyde (PFA) for 2 hours at room temperature after removing the PBS from the final wash. PFA was then aspirated and replaced with a 30% sucrose solution (in PBS) and incubated for 3 hours. This solution was then removed, and spheroids were transferred to moulds where they were then embedded in optimal cutting temperature (OCT) media (Thermo Fisher), snap frozen in liquid nitrogen before being transferred to -80°C for storage.

Cryosectioning of spheroids

Resulting OCT spheroid blocks were then sliced at 7 μM by Cryostat (Bright OTF5000 Cryostat) and transferred to glass slides before being stored at -20°C.

Staining spheroid sections

Slides were removed from -20°C and thawed at room temperature for 30 minutes before being rehydrated in PBS for 10 minutes in a Coplin jar also at room temperature. Slides were fixed and stained using ApopTag® Red In Situ Apoptosis Detection Kit (Sigma-Aldrich) following the provided protocol for tissue cryosections. Hoechst was used as a nuclei counterstain with slides mounted using ProLong® gold antifade mounting solution (Thermo Fisher). Slides were imaged using an Olympus BX40 microscope

with Zen Blue software. Images were processed using ImageJ software to allow for calculation of corrected total spheroid fluorescence (CTSF). The formula for this calculation is as follows: CTSF = Integrated Density – (Area of selected spheroid section X Mean fluorescence of background readings).

Data analysis

Graphs and statistical significance were produced and calculated using PRISM 9 software (GraphPad).

Ki-67 staining

Harvested cells were first washed in PBS (3x) to remove residual media, fixed with 4% PFA (20 minutes, RT), washed in PBS again (3x), and permeabilised (0.1% Triton X-100, 20 min). Cells were then washed 3 times with cell staining buffer (BioLegend) with proper fluorochrome-conjugated Ki-67 antibody (BioLegend) then being added to this solution after the final wash at the concentration of 1 µl per 1 million cells. The cells were then left to incubate in the dark for 30 minutes before running these samples on the Fortessa flow cytometer (BD Biosciences) machine. Compensation and analysis were performed using Flowjo software.

Producing knockout cell lines

Overnight cultures were produced using LB broth supplemented with ampicillin (1:1k) and scrapings taken from glycerol stocks. The resulting pellets were processed using the QIAprep Spin Miniprep Kit (Qiagen). The concentration of resulting DNA was determined before being used in transfections. Both FuGENE (Promega) and DNA were diluted in Optimem (GIBCO) before these two dilutions were combined and allowed to incubate for 20 minutes. The resulting solution was then added to cells and allowed to incubate overnight before the media was exchanged the following morning.

Table 2: shRNA target sequences.

Target Gene	Mature Antisense
HRD1	GAGACAGTTTCAGATGATT
HRD1 (Dox inducible)	ATGGGTACCAGTCTTAGGG
SEL1L	TAATATACAAGAGCCTTTG
HERPUD1	TTTGGGAAGTTCTGAACCG
HERPUD1 (Dox inducible)	TTGAAGACAAGCCATGCTG
FAM8A1	TAATACTTGAATTTAACAG
UBE2G2	AATAAATTCCCAGTGCATC
UBE2J1	TAAAGCTTATTTGCCTAGC
OS9	TTCATCATCCCAGTCGAAG
XTP3B	TATACAGTAACAGCATGAG

Table 3: primary antibodies used for western blotting. All were diluted in 5% PBST

Antigen	Host	Source
ATF4	Rabbit	Cell Signaling Technology
AUP1	Rabbit	Atlas Antibodies
BIP	Rabbit	Cell Signaling Technology
CD147	Rabbit	Santa Cruz
CHOP	Mouse	Cell Signaling Technology
DERLIN 2	Rabbit	Abcam
FAM8A1	Rabbit	A kind gift from Ron Kopito's Lab
HERPUD1	Rabbit	Abcam
HRD1	Rabbit	Cell Signaling Technology
OS9	Rabbit	Proteintech
Phosphoe-eIF2α	Rabbit	Abcam
TUBULIN	Mouse	Cell Signaling Technology
UBE2G2	Rabbit	Cell Signaling Technology
UBE2J1	Rabbit	Abcam
XBP1-S	Rabbit	Cell signaling Technology

XTP3B	Rabbit	A kind gift from Ron Kopito's Lab

Table 4: Secondary antibodies.

Name	Host	Source	Working concentration
Goat	Donkey	Invitrogen	1:25k
Rabbit	Goat	Bethyl	1:35k
Mouse	Goat	Bethyl	1:25k

Primers were reconstituted to make 100 µM primer stocks and then diluted to form 10 µM combined forward and reverse stocks.

Table 5: Primer sequences. All primer sets are for qPCR analysis with the exception of those targeted for XBP1.

Target	Forward or reverse (F/R)	Sequence
ACTIN	F	AGCACAGAGCCTCGCCTT
ACTIN	R	CATCATCCATGGTGAGCTGG
DERLIN 2	F	TGCAGTTGGAATTGATCACACC
DERLIN 2	R	GGCCTGGCCCAAGAAAACTA
FAM8A1	F	AAAATGATGGTTGTGGCACTTA
FAM8A1	R	TGTATCACATGTCACAACTCGAA
HERPUD1	F	GCTTCCAAAGCAGGAAAAACG
HERPUD1	R	GTCCCCGATTAGAACCAGCA
HRD1	F	TCTTCCTCAAATGTTTCCACTG
HRD1	R	TCGTCATCAGGATGGCATAA
OS9	F	CTTCCCTACAGCCTGAGGAGTA
OS9	R	CCAGACTTGGTCTCACTCCACA
SEL1L	F	GAAACCAGCTTTGACCGC
SEL1L	R	ATCTGCCGTCTCTTAGCAGC
UBE2G2	F	CCCAGAAGACACCTGCTTTGAG

UBE2G2	R	GGAGGATGGAAATGCAGACTCTC
UBE2J1	F	CCACCAGAGTATCCCATGAAACC
UBE2J1	R	ACTCCACGAAGGCTGCCAAGTT
XBP1_1	F	TTACGAGAGAAAACTCATGGC
XBP1_1	R	GGGTCCAAGTTGTCCAGAATGC
XBP1_2	F	CCTGGTTGCTGAAGAGGAGG
XBP1_2	R	CCATGGGGAG ATGTTCTGGAG
XTP3B	F	GTCAATCACTGCCAGGATCTCC
XTP3B	R	CGACTTGTGGATCGCTGGAAATC

Table 6: reagent quantities for producing a PCR master mix.

Reagent	Quantity (µl) for one reaction
Taq Polymerase	25
Forward and reverse primer mix	2
Nuclease free water	13

Table 7: Drug treatments: the following are the final concentration used unless otherwise stated.

Drug	Concentration (µM)
Thapsigargin	1.0
4u8C	5.0
Ceapin-A7	5.0

Results

Modelling ER stress in Triple-Negative Breast Cancer

ER stress is often a hallmark of triple-negative breast cancer (TNBC). To investigate this, we selected the MDA-MB-231 and the MDA-MB-436 cell lines as models for TNBC (Figure 5). From literature currently available, there is no consensus as to the level of ER stress various breast cancer cell lines display. A commonly used assay for ascertaining the presence of ER stress is through the detection of the spliced form of XBP1, known as the XBP1 splicing assay. XBP1 mRNA is a substrate for the endoribonuclease activity of IRE1 (Lee et al., 2002), which upon ER stress, splices this mRNA.

The spliced XBP1 ($XBP1_s$) is translated, which then goes on to the nucleus to function as an active transcription factor – transcriptionally activating genes that aid in stress resolution. The primers used in this assay recognise both $XBP1_s$ and unspliced forms of XBP1 ($XBP1_u$) as well as a hybrid species ($XBP1_{h)}$ that forms from one strand of each of these two variants, creating a loop that migrates more slowly through the agarose gel. In this assay thapsigargin (Tg) is commonly used as a positive control. Tg is a drug that induces ER stress by blocking the action of pumps for $Ca2^+$, reducing calcium stores in the ER (Yamarnoto et al., 1995).

A paper from 2014 (Chen et al., 2014) presents a panel of various breast cancer cells (those falling into the TNBC category as well as those that do not). This work suggested that both MDA-MB-436 and MDA-MB-231 display XBP1 splicing, and therefore constitutive ER stress, before the addition of any additional ER stressor (Tg), with MDA-MB-436 showing a greater degree of splicing than the other with a more intense spliced XBP1 band being present. This suggests MDA-MB-436 experience more intense levels of basal ER stress out of these two lines. This is despite MDA-MB-231 cells being viewed as the more aggressive cancer of the two due to its greater metastatic potential (Sheridan et al., 2006).

However, a paper from the Ashkenazi lab (Harnoss et al., 2020) using western blotting rather than agarose gels, shows levels of XBP1s in these two cell lines are undetectable in a 2D context, unless Tg is added. They then demonstrated that this differs in a 3D context, with MDA-MB-231 cells showing expression of $XBP1_s$ at a basal state (this 3D expression did not seem to be tested in MDA-MB-436 cells).

Based on reported observations, we tested two different primer sets (XBP1_1, XBP1_2) in an XBP1 splicing assay on both MDA-MB-436 and MDA-MB-231 cells. XBP1_1 refers to the primer set we use ordinarily lab

taken from a separate publication (Hiramatsu et al., 2011). XBP1_2 refers to a set of primers reported previously by the Glimcher lab (Chen et al., 2014) and were included to confirm results. Both primer sets detect all three variants of XBP1, and therefore have been used interchangeably throughout, but there is a slight difference in the size of the fragments produced. The XBP1_1 splicing primers produce a unspliced band of 283 bp and a spliced of 257 bp meaning just a 26 bp difference between the two. The XBP1_2 primers produce an unspliced band of 146 bp and a spliced band of 119 bp, meaning another small difference of just 27 bp between the two.

In our hands, both cell lines appeared to display comparable levels of XPB1 splicing, with a very faint $XBP1_s$ band but a clear prevalence of a $XBP1_h$ band. This indicates that some XBP1 splicing must be occurring to enable formation of the hybrid amplicon. When treated with Tg, XBP1 splicing is enhanced, meaning these cells are not at a maximal level of ER stress when at a basal state and are capable of experiencing higher levels of ER stress (Figure 6A).

This observation led me to conclude that both cell lines were suitable for use in this project as they both appear to have some degree of constitutive ER stress. The available literature has suggested that MDA-MB-436 experienced higher ER stress levels of the two and so experiments were first trialled and refined in this cell line before testing the MDA-MB-231 cells. MDA-MB-231 cells were also included as they were more suitable for some experiments due to their shorter doubling time and enhanced ability to form colonies (allowing for the performance of a crystal violet assay for example).

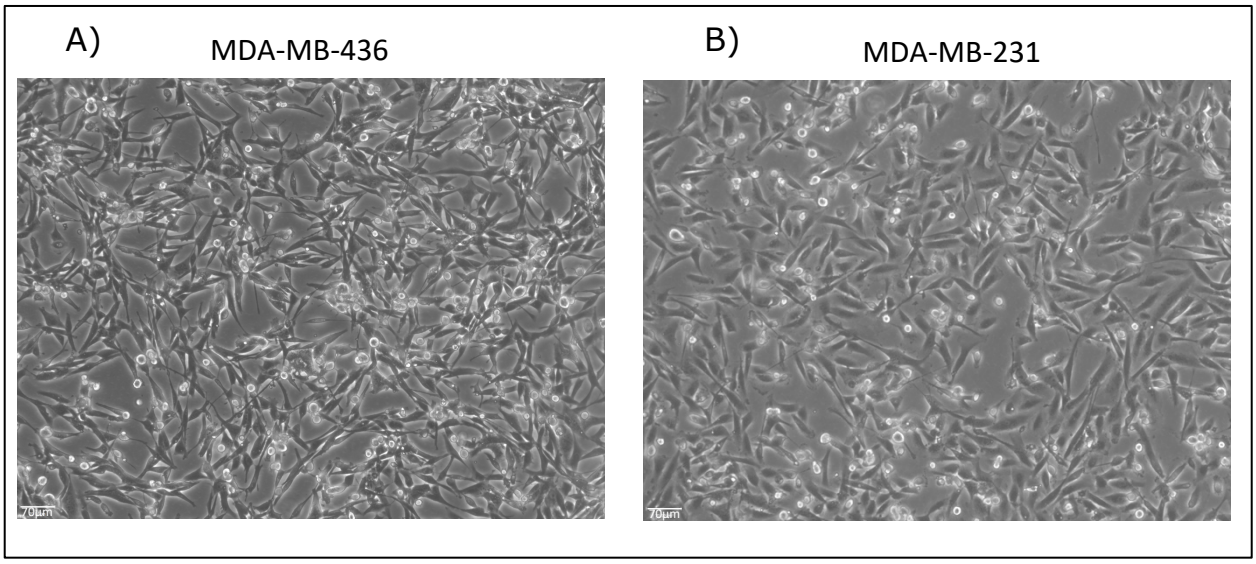


Figure 5: Triple negative breast cancer lines A) MDA-MB-436 cells. B) MDA-MB-231 cells. Both images have been acquired using a 10X lens with phase contrast, a scale bar has been included (70 µm).

To complement analysis of the two TBNC cell lines, I also included other cancer cell lines that either exhibited low/no ER stress (HeLa-epithelial/cervical) or "chronic ER stress" (AMO-1 – multiple myeloma (Chen et al., 2022)) (Figure 6A and B). HeLa cells did not produce either a hybrid or spliced XBP1 band, whereas AMO-1 cells exhibit both, even before addition of an ER stressor. Addition of Tg to AMO-1 cells resulted in the loss of $XBP1_u$ band and increasingly intense $XBP1_s$ band. This data collectively suggests that these TNBC cell lines (MDA-MB-436 and MDA-MB-231) sit in the middle of the ER stress spectrum - exhibiting a modest level of constitutive ER stress but not as much as some other cancers (e.g., multiple myeloma).

XBP1 splicing assays were also performed in both cell lines in the presence of the UPR inhibitors 4μ8c and Ceapin-A7. As mentioned previously, Tg increases ER stress levels and results in the production of the $XBP1_s$ band (Figure 6C, lane 1). 4μ8c is an inhibitor of IRE1, the enzyme that splices XBP1. 4μ8c blocks IRE1 RNase activity and prevents XBP1 splicing and the formation of the spliced and hybrid amplicons (Figure 6C, lane 4). Ceapin-A7 is an ATF6 inhibitor that works by fixing ATF6 to the ER membrane and preventing their entry into COPII vesicles. As ATF6 is an independent branch of the UPR, Ceapin-A7 does not directly affect XBP1 splicing and treated samples mirror the untreated condition (Figure 6C, lane 3 and Figure 6D, lane 2). Splicing assays for both MDA-MB-436 and MDA-MB-231 exhibit the same effects caused by these treatments. Although there was an issue with the 4μ8C lane on the MDA-MB-231 gel (Figure 6D, lane 3), the inhibitory effect of this drug on splicing is displayed in the lane with both 4μ8c and Ceapin-A7 in which no splicing is present (Figure 6D, lane 4).

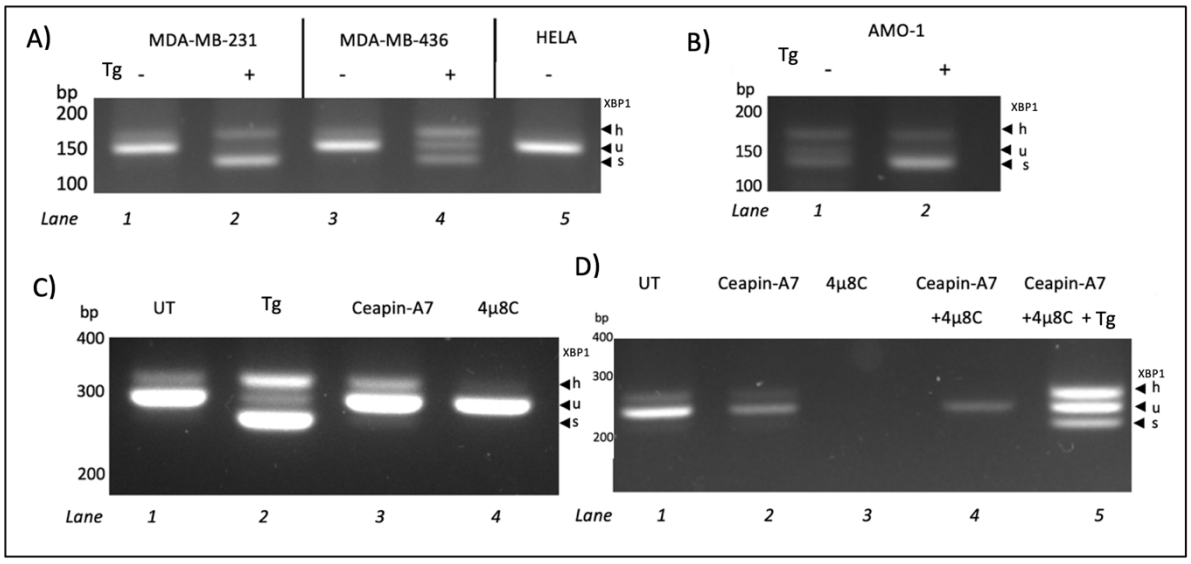


Figure 6: various XBP1 splicing assays performed as a method for determining ER stress A) and B) a comparison of ER stress and ER stress induction in MDA-MB-231, MDA-MB-436, HELA and AMO-1 cells using the XBP1_2 splicing set. C) and D) show responses to various drug treatments using the XBP1_1 splicing set in MDA-MB-436 AND MDA-MB-231 cells respectively. Each assay was repeated a minimum of three times with the same effects being seen. Thapsigargin was given at a final concentration of 1 μM whereas both UPR inhibitors (4μ8c and Ceapin-A7) applied with a final concentration of 5 μM. All cells were harvested 16 hours after drug treatment.

Figure 6, lane 5, shows the effect of the two UPR inhibitors when ER stress is upregulated. This appears as though there is less of a prominent spliced band and a more prominent unspliced band than with Tg alone (Figure 6A), suggesting 4μ8C has worked to inhibit IRE1 but, as Tg is such a potent ER stressor, some splicing still occurs. Pre-treatment with 4μ8C would likely prevent this effect.

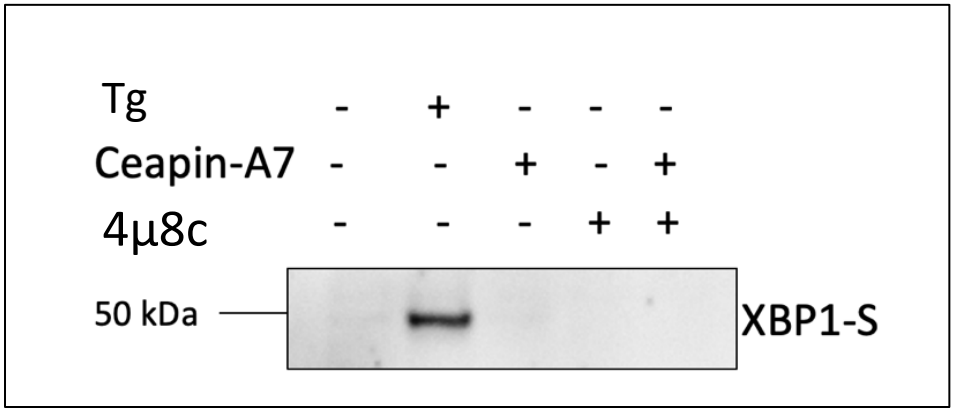


Figure 7: A western blot to detect the spliced variant of XBP1 in MDA-MB-436 treated with thapsigargin (Tg) and UPR inhibitors (Ceapin-A7 and 4μ8C) for 16 hours.

These observations were confirmed in MDA-MB-436 cells by western blot using an antibody that detects the spliced variant of XBP1 (Figure 7). An $XBP1_s$ band was only detectable after Tg treatment. UPR inhibitors had no effect without additional stressor treatment. This supports the data from the above splicing assays and emphasises the potency of Tg as an ER stress inducer.

The Effect of UPR Activation in TNBCs at the Protein Level

ER stress induced activation of the UPR leads to the transcriptional upregulation and production of ER proteins to promote proteostatic resolution. To investigate this, I analysed protein levels of various Hrd1 complex components that mediate ERAD as well proteins implicated in the UPR by western blot. Specifically, I wished to monitor basal levels of these proteins and observed any changes that may occur with different

treatments. Compounds (Tg, 4μ8c, and Ceapin-A7) used above in splicing assays were also included in assays that were performed in both MDA-MB-436 and MDA-MB-231 cell lines (Figures 8 and 9, respectively).

The most notable changes in protein levels were seen upon addition of Tg and ER stress induction. Tg addition caused upregulation of various factors involved in the UPR such as BiP, IRE1, ATF4 and CHOP, the latter two being transcription factors in the PERK pathway. Various components of the Hrd1 complex also appear upregulated in this response with the most notable being HRD1 itself as well as HERPUD1. These data are consistent with a model where components of the Hrd1 complex are upregulated by ER stress in these TNBC cell lines. For the initial experiment in MDA-MB-436 cells, two time points were included for the combined inhibitor treatment with variations being seen between these two points (Figure 8). For example, HRD1 appears upregulated from basal levels at 16 hours but this affect is no longer seen at the 24-hour mark giving a rough time frame for stress resolution. In contrast, levels of ATF4 appear higher at 24 hours, suggesting it may take longer for the full effects of this upregulation to be seen. CHOP expression is seen in all samples but not in the parental line meaning all of these synthetic disruptions in turn may contribute to an increase in apoptotic events (Figure 8).

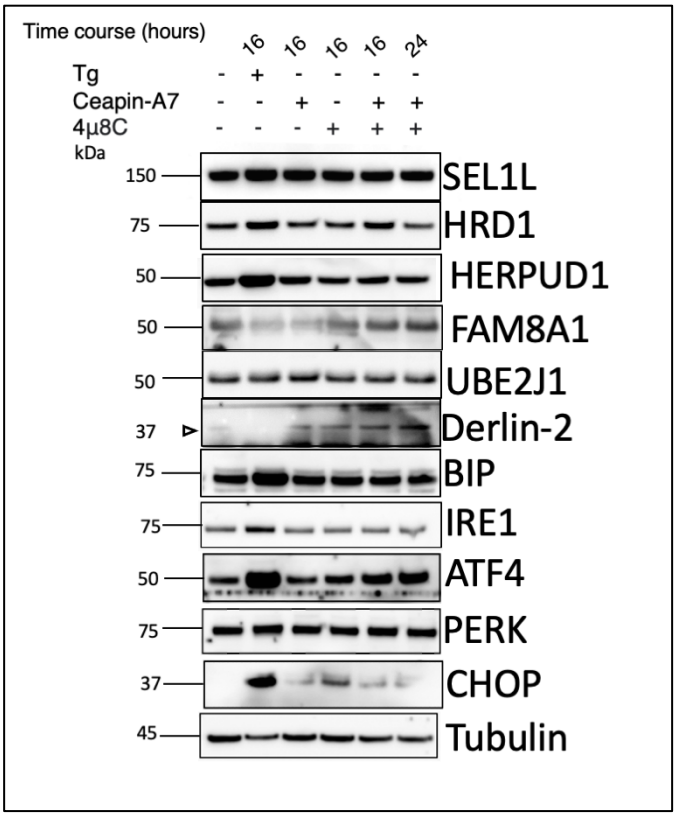


Figure 8: a western blot performed by drug treating MDA-MB-436 cells with thapsigargin (Tg) as well as Ceapin-a7 and 4μ8C for 16 hours, with an additional timepoint of the combined treatment of 24 hours. Various components of the Hrd1 complex, as well as proteins involved in the UPR, have been blotted for. A tubulin loading control has been included

This experiment in MDA-MB-231 cells (Figure 9) recapitulated similar data to those produced by MDA-MB-436 cells with Tg again causing UPR activation (BIP, CHOP, ATF4 and IRE1 upregulation). HRD1 complex components: HERPUD1, HRD1 and Ube2j1 also showed upregulation upon the addition of Tg. Treatment with UPR inhibitors (both separately and combined) appeared to cause little change in these investigated proteins.

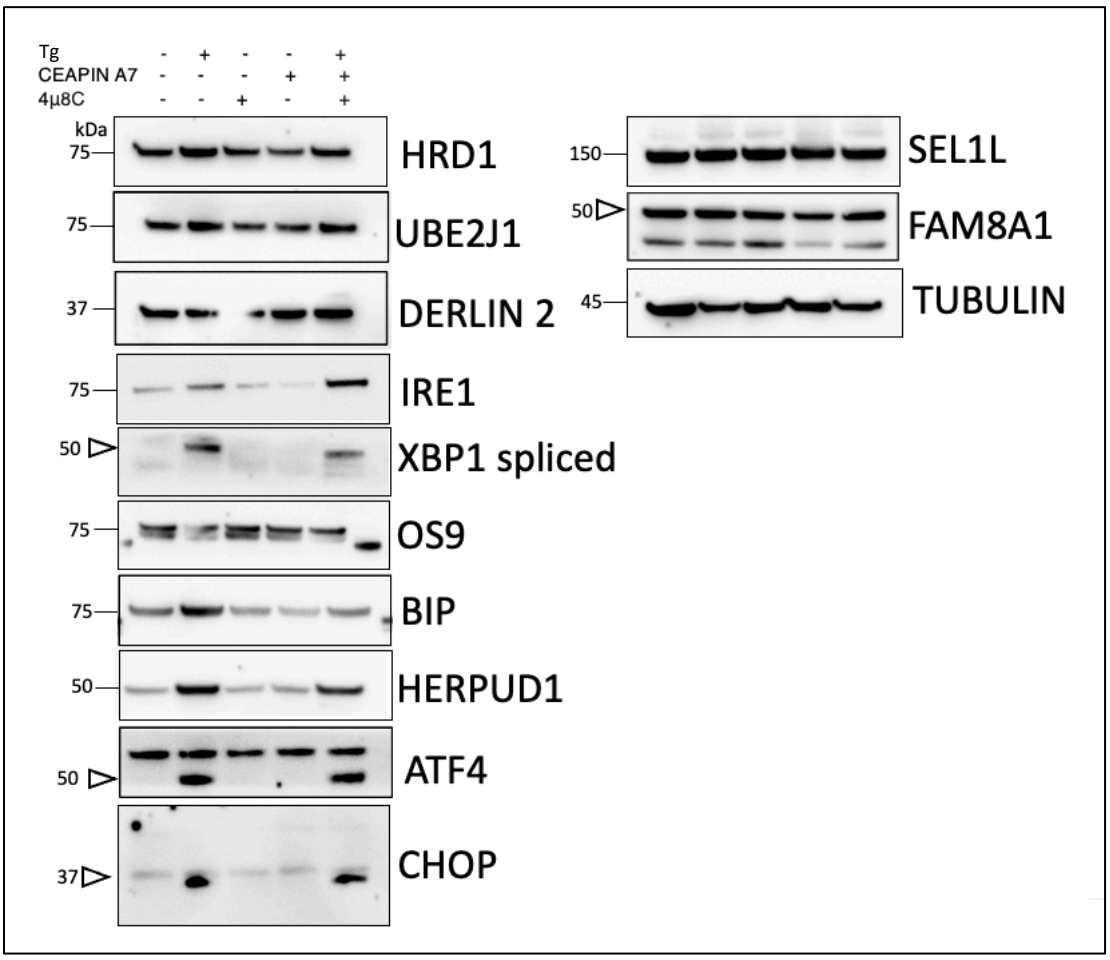


*Figure 9: a western blot performed by treating MDA-MB-231 cells with thapsigargin (Tg), Ceapin-A7 and 4*μ8c for 16 hours*. Various components of the Hrd1 complex, as well as proteins involved in the UPR, have been blotted for. A tubulin loading control has been included.*

Demonstration of Synthetic Lethality in TNBC Cells

Although the outlined UPR pathway inhibitors are not reported to be toxic to unstressed cells (Cojocari et al., 2013; Gallagher et al., 2016), inhibiting the UPR in cancers constitutively experiencing ER stress may be lethal if they rely on the UPR (and ER stress resolution) for survival. With such synthetic lethality, cells become unable to tolerate elevated stress levels and consequently may be forced into an apoptotic fate. This premise underlies the rationale for targeting the UPR as a therapeutic strategy in cancer.

To investigate this further, varying concentrations of 4μ8C and Ceapin-A7 were added to MDA-MB-436 cells and their impact on cell viability determined (Figure 10). Higher concentrations of either UPR inhibitor (>5 μM) caused statistically significant decline ($P<0.05$). At very high concentrations of the inhibitors (125 μM) almost no viable MDA-MB-436 cells remained, but as this is more than 20x the IC50 values for these compounds, this could be the result of off-target effects. I added both inhibitors to test for synergy when interfering with two distinct UPR branches (Figure 10c), but no difference in cell viability was observed, indicating that inhibition of either branch was sufficient to kill cells.

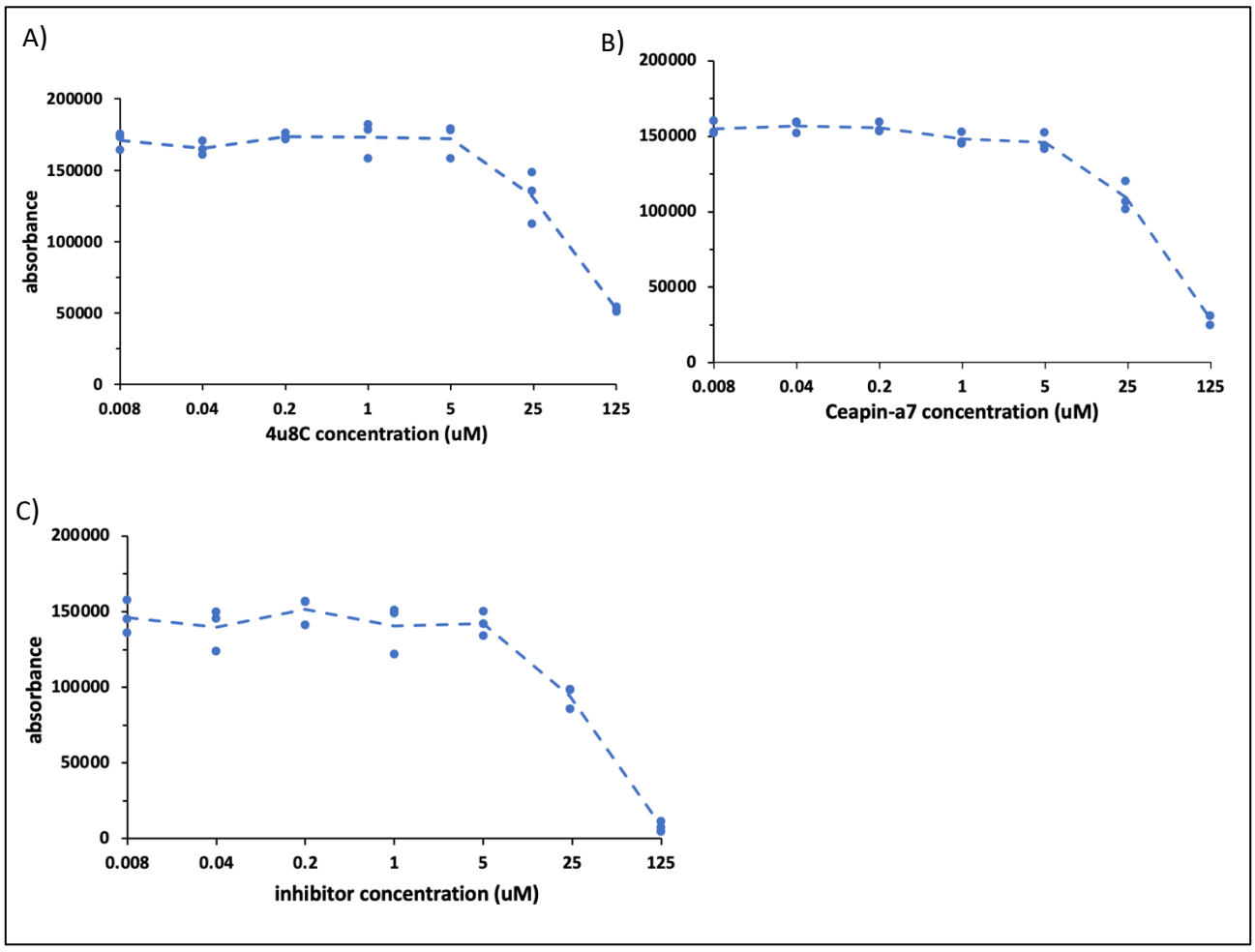


Figure 10: Alamar Blue data for the treatment of MDA-MB-436 cells with varying concentrations of both 4μ8c and Ceapin-A7, inhibitors of the UPR, for 16 hours, n=3. A) 4μ8c alone, B) Ceapin-A7 alone and C) combined 4μ8c and Ceapin-A7.

Knockdown of Hrd1 Complex Components

To determine the contributions made by individual components of the Hrd1 complex to cell survival, I stably introduced shRNAs to systematically reduce the availability of each factor. shRNAs expressed from the pGIPZ plasmid (Figure 11) were acquired from the Target Discovery Institute (Oxford). The pGIPZ vector also contains a GFP cassette and puromycin selection marker to identify and select shRNA expressing cells. The Hrd1 components I targeted were chosen based on availability within the library (Table 2).

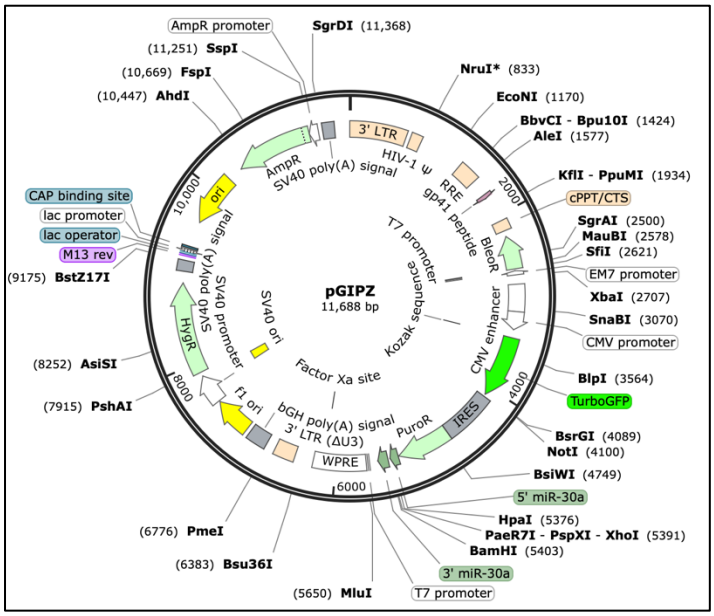


Figure 11: the PGIPZ plasmid used in the shRNAs for the production of knockdowns.

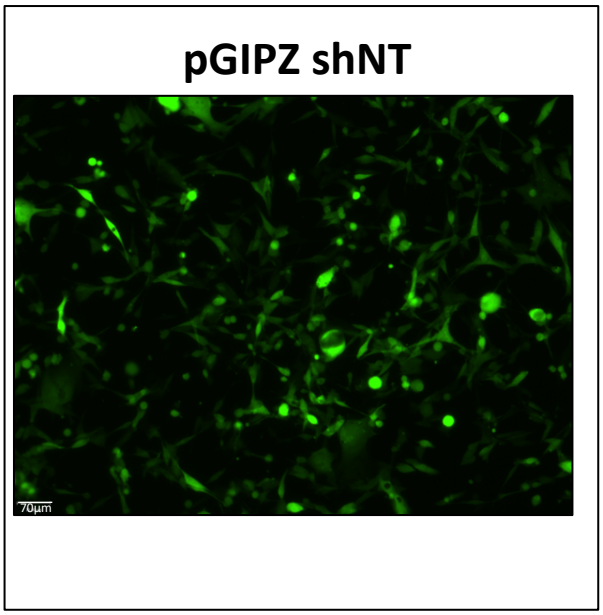


Figure 12: MDA-MB-436 cells that have been stably transduced with an shRNA lentiviral plasmid containing a non-targeting sequence. Image was taken under a blue light to show GFP expression, a scale bar has been included.

A non-targeting control was also included in experiments with the knockdowns, as transduction can have off-target effects on other cellular processes so a parental cell line would not be appropriate for these experiments (Figure 12). The non-targeting control contains a scrambled sequence expressed from the pGiPZ vector.

Validating Knockdown of Hrd1 Complex Components

Knockdown efficiency of shRNAs in TNBC cell lines was determined both at the transcript (qPCR, Table 4) and protein levels (western blot). I observed

>75% reduction in HRD1, HERPUD1, UBE2J1 and XTP3-B transcripts in both MDA-MB-436 and MDA-MB-231 cell lines and ~50% reduction for SEL1L, FAM8A1 and OS9 (Figure 13). However, corresponding reduction to protein levels was only observed for Hrd1, HERPUD1 and FAM8A1 with others (SEL1L, Ube2j1, XTP3-B and OS-9) exhibiting only very modest change (Figure 14).

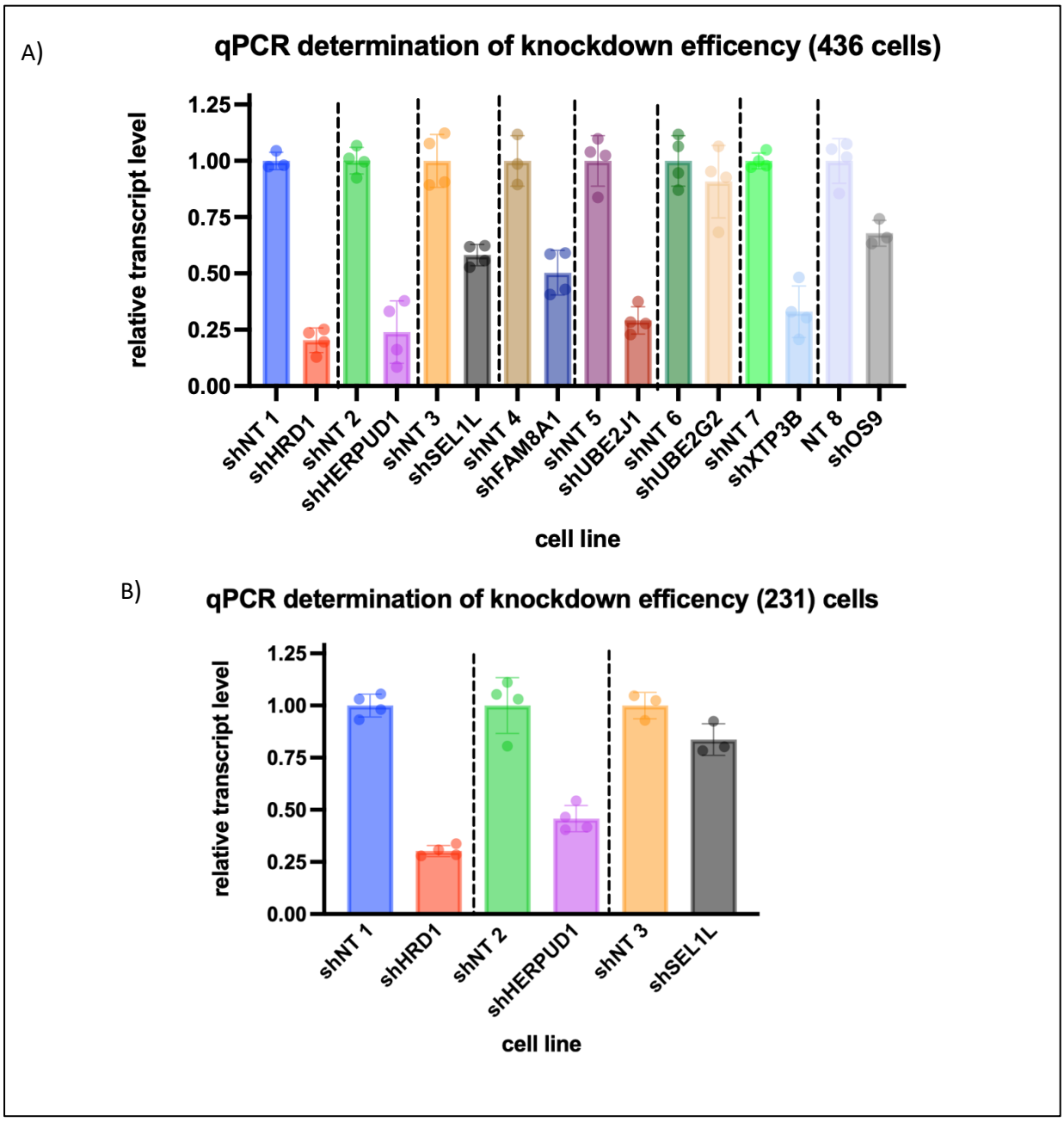


Figure 13: determining the knockdown efficiency at the transcript level of various shRNAs. The dashed lines separate the bars by targets with non-targeting cDNA ran, with the primers for each target, as a control. Each point represents a well in the qPCR plate (technical replicates) with samples collected at the same time point post selection. A) performed using MDA-MB-436 cells. B) performed using MDA-MB-231 cells.

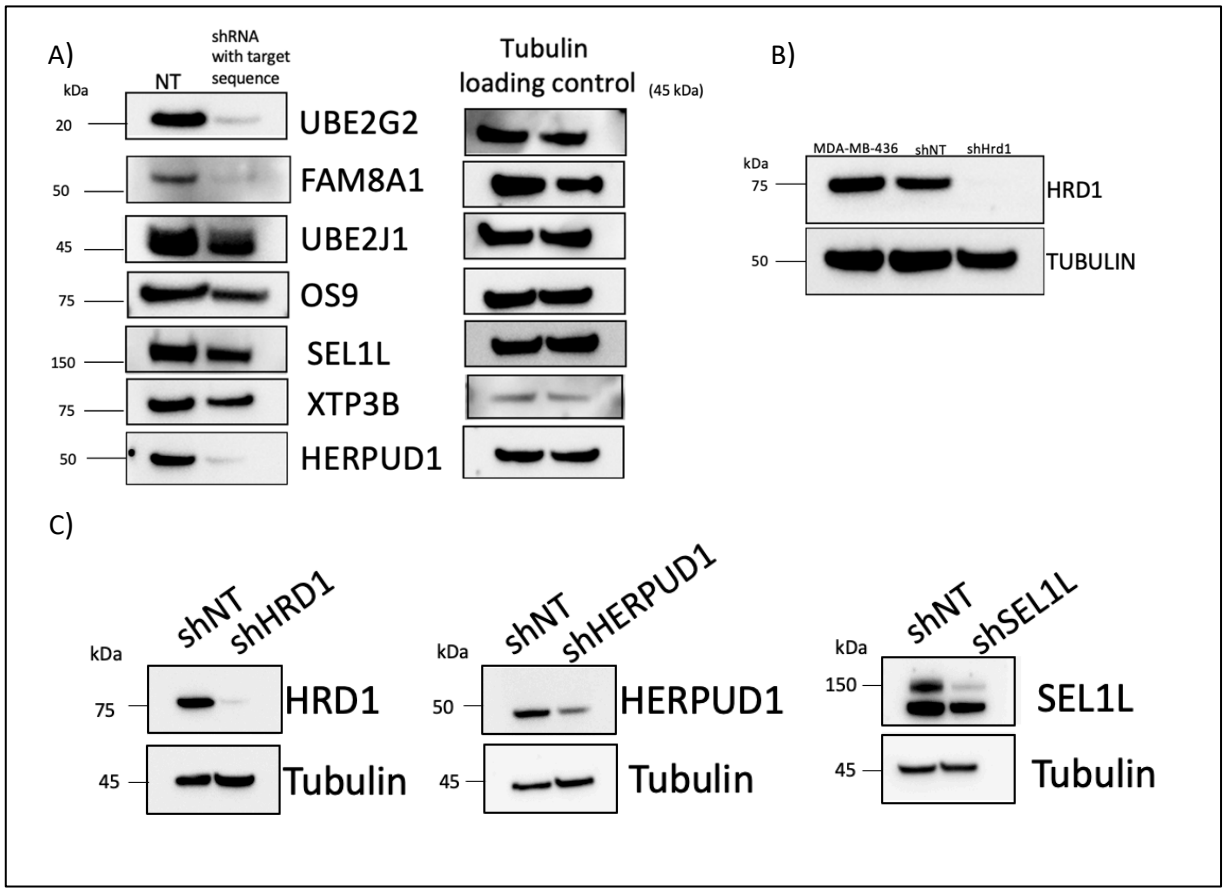


Figure 14: western blots for determining the extent of knockdown at the protein level for shRNAs in A) MDA-MB-436 cells, B) MDA-MB-436 cells and C) MDA-MB-231 cells. These lines have been selected with puromycin prior to testing.

Table 8: MDA-MB-436 shRNA knockdown summary

Target	Knockdown at transcript level? Percentage reduction included	Knockdown at protein level?
HRD1	Yes - 80%	Yes
HERPUD1	Yes	Yes
SEL1L	Yes – 42%	Slight reduction
FAM8A1	Yes – 52%	Yes
UBE2J1	Yes – 71%	Slight reduction
UBE2G2	No	Yes
XTP3B	Yes -67%	Slight reduction
OS9	Yes – 32%	Slight reduction

Table 9: MDA-MB-231 shRNA knockdown summary

Target	Knockdown at transcript level? Percentage reduction included	Knockdown at protein level?
HRD1	Yes – 70%	Yes
HERPUD1	Yes – 54%	Yes
SEL1L	No	Yes

Curiously, Ube2g2 protein level but not transcript levels were reduced. After repeating both the western blots and qPCRs, these observations held. Transcript levels can correlate poorly with protein levels (Fukao, 2015) but this mismatch may instead be down to off-target effects of the shRNA or issues with primer specificity and would require further investigation.

Due to time constraints, I chose to pursue knockdown lines that showed both a decrease at the transcript level and the protein level for increased certainty the phenotype of the loss of this component may be seen. From this it was determined that shHRD1, shFAM8A1, shSEL1L, shUBE2J1 shXTP3B and shHERPUD1 would be included in future experiments. To streamline the project to accommodate a short timeline, I focussed on shHRD1, shHERPUD1, shSEL1L and shFAM8A1. This was due to them exhibiting sufficient knockdown, their perceived importance in the Hrd1 complex, and their regulation (or lack of) by the UPR. With this in mind, MDA-MB-231 cell lines expressing shHRD1, shHERPUD1 and shSEL1L were generated.

An Inducible shRNA System

shRNAs were initially introduced with constitutive expression and selection however, over time this cell population could become dominated by cells that have adapted to the knockdown and therefore do not exhibit a phenotype that might be expected from knocking down the chosen component (Figure 15).

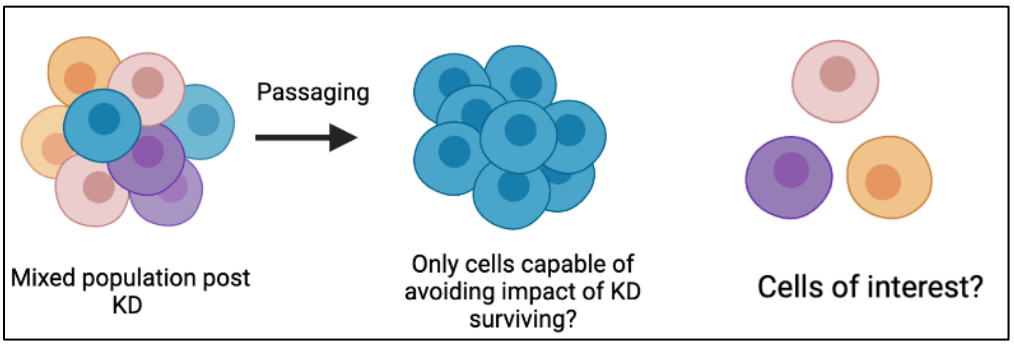


Figure 15: a diagram representing the rational for the move to a doxycycline inducible system. In theory, Cells displaying the phenotype of interest after transduction with the shRNA are lost over time with only cells capable of circumventing the consequences of the knockdown capable of survival. (Created with Biorender.com)

To test viability of shRNA-containing cells post-transduction preselection, I used the Celigo imager (Figure 16). Propidium iodide (PI) stain is a red fluorescent dye that is not permeable to live cells but can enter dead cells allowing for the detection of apoptotic and necrotic cells. As transduced cells express GFP, cells that were simultaneously both green and red could be detected using this system. Very few cells (one or two per well- circled in blue, Figure 16e) appeared to contain both GFP and PI. A low proportion of double positive cells being detected led to the conclusion that it is unlikely a large population of cells are dying due to expression of the shRNAs. Therefore, these cell lines could still provide valuable insight as to what happens in TNBC cells when these components are depleted and could be included in further experiments.

However possible low levels of GFP expression caused by transduction occurring only recently as well as possible GFP leakage from dead cells could have affected the findings of this experiment. To supplement this data, this effect on viability shortly following transduction was also looked at by performing an Alamar Blue assay 5 days post-transduction (Figure 17). There was little variation in cell number across the cell lines with the exception of shFAM8A1, which appeared to show ~85% increase in viability compared to the non-targeting control, which could not be easily explained.

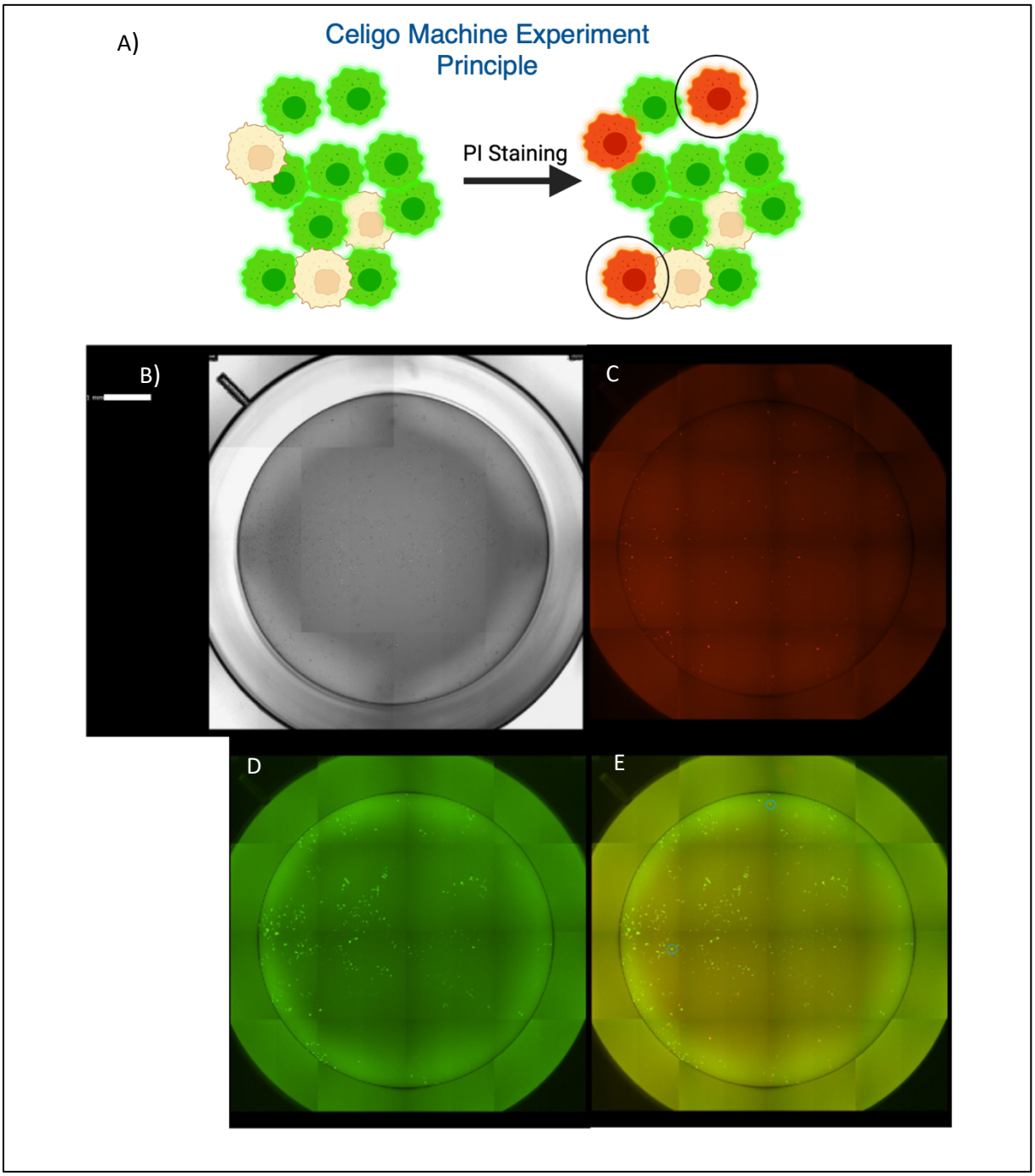


Figure 16: An experiment performed using a Celigo imager to investigate the effect of shRNA expression on cell viability. A) outlines the principle behind this experiment with GFP expressing cells depicted in green and Propidium Iodide (PI) stained cells shown in red. This allows the detection of cells that are both GFP expressing and PI positive dual expressing cells) and therefore have died after, and possibly as a consequence of, expression of the shRNA. MDA-MB-436 cells post transduction with lentiviral shHRD1 were plated at 500 cells per well pre-selection. 5 days after transduction these plates were then imaged B) brightfield channel = all cells, C) PI positive cells, D) GFP positive cells, E) an overlay of images C & D in order to detect double positive cells (PI stained GFP expressing cells). These double positive cells have been circled on this image; no numerical analysis was performed on this data due to the extremely limited number of cells falling into this category. Plates transduced with a non-targeting shRNA were ran as a control.

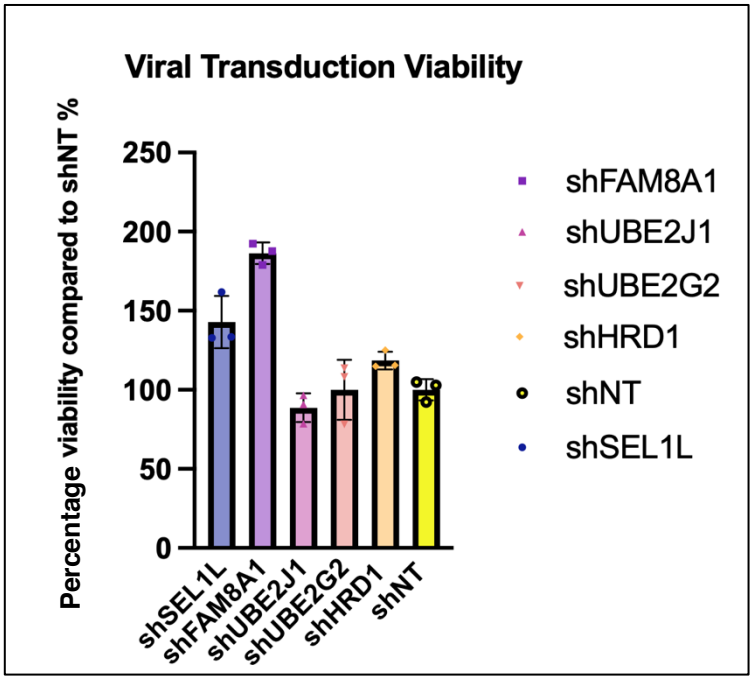


Figure 17: determining the viability of various shRNA transduced MDA-MB-436 cell lines 5 days post-transduction, pre-selection, compared with the number of living shNT cells. This was done by performing an Alamar Blue assay with 3 technical replicates performed for each line.

Due to unpredictable effects of long-term shRNA expression on cell growth/ we chose to supplement this study with a doxycycline (DOX) inducible expression system for shRNAs that would allow for transduced cells to grow without expressing the shRNA until required for assays (Figure 18).

The SMART vector (Horizon) contains a TET repressor that expresses the shRNA and GFP only upon the addition of DOX (Figure 18A). Successful expression of shRNA can be visualised by microscopy (detectable ~10 hours after DOX addition). A dose-response test for DOX was also done by western blot to determine the lowest concentration able to cause adequate Hrd1 depletion (100 ng/ml, Figure 18B). Once knockdowns were validated by a preliminarily western blot and qPCR, additional durations of DOX treatment were trialled to monitor both Hrd1 protein levels and transcription.

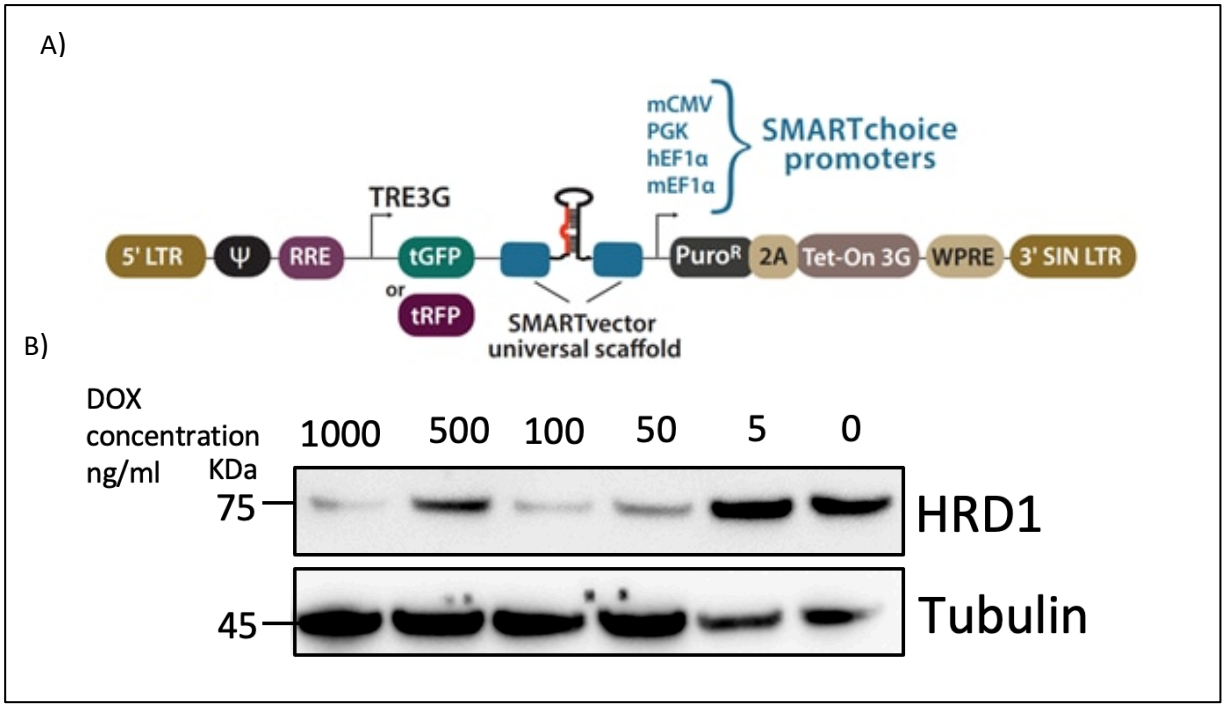


Figure 18: using a doxycycline inducible system to produce shRNA knockdowns. A) the SMART™ construct used in this system (Horizon). B) a dose-response test for doxycycline 64 hours after addition to MDA-MB-436 cells to determine a suitable concentration of Doxycycline to cause sufficient knockdown of Hrd1. A tubulin loading control has been included.

Once the success of the knockdown was determined via a preliminarily western blot and qPCR, additional time points were tested to see how the availability of Hrd1 reduces at the protein level overtime and how transcription of Hrd1 is affected by the addition of DOX to this system at various time points. This was first done producing a qPCR, using the chosen concentration of DOX, at various time points (Figure 19). This determined that 8 hours of DOX treatment in MDA-MB-436 cells was sufficient for a ~75% reduction in Hrd1, but this took up to 24 hours in MDA-MB-231 cells.

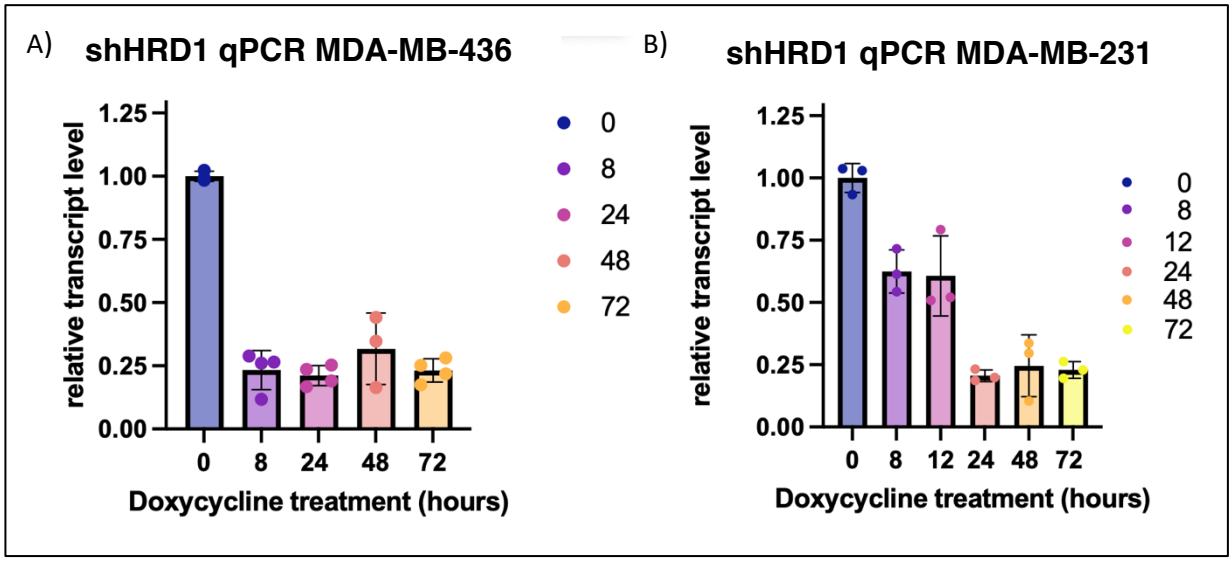


Figure 19: qPCR data for assessing transcript knockdown over time for: A) doxycycline inducible shHRD1 MDA-MB-436 cells, B) doxycycline inducible shHRD1 MDA-MB-231 cells. 100 ng/ml of doxycycline was given. Each point represents a technical replicate.

Visualising Dox-Induced Depletion of Hrd1

After determining DOX and the shHRD1 inducible system was sufficient to deplete Hrd1, to ensure that the doxycycline was having no off-target effects, a western blot was a performed to validate the effects of DOX on shHRD1 MDA-MB-436 cells as well as on an MDA-MB-436 inducible non targeting control that also expresses GFP (Figure 20). Cells expressing shHRD1 treated with DOX exhibited significant reduction in Hrd1 levels while DOX treating those with the non-targeting sequence (shNT) showed no effect. Moreover, DOX alone does not activate the UPR (assessed by BiP levels), nor does it alter Hrd1 levels unless shHRD1 is present.

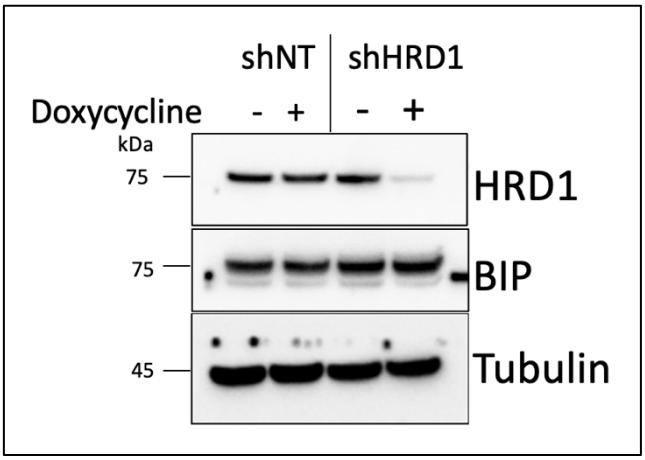


Figure 20: a western blot performed for dox inducible shHRD1 in MDA-MB-436 cells with its non-targeting counterpart included. Cells were treated with 100 ng/ml doxycycline for 64 hours before harvesting. A Tubulin loading control has been included.

After verifying that DOX addition reduces Hrd1 levels, the impact on its cofactors, on ERAD, and on the UPR could be monitored. With temporal control over Hrd1 reduction, any effects can be monitored in 'real time' as levels diminish. Cell lysates at various time intervals after DOX addition were harvested and the resulting western blots show selected UPR proteins increasing in abundance, suggesting that these cells lose the capability of resolving proteotoxic stress in the absence of Hrd1 (Figure 21).

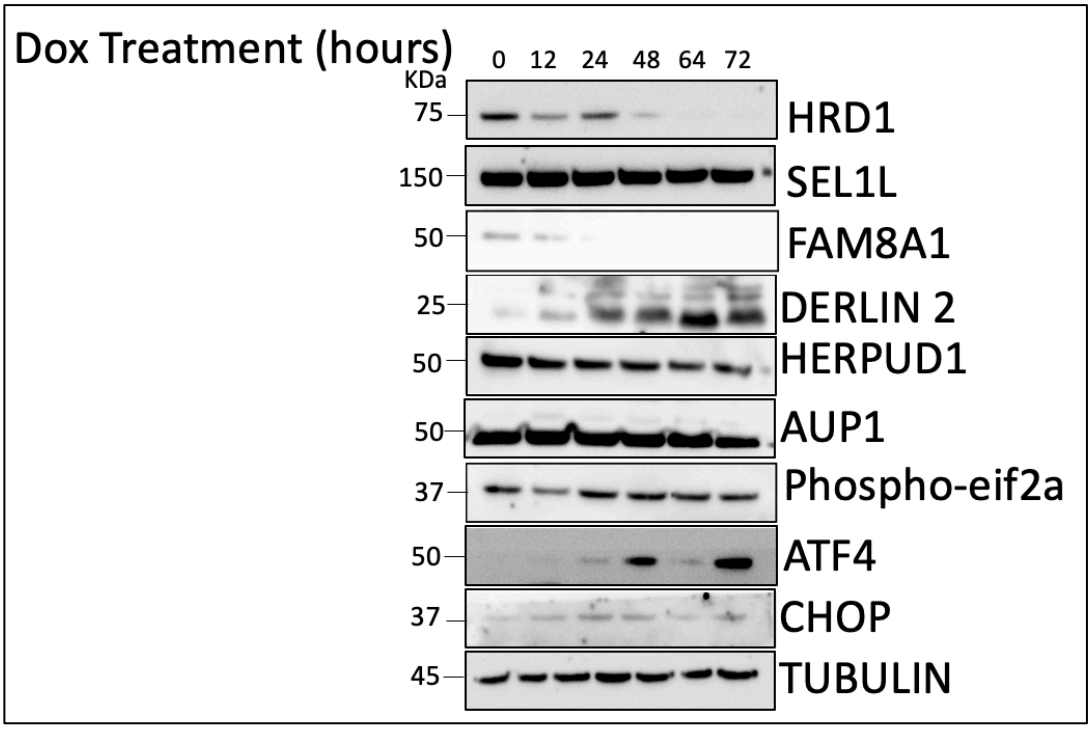


Figure 21: Doxycycline treatment time point assay (up to 72 hours) using shHRD1 MDA-MB-436 (doxycycline inducible). Various components of the Hrd1 complex, as well as proteins involved in the UPR, have been blotted for. 100 ng/ml of doxycycline was added, a tubulin loading control has also been included.

These data are consistent with the current model where Hrd1 provides a scaffold for the other proteins of the complex, with other components being destabilised as a consequence on reduced Hrd1 availability. I repeated this experiment with slightly different time points (Figures 22 and 23) including a longer time course since little change was observed at shorter time points.

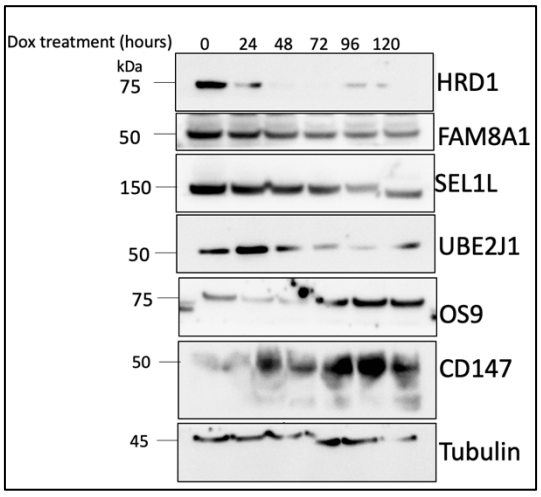


Figure 22: Doxycycline treatment time point western blot (up to 120 hours) using shHRD1 MDA-MB-436 (doxycycline inducible). The hours represent the time after a 100 ng/ml dose of doxycycline was given. Various components of the Hrd1 complex, as well as proteins involved in the UPR, have been blotted for. The distorted tubulin is due to stripping and reblotting of the membrane.

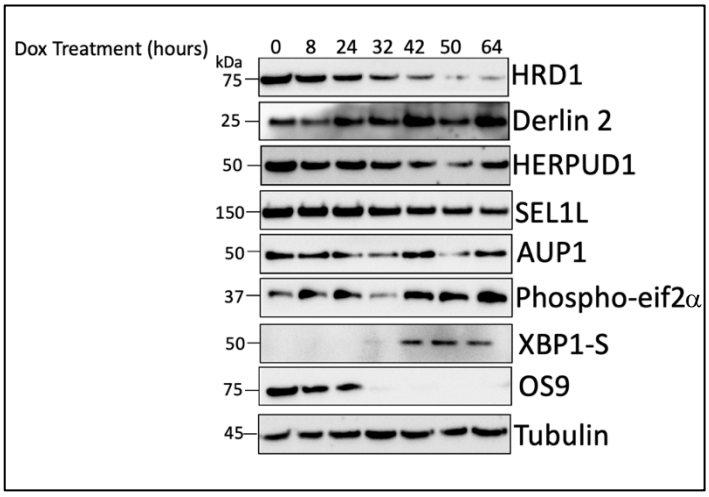


Figure 23: Doxycycline treatment time point western blot (up to 64 hours) using shHRD1 MDA-MB-436 (doxycycline inducible). The hours represent the time after a 100 ng/ml dose of doxycycline was given. Various components of the Hrd1 complex, as well as proteins involved in the UPR, have been blotted for. Tubulin has been included as a loading control.

To investigate the effect of induced Hrd1 loss on ERAD, I monitored the abundance of an endogenous Hrd1 substrate, CD147. The majority of CD147 assembles and is deployed to the cell surface, while unassembled forms are engaged with SEL1L and are targeted to ERAD (Tyler et al., 2012). Importantly, immature CD147 can be observed to accumulate upon loss of Hrd1 (Figure 22). Additionally, OS-9 is also a substrate of Hrd1, but this relationship is more complex since OS-9 is also a functional component of the Hrd1 complex. Cellular OS-9 levels are initially depleted as Hrd1 levels drop (not detected between hours 24-64, Figure 22). After this time OS-9, like CD147, appears to accumulate (hours 72- 120, Figure 22). As OS-9 is upregulated by the UPR, this could offer an alternative explanation for this late-stage accumulation.

In terms of proof of upregulation of the UPR: phospho-eIF2α, ATF4 and $XBP1_s$ were all upregulated upon the loss of Hrd1 with XBP1 splicing first detected at 32 hours and increased significantly by 42 hours.

AUP1 expression remain largely unchanged although slight effects can be noted (32 and 52 hours) but SEL1L appears to decrease from 32 hours onwards, consistent with its requirement for co-assembly with Hrd1 for stability (Sun et al., 2014). Interestingly, levels of Derlin-2 appear to increase with Derlin-2 thought to be stress regulated but to a lesser extent than Derlin-3 as previously mentioned. Unfortunately, antibody reagents able to probe for Derlin-3 are not currently available.

To evaluate robustness of these observations, Hrd1 was inducibly depleted from MDA-MB-231 cells using a similar strategy (Figure 24). Overall, these cells exhibited the same general trend of UPR activation upon Hrd1 depletion as well as the concurrent reduction of various other Hrd1 components with some appearing to remain unaffected. SEL1L decreases consistently throughout the time course while the E2s, Ube2g2 and Ube2j1, are both lost to a level hardly detectable by 96 hours. Only 96 hours after DOX application and maximum loss of Hrd1 does BIP appear to accumulate.

Unlike MDA-MB-436 cells, OS-9 levels appear steady throughout the time course MDA-MB-231 cells. Moreover, spliced XBP1 appears in untransduced MDA-MB-231 cells (0 hour). Derlin-2 does not accumulate concomitantly with the depletion of Hrd1 in MDA-MB-231 cells and instead is lost by 72 hours.

In summary, depleting Hrd1 using the DOX inducible shRNA system produced similar outcomes in both of the trialled TNBC lines in terms of levels of various proteins. As a general trend proteins involved in the UPR appeared to show upregulation as ERAD function was impaired through the

loss of Hrd1 whilst Hrd1 components themselves depleted as the complex destabilised.

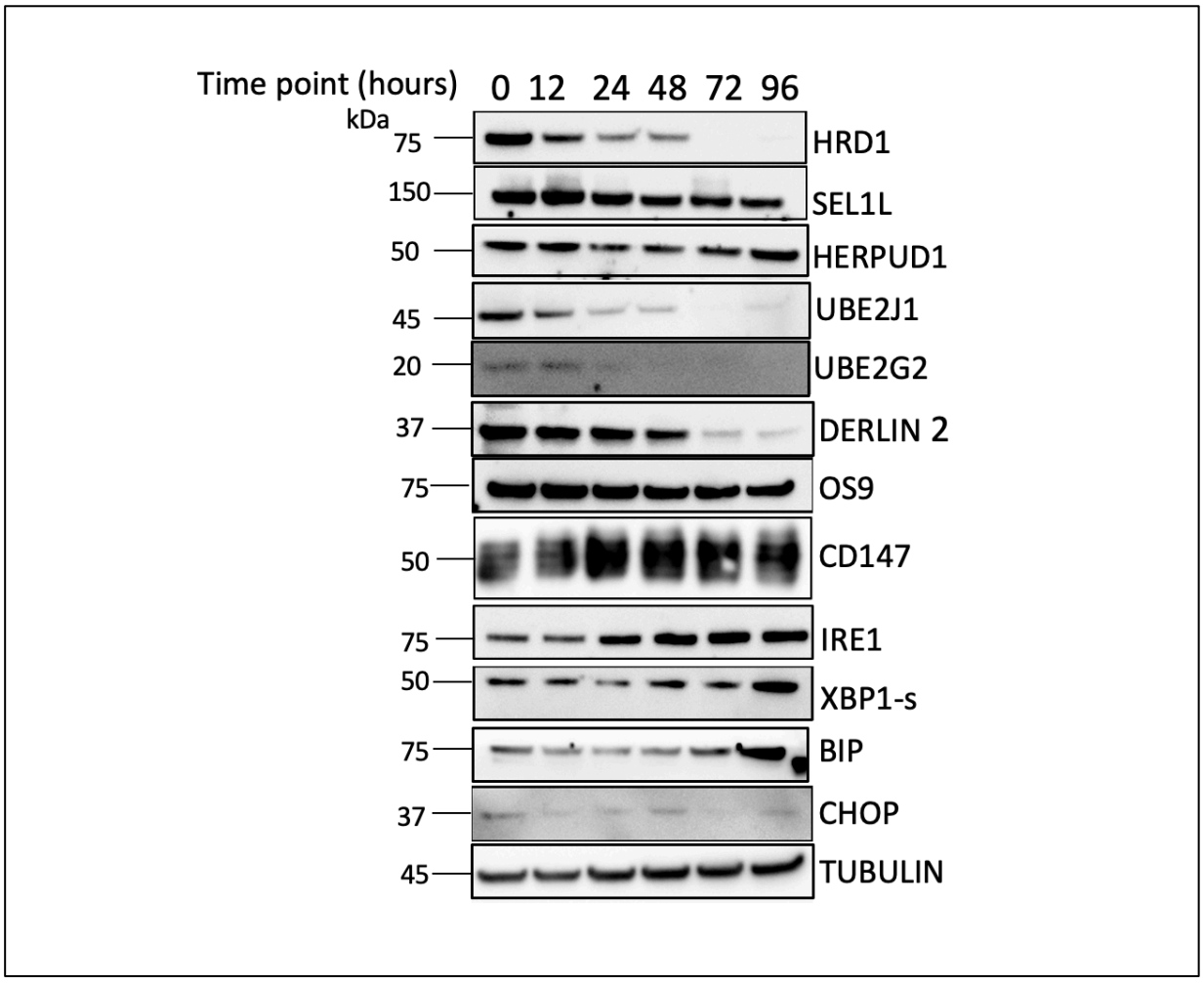


Figure 24: a western blot performed for doxycycline inducible shHRD1 in MDA-MB-231 cells showing the depletion of HRD1 overtime (up to 96 hours). The hours represent the time after a 100 ng/ml dose of doxycycline was given. Various components of the Hrd1 complex, as well as proteins involved in the UPR, have been blotted for. A tubulin loading control has also been included.

Inducible Depletion of HERPUD1

To build on findings from loss of Hrd1, I generated cells with DOX-inducible knockdown of HERPUD1. As above, DOX was given for different durations and the impact of HERPUD1 loss on other proteins determined by western blot (Figure 25).

Similar to Hrd1, depletion of HERPUD1 resulted in loss of various Hrd1 complex components it coassembles with, as well as upregulating those

involved in the UPR. One notable difference is that HERPUD1 is more rapidly turned over than Hrd1 as it is undetectable by western blot much earlier than Hrd1 was (24 hours vs 72 hours in MDA-MB-231 cells, Figures 24 and 25). qPCR also revealed an over 50% reduction in HERPUD1 levels by 8 hours whereas this took up to 24 hours to achieve for Hrd1 in the same MDA-MB-231 cell line (Figure 26 and Figure 19B).

Despite rapid depletion of HERPUD1- the corresponding depletion of Hrd1 was only seen at 96 hours, indicating that Hrd1 stability is not entirely dependent on HERPUD1. Derlin-2 on the other hand, was lost on a timescale that corresponded to HERPUD1, suggesting some co-dependency for stability.

UPR activation was however, observed to begin earlier, with increased IRE1 at 24 hours and sustained until 96 hours. An alternative hypothesis for this marked increase in IRE1 is that IRE1 stability is HERPUD1 dependent, as has been previously implicated with SEL1L (Sun et al., 2015). Additionally, As with the doxycycline inducible shHRD1 in MDA-MB-231 cells, $XBP1_s$ is detectable before the addition of any doxycycline but with detected levels highest at 96 hours. CHOP exhibits little change in abundance across the time course but this could be attributable to the quality of the detecting antibody. To look at ERAD, I blotted for CD147 to see if reducing HERPUD1 levels disrupted substrate processing. CD147 levels were reduced at 24 hours and beyond, which correlated with loss of HERPUD1 but notably not Hrd1 (Figure 25).

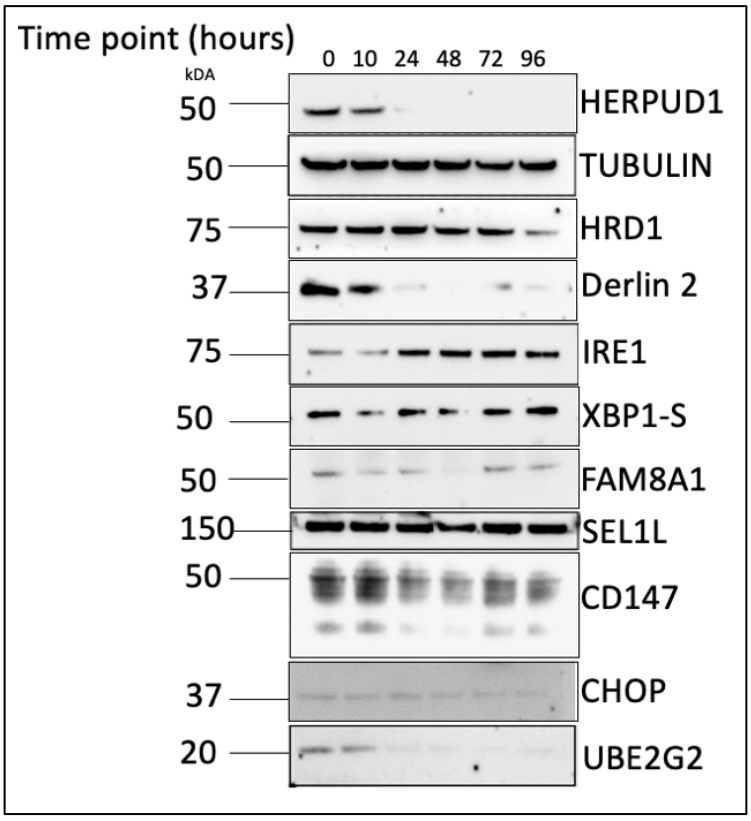


Figure 25: a western blot performed for doxycycline inducible shHERPUD1 in MDA-MB-231 cells showing the depletion of HERPUD1 overtime (up to 96 hours). Various components of the Hrd1 complex, as well as proteins involved in the UPR, have been blotted for. A Tubulin loading control has been included.

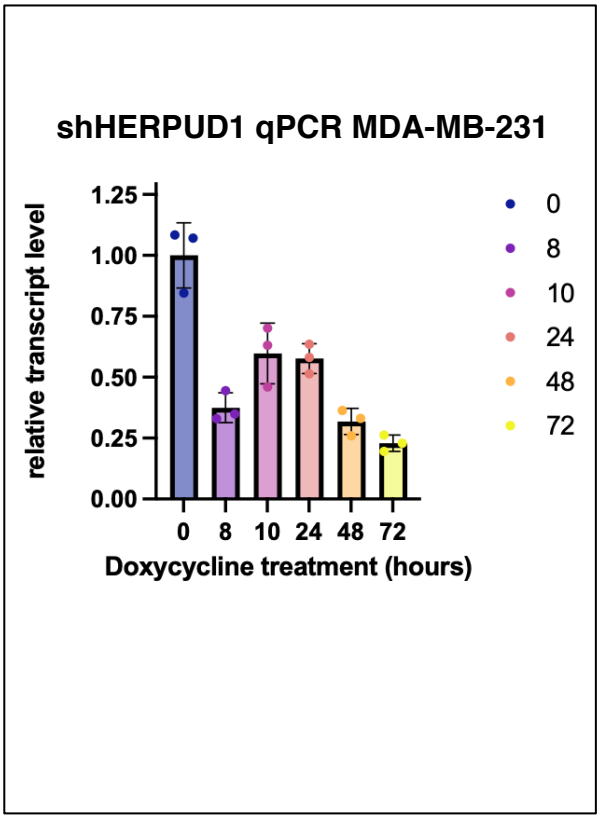


Figure 26: qPCR data for assessing transcript knockdown over time for: doxycycline inducible shHERPUD1 MDA-MB-231 cells. 100 nm Each point is representative of a technical replicate.

Generation of Hrd1 Knockout cells:

I sought to create knockout MDA-MB-436 cell lines for Hrd1 and HERPUD1 to determine whether phenotypes would only be revealed upon complete loss of these two proteins. I first performed a pilot experiment to optimise transfection of this cell line with. GFP plasmid. However, after transfection with miniprepped DNA for plasmids containing my chosen target sequences, no viable cells remained post-selection. This could suggest that these cells are reliant on these components for survival and therefore their complete removal results in lethality.

Splicing Assay for Hrd1 Depleted Cells

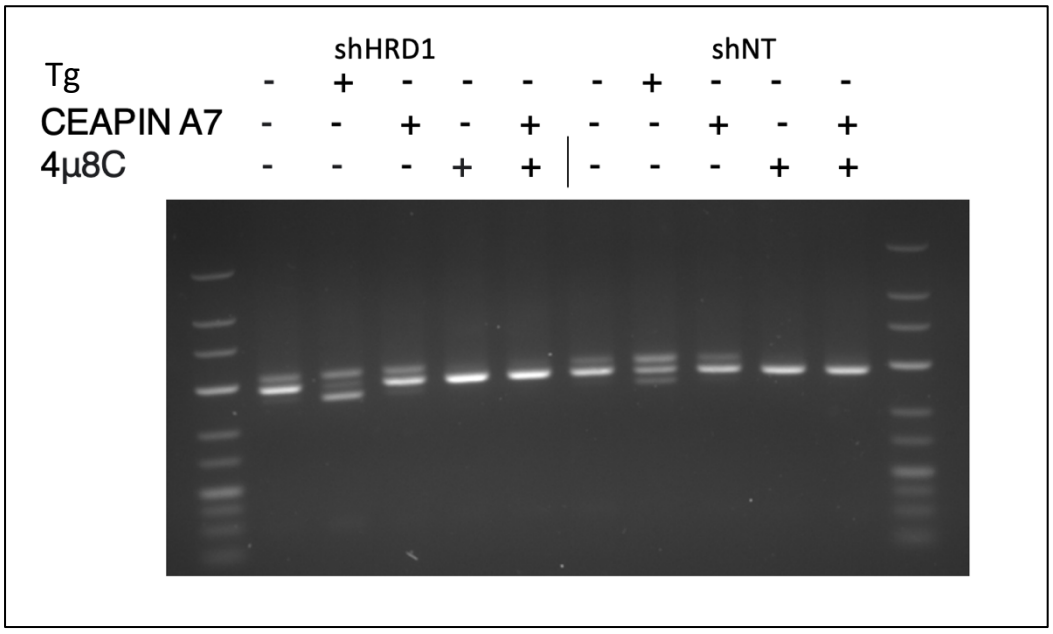


Figure 27: an XBP1 splicing assay for HRD1 depleted MDA-MB-436 cells treated with thapsigargin as well as Ceapin-A7 and 4μ8c, compared to a non-targeting control. This assay has three technical replicates.

To determine if Hrd1 depletion affected ER stress levels or impacted response to compound treatments, I monitored XBP1 splicing in depleted cells under a variety of conditions (Figure 27). The only difference seen between these cells is a more intense spliced XBP1 band relative to the unspliced band in shHRD1 cells treated with Tg compared to the shNT cells. This suggests that Tg causes greater upregulation of ER stress when Hrd1 is depleted.

Reducing Hrd1 Abundance Disrupts Cell Viability and Reduces Tolerance to Stress When Grown in 2D

MDA-MB-436 cells displayed reduced cell viability under Hrd1 insufficiency. Cells were grown as a monolayer (2D) in tissue culture plates and assayed by Alamar Blue assay. In this assay, a blue dye (resazurin) is reduced by living cells to give a pink colour, allowing for absorbance to be used as a readout for cell viability. This assay was done by using various concentrations of the ER stress inducer Tg (Figure 28A). Enhanced loss of cell viability at each Tg concentration was seen in the shHRD1 cells when

compared to shNT cells. This suggest that Hrd1-depleted cells were less tolerable of additional synthetic stress.

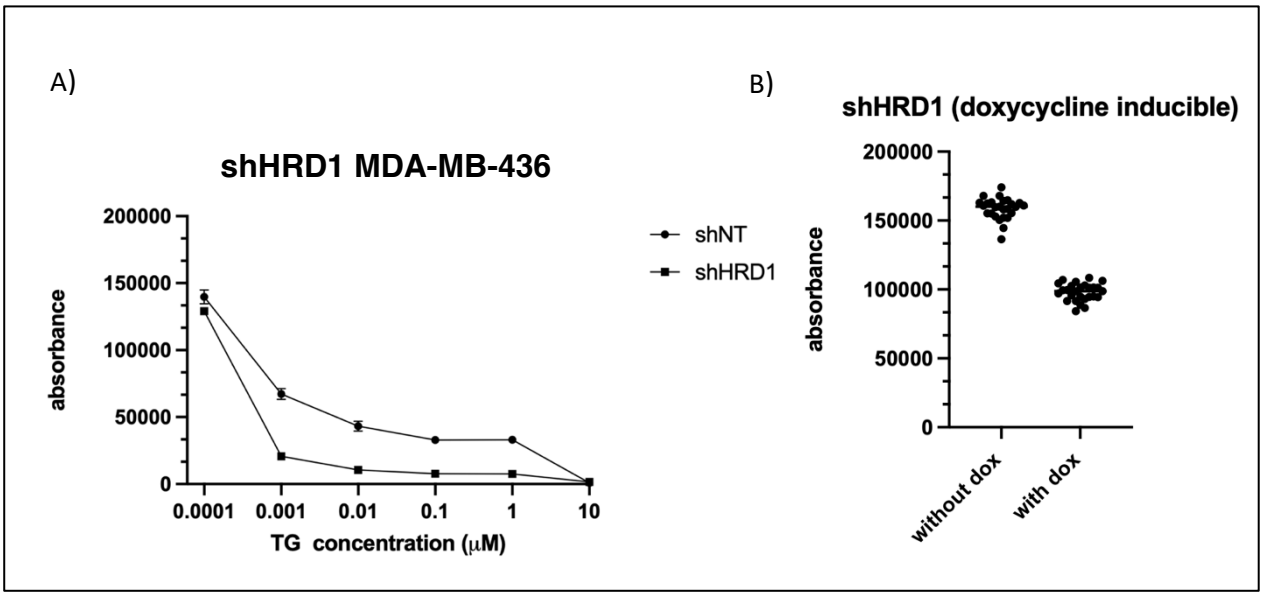


Figure 28: Alamar Blue data for HRD1 depleted MDA-MB-436 cells A) with increasing concentrations of thapsigargin treatment with three technical replicates per concentration. B) with and without doxycycline treatment using the inducible system with doxycycline addition, triggering the expression of the shRNA. This was done using a 100 ng/ml dose of doxycycline. Each point is representative of a well in a 96 well plate. Both experiments were repeated at least 3 times with the same outcome/trend being shown.

While performing these experiments, I observed that there were consistently fewer shHRD1 than shNT cells at the end of the assay, even though they were untreated. This observation prompted me to plate multiple untreated plates to compile data on how shHRD1 cells grew over 5 days without any drug treatment, relative to shNT cells (Figure 28B). shHRD1 cells consistently displayed diminished viability when compared to cells with undisrupted levels of Hrd1. This demonstrates that these cells show reduced viability, even without any additional synthetic stress and indicate a role for Hrd1 in viability of MDA-MB-436 cells.

This viability assay was also used with the other knockdown cell lines to determine the effect of losing other Hrd1 components on Tg induced cell death (Figure 29). Using the Alamar Blue assay, I observed that depleting Ube2g2 also attenuated tolerance to Tg of MDA-MB-436 cells compared with the shNT cell line (Figure 29C). Like with Hrd1 depletion, cells with SEL1L insufficiency consistently seemed to display reduced viability (Figure 29A), compared to the shNT cells even without any additional synthetic stress (0.0001 μm (= untreated to allow plotting on a logarithmic scale), Figure 29A). However, the additional untreated Alamar Blue assays were not performed with this cell line due to time limitations.

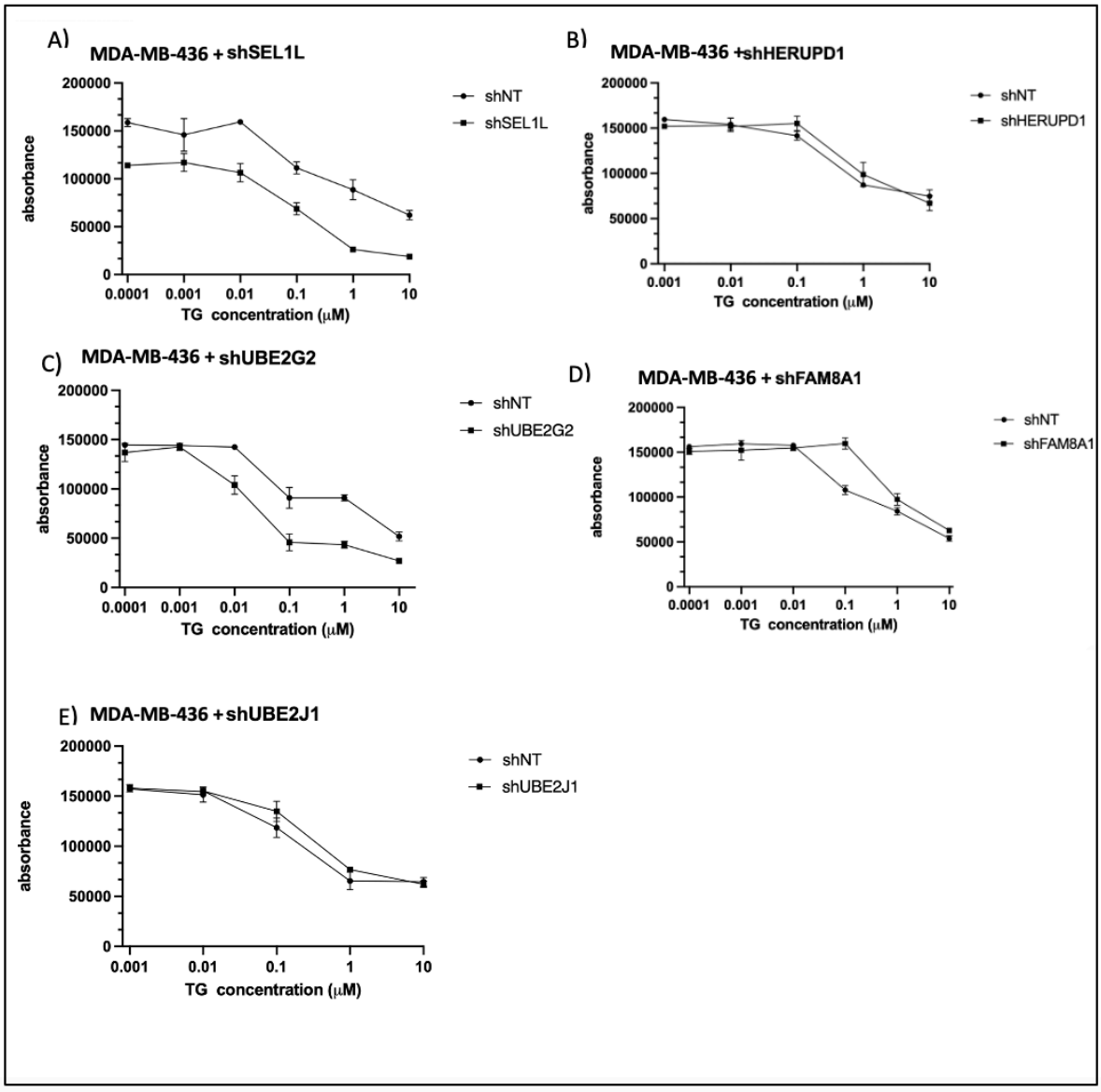


Figure 29: Alamar Blue data for application of various thapsigargin concentrations to knockdown cell lines using MDA-MB-436 cells; A) SEL1L B) HERPUD1, C) Ube2g2, D) FAM8A1 and E) Ube2j1. Each treatment group contains 3 replicates, and all experiments were repeated at least 3 times with the same outcome/trend being shown.

Interestingly, depleting FAM8A1 had the opposite effect, actually appearing to increase Tg tolerance and hence viability, at least at this time point in a 2D context (Figure 29D). Reducing levels of either HERPUD1 or Ube2j1 did not appear to effect viability compared to the non-targeting control at all trialled concentrations of Tg (Figure 29B and E).

These experiments were then repeated in MDA-MB-231 cell lines (Figure 30). In this line, depleting Hrd1 produced the same effect as in MDA-MB-436 cells with a corresponding decrease in viability seen as a result of Tg treatment as well as without (0.0001 μM (= untreated), Figure 30A). Here, SEL1L depletion did not produce a corresponding decrease in cell viability and were comparable to the shNT non-targeting control. This may be due to differences between cell lines in terms of SEL1L dependence or more likely due to the differing levels of knockdowns achieved (Figures 15 and 16).

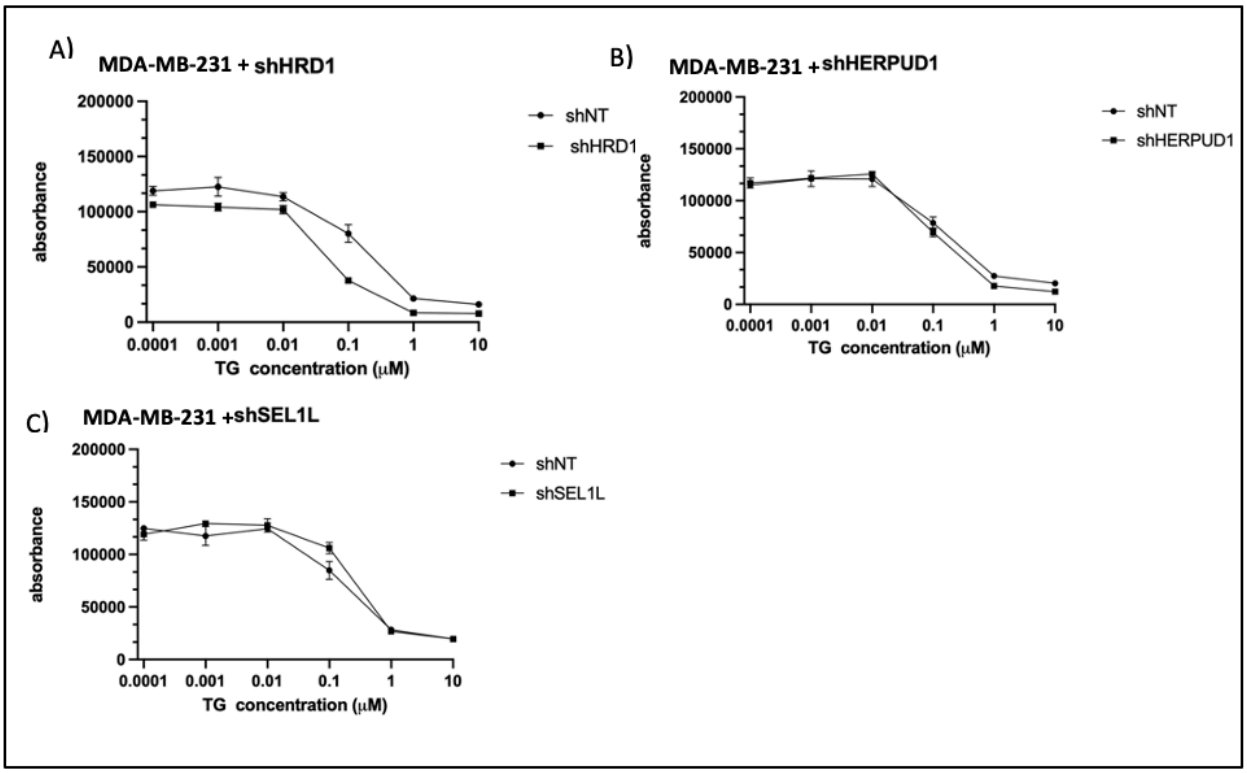


Figure 30: Alamar Blue data for increasing concentrations of thapsigargin applied to knockdown cell lines using MDA-MB-231 cells; A) shHRD1 B) shHERPUD1 and C) shSEL1L. Each treatment group contains 3 replicates, additionally, all experiments were repeated at least 3 times with the same outcome/trend being shown.

Reducing cellular levels of either HERPUD1 or Ube2j1 with shRNA knockdowns did not appear to effect viability in MDA-MB-436 cells. This suggests these components are not essential for cell survival in this line. Alternatively, a stronger knockdown with a greater reduction in cellular levels or a compl nockout may expose a phenotype. Some mitigation by homologs (e.g., HERPUD2) might also be a contributing factor.

Further Assessing Viability of Hrd1 depleted cells in 2D cultures

MDA-MB-231 cells depleted of Hrd1 (shHRD1) and its non-targeting counterpart (shNT) were seeded for crystal violet assays using an optimal initial seeding density chosen to be 6,000 cells/well (Figure 3A-C). Cell line viability was compared using crystal violet staining after treatment with varying concentrations of Tg. Fewer cells remain in shHRD1 than in shNT wells treated with the same Tg concentration, indicating that without Hrd1, MDA-MB-231 cells were sensitised to synthetic stress produced by Tg Figure D & E). However, shHRD1 also showed reduced viability without any additional stressor treatment when plated at high and medium cell densities but with similar viability seen between shHRD1 and shNT with a low initial seeding density. At this low seeding density, the increased reduction in viability of shHRD1 cells relative to shNT treated with Tg is seen.

Crystal violet assays were also attempted for MDA-MB-436 cells but each time colonies lifted and failed to remain attached to the tissue culture treated plated after the fixation step meaning no useable numerical data was collected.

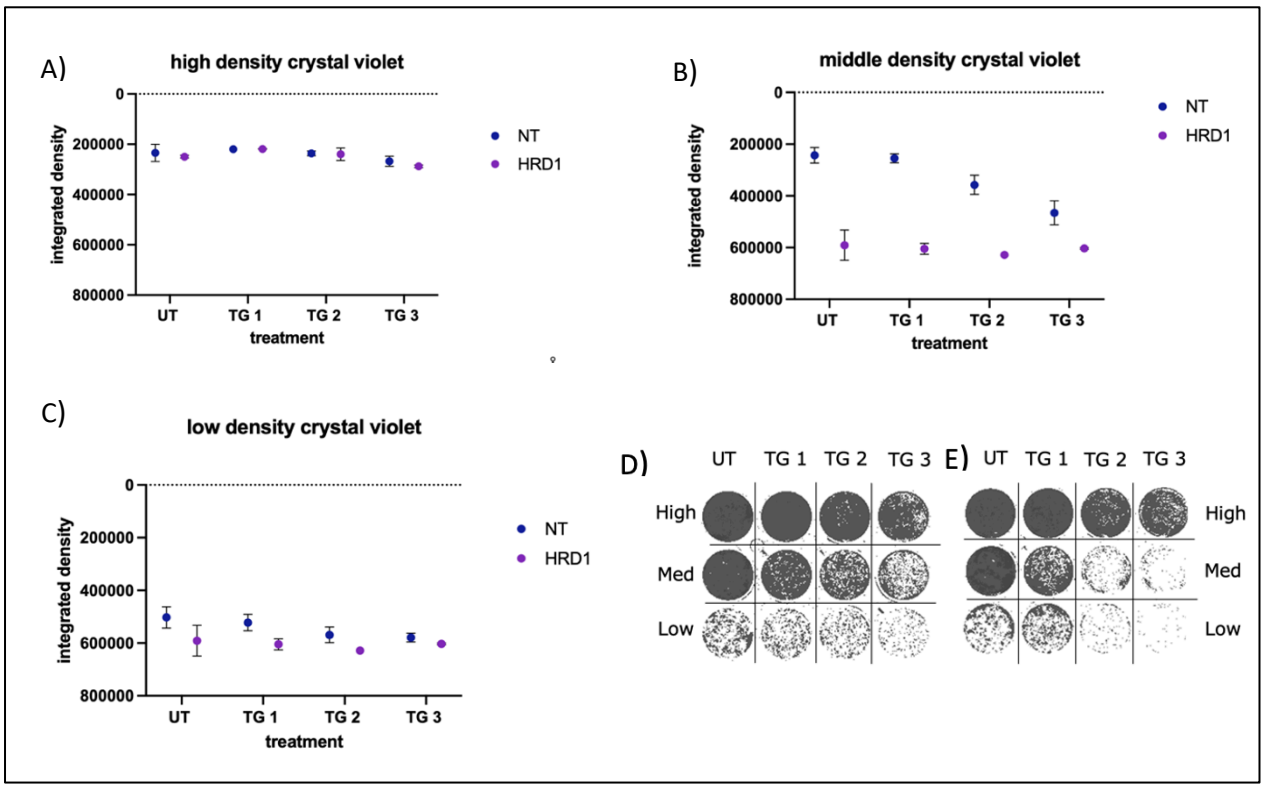


Figure 31: crystal violet viability data for MDA-MB-231 cells showing depleted Hrd1 levels. Integrated density values are shown for wells seeded with the lowest (A- 1,200 cells), middle (B – 6,000 cells) and highest (C- 30,000) initial seeding densities. Varying levels of thapsigargin were used: TG 1= 10 nM, TG 2 =100 nM, TG 3 = 1 μM. A scan of a plate for each of the cell lines, NT (D) and shHRD1 (E) has been included.

Using Spheroids as a 3D Growth Assay

Spheroids (sometimes referred to as tumorspheres) are 3D cell aggregates. While called spheroids, these structures are more ellipsoid (disc-like) in shape making area a more representative measure than volume when analysing images (Figure 32). Spheroid production aims to create conditions *in vitro* more similar to their *in vivo* counterparts. These 3D structures aim to model solid tumour cancers by creating a necrotic hypoxic core to recapitulate the hypoxic nutrient-depleted environment in which they ae found within the human body (Figure 32B). These conditions in turn could therefore exaggerate the ER stress these cells experience and cause further UPR activation.

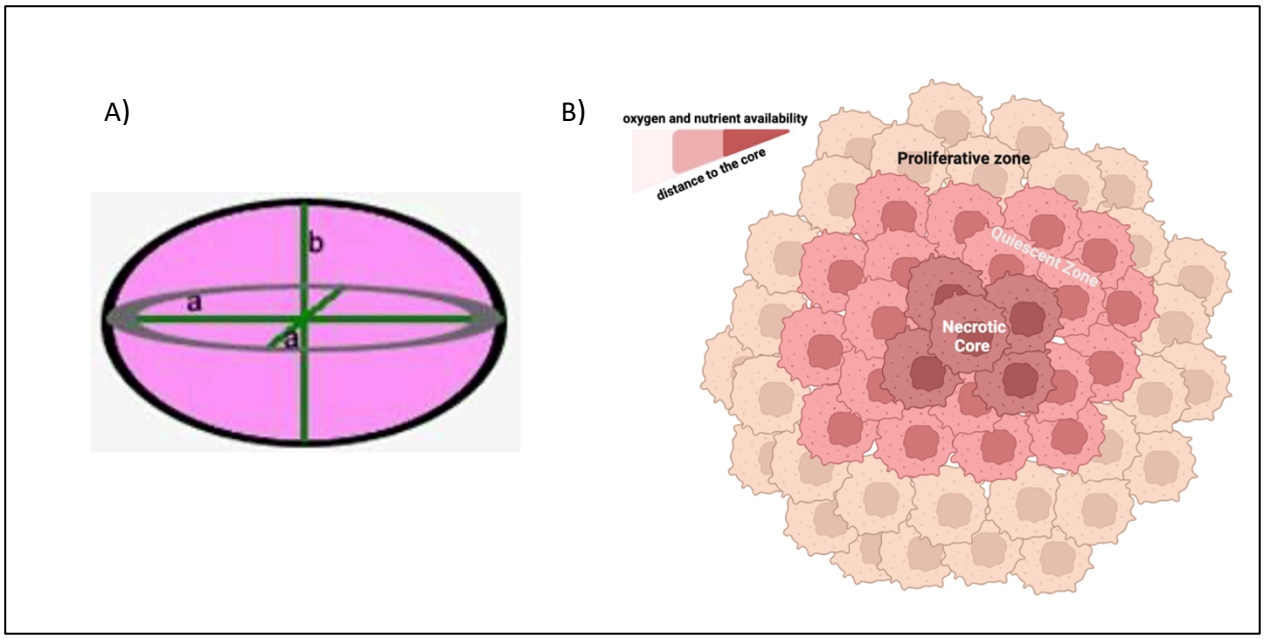


Figure 32: the structure of a 3D cultured spheroid A) the shape of a spheroid (a rotational ellipsoid) and B) the composition of a spheroid cross section outlining the three layers (necrotic core, quiescent zone, and proliferative zone) – created using Biorender.com.

I monitored formation and growth of spheroids from MDA-MB-436 cells that were knocked down for Hrd1 complex components. Reducing levels of Hrd1 attenuated growth of 3D spheroids over the time period compared to those of non-targeting controls (shHRD1- 4.3-fold, shNT – 7.6 fold) (Figure 33B). Knockdown cell lines targeting other Hrd1 complex components produced spheroids that were similarly smaller than those of the non-targeting control (shNT).

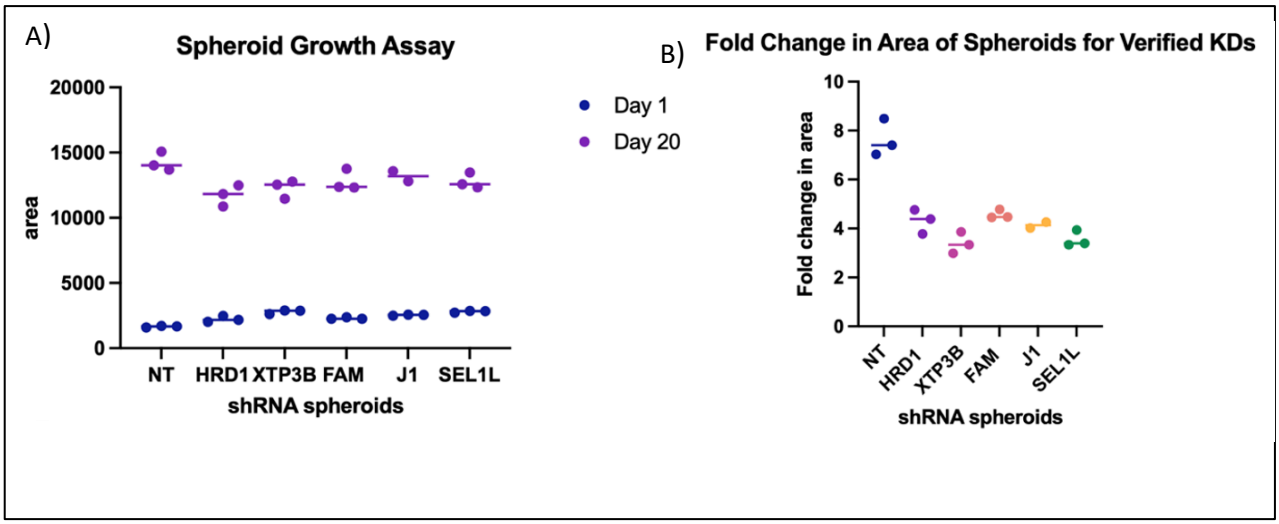


*Figure 33. A) Spheroid areas of HRD1, XTP3B SEL1L, FAM8A1, Ube2j1 (shown as J1 in the figure) and SEL1L depleted cells, with a non-targeting control included, at the beginning and end of the assay. B) The fold change of these same spheroids calculated from their initial and final area measurements.*This experiment was done with the lab's old imaging system where images did not have a scale bar, but all images were to scale with each other therefore image pixels were used for calculations in ImageJ, n=3.*

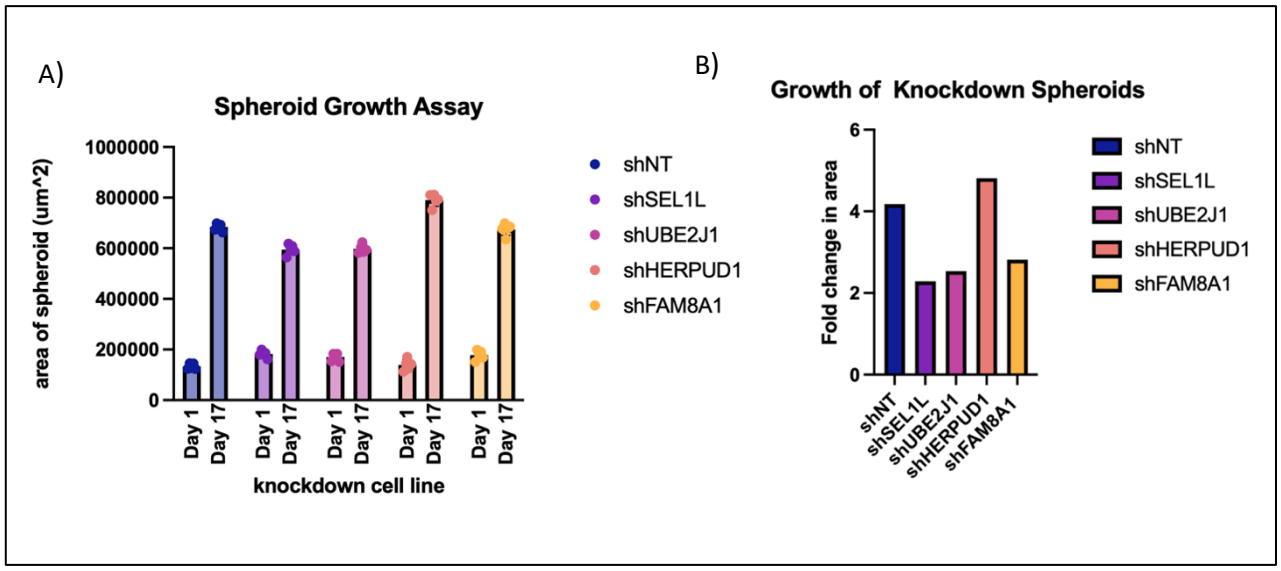


Figure 34: spheroid experiment two - a repeated 3D growth assay of MDA-MB-436 cells depleted of Hrd1 complex proteins with a narrower range of knockdown cell lines with the addition of HERPUD1 as a target. A) measured area of TNBC spheroids at the beginning and end of the assay with fold change of this growth also being calculated B). 5 technical replicates were produced for each group.

This assay was then repeated using a new imaging system (Volocity), and included cells depleted for HERPUD1 (Figure 34). These data recapitulated that of the previous assay with knockdowns of each Hrd1 component resulting in a corresponding decrease in spheroid size. HERPUD1 appeared to be the only component tested that when reduced in abundance causes larger spheroids to be reduced than by the non-targeting control, but why this occurred was not clear.

Culturing MDA-MB-231 Spheroids

When performing this growth assay MDA-MB-231 cells, spheroids appeared to form structures that were less compact than those of MDA-MB-436 cells (Figure 35). Single cells appeared visible on the external layers forming a less homogenous structure and creating a 'fluffy' appearance. It has been reported previously that spheroid morphology tends to fit into one of three

categories: rounds, mass, and aggregate (Kang et al., 2019). In terms of this study is worth noting that MDA-MB-436 cells grew as 'round' spheroids whereas MDA-MB-231 cells tended to favour a 'mass' spheroid structure (Figures 35B and D) and when both cell lines initially form spheroids, they adopt an aggregate appearance (Figures 35A and C). Unfortunately, time constraints meant that varying culture conditions could not be trialled in this cell line to determine if structures resembling 'round spheroids' and those previously cultured could be reproduced in the MDA-MB-231 cell line. Spheroids were then formed from MDA-MB-231 cell lines knocked down for Hrd1, SEL1L or HERPUD1 as well as from a non-targeting control (Figure 36). Like MDA-MB-436 cells, depletion of Hrd1 resulted in spheroids with reduced areas, indicative of slower growth. MDA-MB-231 cells depleted SEL1L or HERPUD1 also exhibited reduced size, indicating their importance for 3D growth.

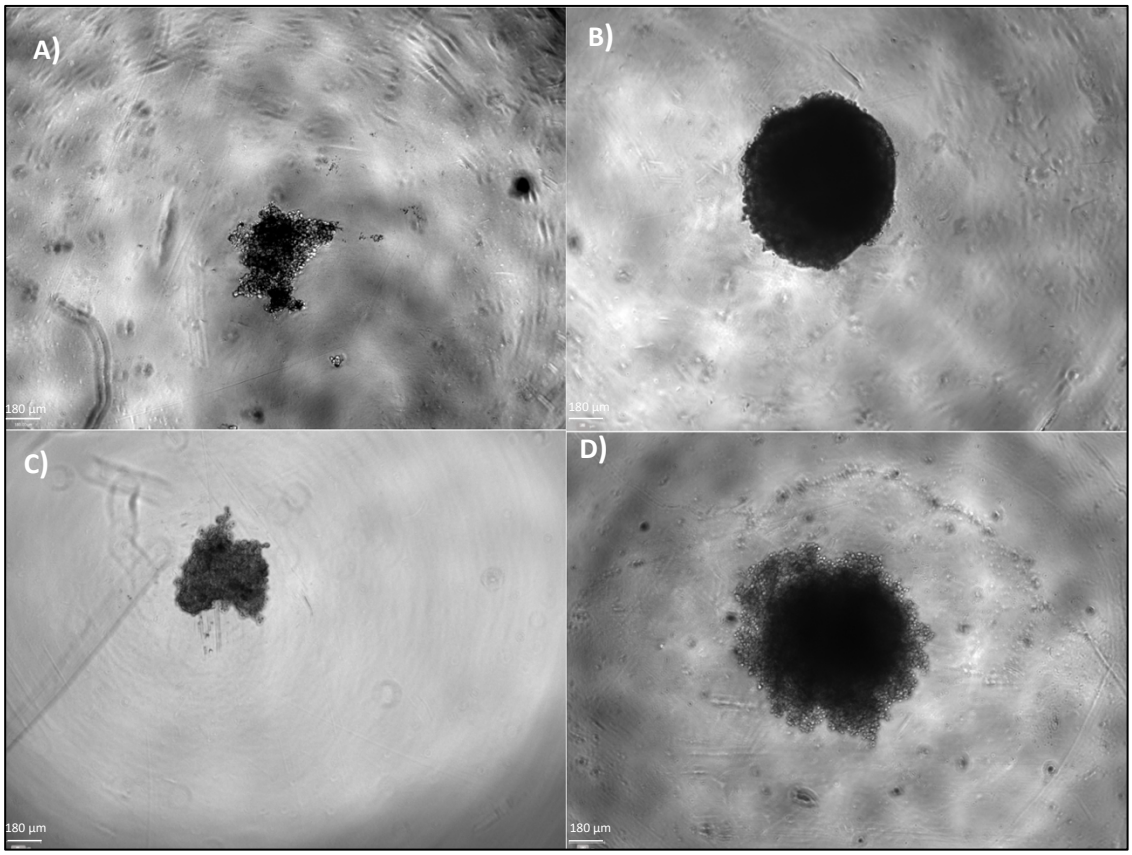


Figure 35: images displaying the various spheroid morphologies. A) MDA-MB-436 spheroid the day after plating B) MDA-MB-436 spheroid 14 days after plating C) MDA-MB-231 the day after plating D) MDA-MB-436 14 days after plating. A scale bar has been included in each image (180 µm).

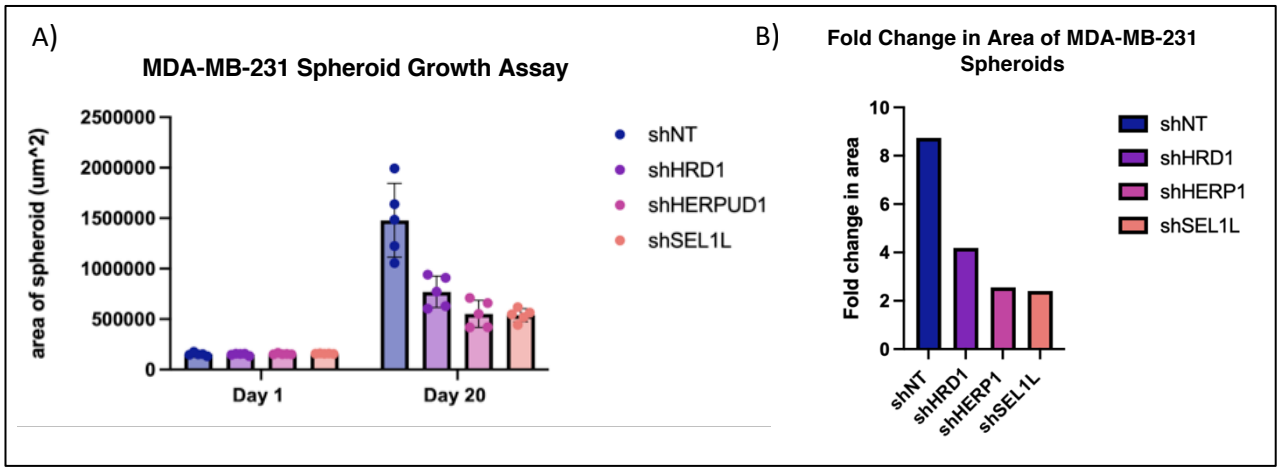


Figure 36: spheroid experiment three - a 3D growth assay of MDA-MB-231 cells depleted of Hrd1 complex proteins. A) Spheroid areas of HRD1, HERPUD1 and SEL1L depleted TNBC cells with a non-targeting control included. B) fold change from these measurements were then calculated and plotted, n=5.

MDA-MB-231 cells containing DOX-inducible shRNAs were also formed to assess their utility in 3D spheroid assays. Upon DOX addition and reduction of Hrd1, spheroids were reduced in size (Figure 37). DOX is generally accepted as inert, lending it to be widely used in these inducible systems, but some literature suggested it can be used to reduce the growth of cancer cells (Alsaadi et al., 2021 and Yang et al., 2015), when used at much higher concentrations then used in this assay. Previous work in our lab has also shown that using DOX at this concentration on non-targeting cells has no effect in growth when compared to its untreated counterpart (unpublished data).

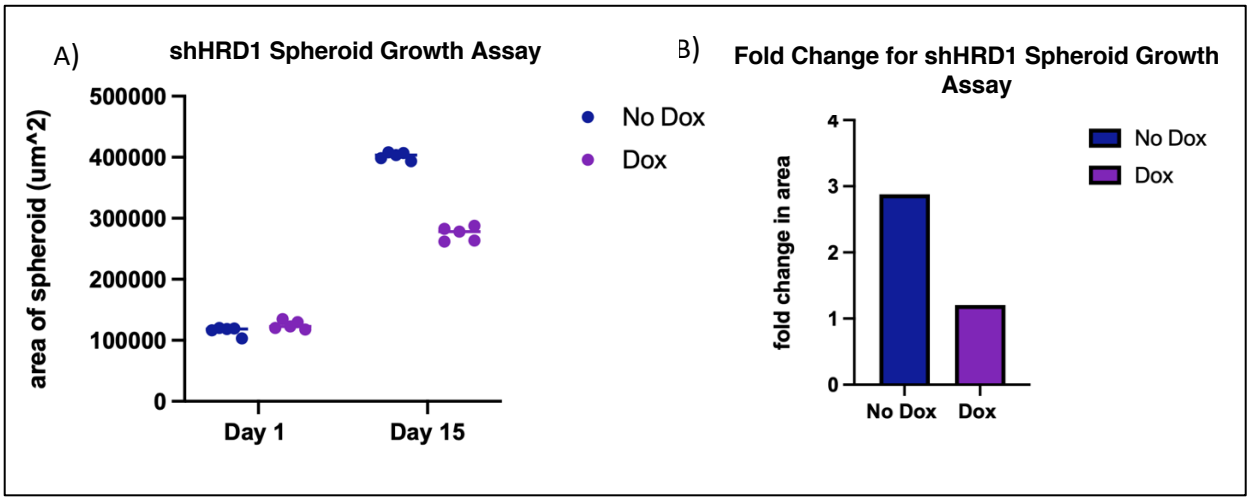


Figure 37: The effect of reducing Hrd1 via the doxycycline inducible system in MDA-MB-231 cells A) spheroid areas at the beginning and end of the growth assay (day 1 and day 15 respectively). B) looking at the change in area of the spheroids across the growth assay in terms of fold change. 5 technical replicates were produced for each group.

Determining Effect of Knockdown Method on TNBC Spheroid Formation

The strategy to knockdown Hrd1 could affect spheroid formation. To test this, I grew MBA-MD-436 cells with DOX-inducible and constitutively expressed shHRD1 side by side as assessed spheroid formation. Both sets of Hrd1 depleted spheroids were significantly smaller than their control line at 20 days: P=0.000026 (non-inducible) p=0.000006 (inducible); no significant difference was detected in both systems at day 0 (Figure 38). These data suggest that DOX-inducible depletion of Hrd1 with the SMART system provides the same outcome as stably transducing TNBC cells with shHRD1 under a constitutively active promoter.

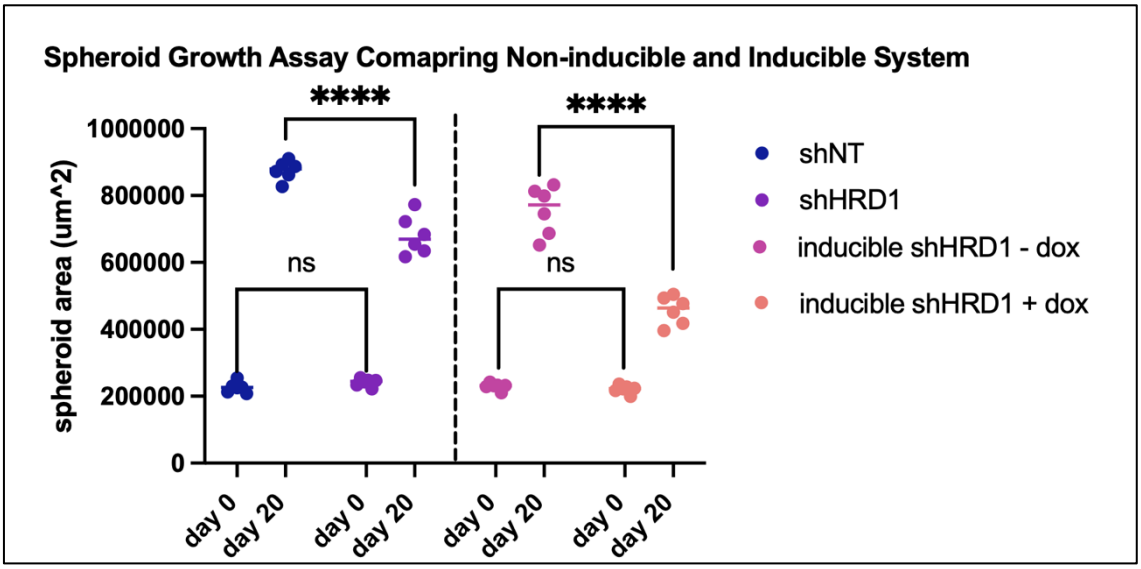


*Figure 38: spheroid growth comparison for the two shHRD1s used in this research project (both the non-inducible and inducible shRNA). This experiment used MDA-MB-436 cells. Statistical significance: * <0.05, ** <0.01, *** <0.001, ****<0.0001.5 technical replicates were performed for each group.*

Effects of Synthetic Stress on the Growth of TNBC Spheroids

The effect of exacerbating ER stress conditions on Hrd1 depleted cells was tested in a 3D context by treating spheroids with the ER stress inducer Tg (Figure 39). Tg was applied at three different concentrations to cells treated

with and without DOX. By plotting the fold change in area for DOX-treated and untreated spheroids at different Tg concentrations, I observed that DOX treated spheroids were smaller for two of the tested concentrations: 10 nM and 100 nM but not at 100 nM (P=0.136). This indicates that Hrd1 contributes to maintenance of the constitutive stress levels of these cancer cells, but an increasing dependence is notable when the system experiences supplementary stress.

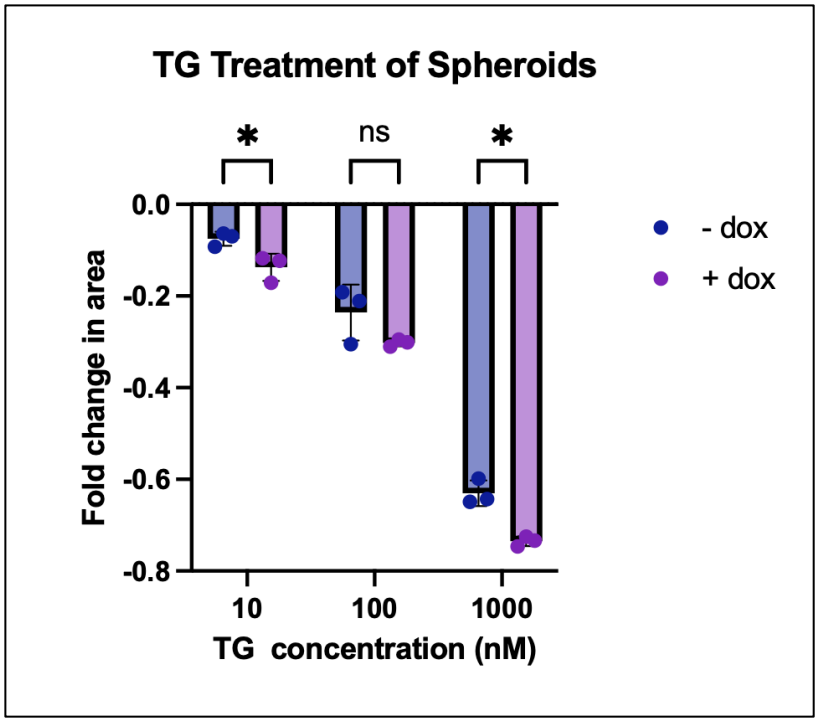


*Figure 39: the effect of thapsigargin treatment on the size of spheroids grown with or without doxycycline using doxycycline inducible shHRD1 MDA-MB-436 cells. Fold change is the final area measurements from the treated group compared to the final measurements from the untreated control. Statistical significance: * <0.05, n=3.*

This subtle effect between -/+DOX groups may be because Tg is a potent stressor and a different, less potent, drug may reveal a response only seen in one group but not the other (for example reduced spheroid size only in Hrd1 depleted cells). This assay is 20 days long and so there may also be issues with half-life of the compounds: both Tg and DOX (although these were replenished throughout) and the cells response (and possible resolution) to these compounds may occur prior to the end of the assay.

Effects of UPR Inhibitors on TNBC Spheroid Growth

To test the contribution of UPR, spheroids were grown in the presence of 4μ8C, Ceapin-A7, or both at a final concentration of 5 μM. Previous work in the lab demonstrated this concentration was able to inhibit the UPR without causing toxicity (unpublished data). Notably, UPR inhibitor-treated spheroids formed from both shNT, and shHRD1-expressing cells were significantly smaller than their untreated counterparts ($P<0.05$) (Figure 40).

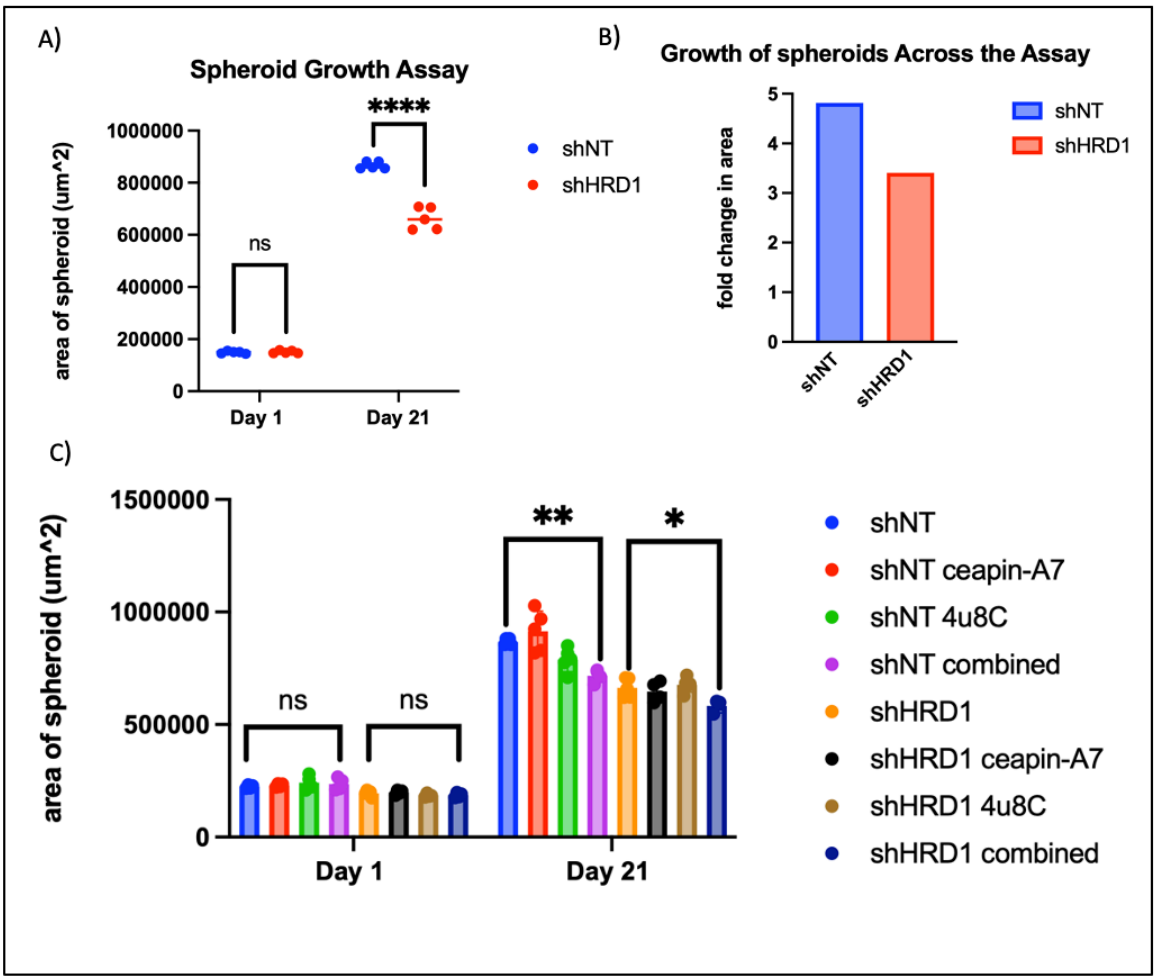


*Figure 40: A) area comparison for MDA-MB-436 spheroids (those showing Hrd1 depletion and the non-targeting control) with fold change in area calculated from this data B). A portion of these spheroids were then treated with UPR inhibitors (C). Statistical significance: * <0.05, ** <0.01, *** <0.001, ****<0.0001. Each group contains 5 technical replicates.*

Lysing Spheroids for Western Blot

In an attempt to gather more data from spheroids, I attempted to extract protein and perform western blots of the Hrd1 complex and UPR components. However, insufficient cell number together with the sturdy nature of the spheroids necessitated the use of needle shearing, which meant the quantity of protein extracted was low - impeding the quality and usefulness of the data produced. Going forwards instead of lysing the cells in this manner, select proteins of interest were chosen and these were visualised on cryosections using immunofluorescent staining.

Assessing Ki-67 Expression in TNBC cells Depleted of Hrd1

Ki-67 is a marker for cell proliferation and can be used as a biomarker for breast cancer patients (Davey et al., 2021). Flow cytometry analysis of Ki-67 stained cells originating from 2D cultures of either DOX-induced shHRD1 or shNT cells was performed to determine if Hrd1 depletion affected Ki-67 expression (Figure 41). However, Ki-67 expression levels were mostly unaffected by depletion of Hrd1. There is a slight reduction in Ki-67 from shHRD1 cells as well as a slight decrease in GFP expression, but this was not significant. This suggests Hrd1 depletion does not affect proliferation of TNBC cells grown in a 2D environment. The reduced growth phenotype may instead be accounted for by induction of apoptotic pathways rather than reduced proliferation. Equally, a 3D culture environment may be required to uncover a relationship between Hrd1 abundance and TNBC proliferation.

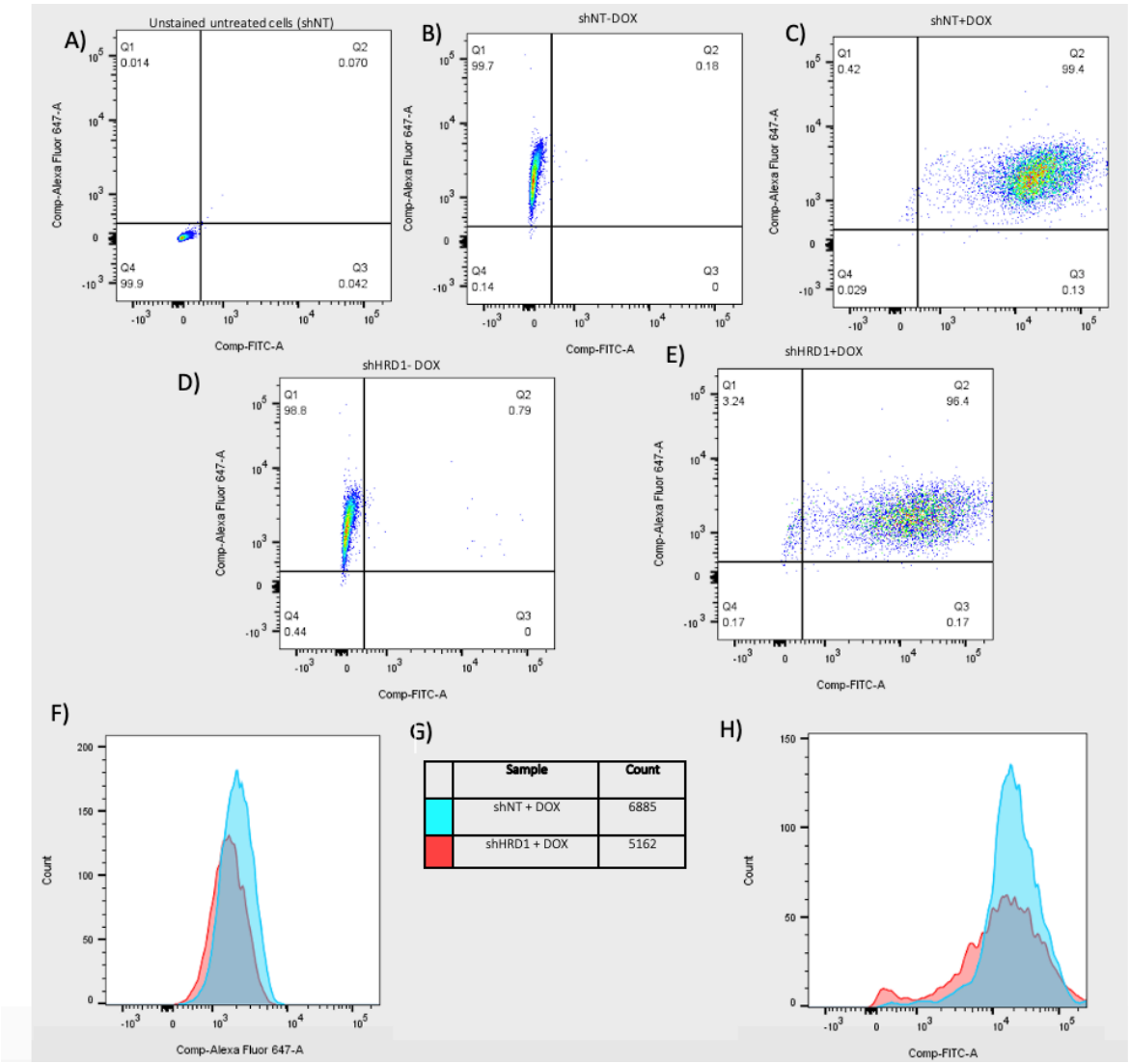


Figure 41: flow cytometry data for ki67 expression in Hrd1 depleted cells vs the control line. A) unstained untreated non-targeting cells. B) non-targeting cells without doxycycline (no GFP expression). C) non-targeting cells with doxycycline (GFP expressing). D) shHRD1 cells without doxycycline (no GFP expression, Hrd1 not depleted). E) shHRD1 cells with doxycycline (GFP expressing, Hrd1 depleted). F) the two doxycycline treated populations samples for ki67. G) the number of singlets in each of the two doxycycline treated samples. H) the two doxycycline treated samples looking at GFP expression.

Assessing Autophagy Dependence in Hrd1 Depleted TNBC cells

There is a rational that if Hrd1 depleted cells can no longer rely on ERAD to manage their cellular stress to be kept below the threshold for apoptosis, that they may resort to an alternative strategy/pathway to allow for functioning of the ER and therefore cellular survival. One hypothesis is that they employ autophagy. This is another protein clearance pathway that

removes misfolded proteins through the functioning of autophagosomes and lysosomal degradation. Although ERAD, tends to be favoured over this process (Wu et al., 2023), its role in managing ER stress, particularly through AMP-activated protein kinase (AMPK) (Rashid et al., 2015) may facilitate cell survival. Specifically in breast cancer, a 2021 publication states that inhibitor resistant cell lines displayed higher levels of autophagy, implying autophagy is important in breast cancer cell survival (Sannino et al., 2021).

Bafilomycin A-1 (BAF-A1) is an autophagy inhibitor that inhibits fusion of autophagosome and lysosome, a crucial step in autophagy. Cells were treated with various concentrations of BAF-A1 to determine how this impacted viability and to compare the response in cells with and without Hrd1. Both cell lines showed reduced viability with increasing concentrations of BAF-A1. Cells deficient in Hrd1 appear to be slightly more sensitive to BAF-A1 treatment at some concentrations (e.g., 1 μM). shNT cells treated with BAF-A1 are 73.9% viable whereas those depleted of Hrd1 (shHRD1) were only 53.2% viable at this concentration. For these calculations, data has been normalised to untreated cells to account for any parental differences in proliferation.

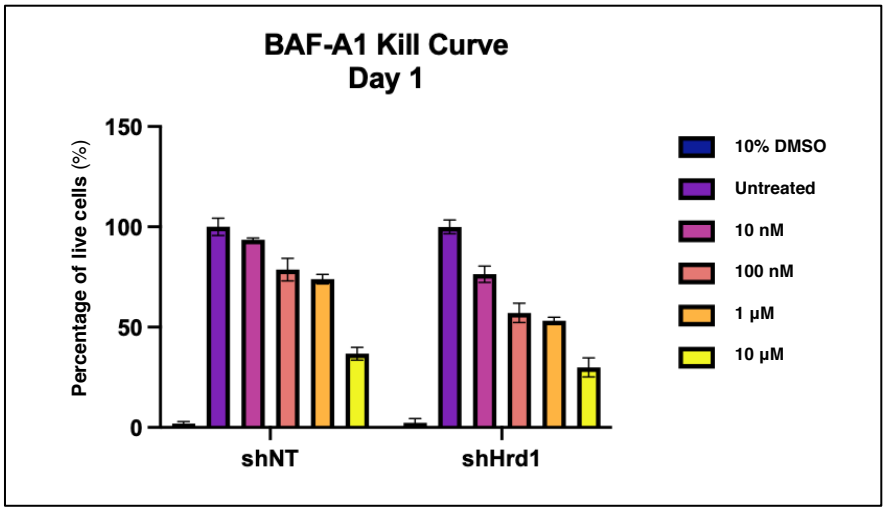


Figure 42: Alamar Blue data to determine percentage of living MDA-MB-436 cells, at various concentrations of BAF-A1 treatment, relative to untreated cells.

The Impact of Hrd1 Depletion on Apoptosis

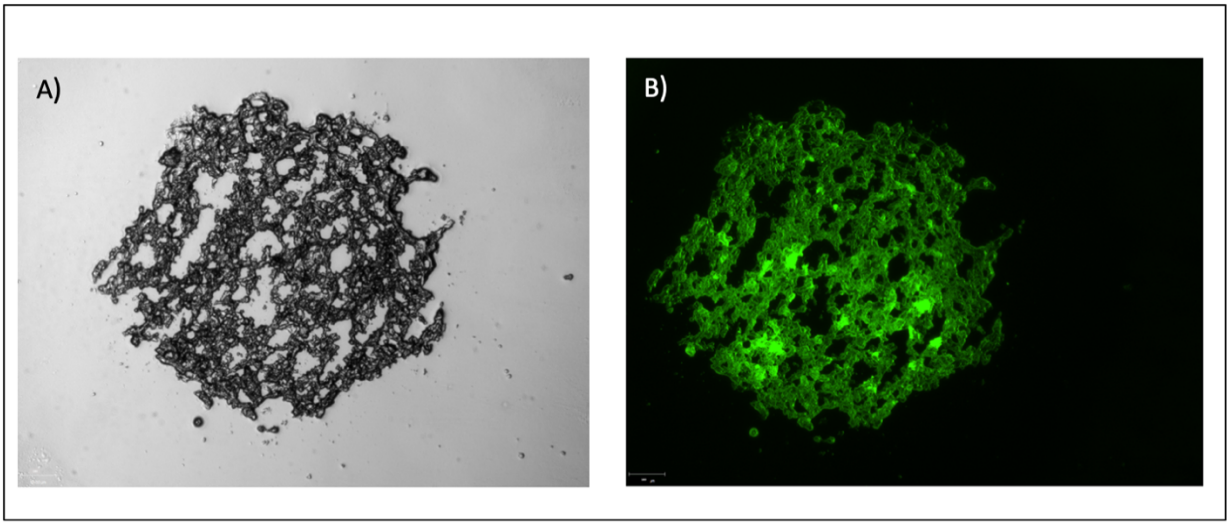


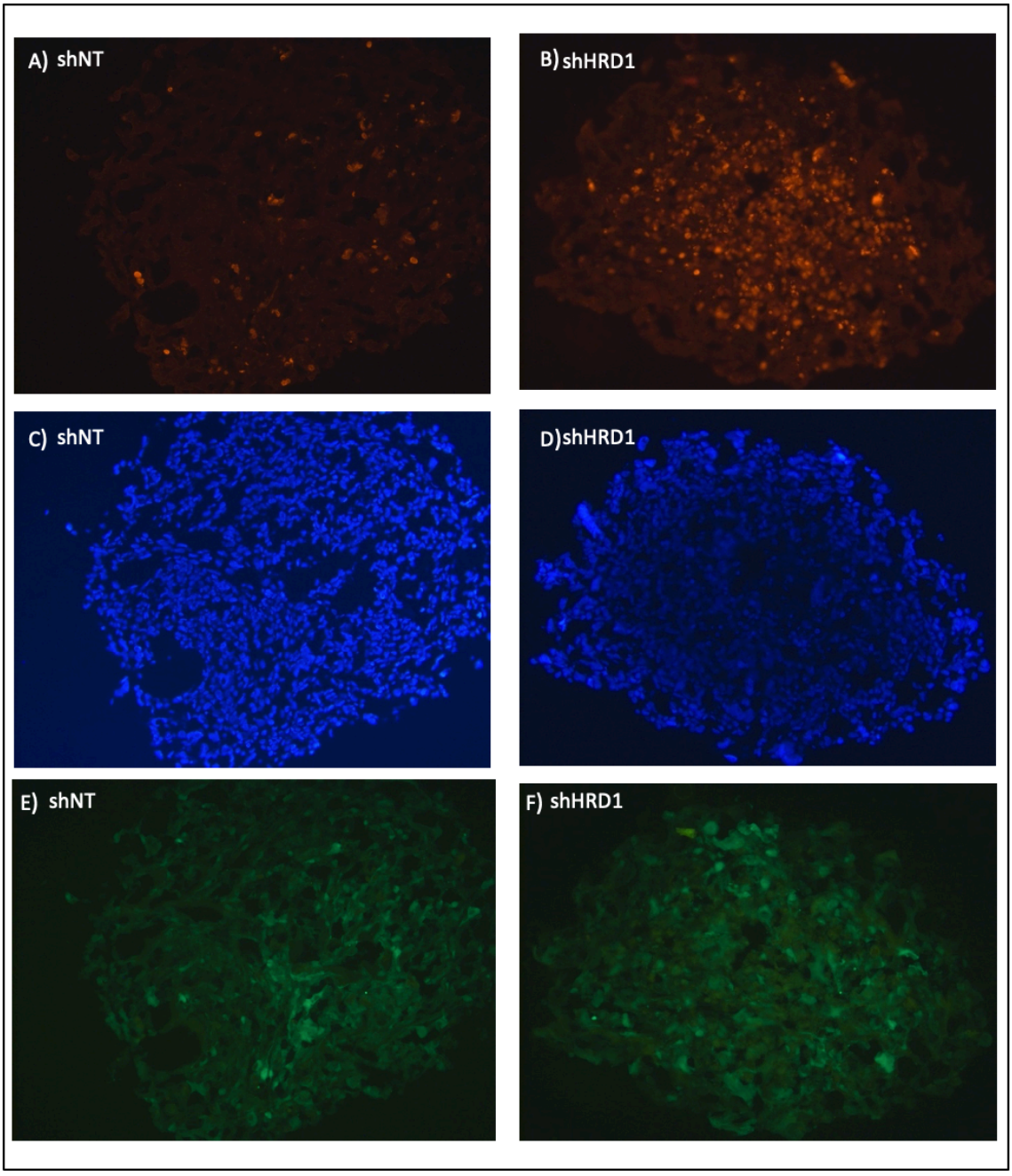
Figure 43: a cryosection of a Hrd1 depleted spheroid imaged prior to staining in bright field (A) and using the FITC channel (B). A scale bar has been included in both images (180 µm).

To determine whether Hrd1 depletion increased the number of apoptotic events within spheroids, spheroids cryosections (Figure 43) were stained using ApopTag kits, as form of (terminal deoxynucleotidyl transferase dUTP nick end labelling) TUNEL assay. TUNEL works by detecting breaks in DNA that occur at the final stage of apoptosis. Apoptosis is distinct from necrosis and is more applicable when looking at cell death brought about by cellular stress and the UPR. This staining method uses a rhodamine fluorochrome, so the slides are imaged with the 'rhodamine' filter on the microscope as well as the 'FITC' filter and 'DAPI' for GFP expression and Hoechst staining respectively. Slides were chosen for staining that contain cryosections believed to be at/near the core of the spheroid. These chosen sections had the largest diameter and were the most intact.

The resulting data revealed that spheroids with Hrd1 deficiency tended to have a higher concentration of TUNEL positive cells with this being statistically significant (P=0.0106), indicating a higher number of apoptotic cells (Figure 44A, B and I). Contrastingly, GFP expression and Hoechst showed no statistically significant difference between shNT spheroids and

shhRD1 meaning the increase in number of TUNEL positive cells is not simple down to increased cell density in shHRD1 spheroids.

These TUNEL positive cells in Hrd1 depleted spheroids seem to be situated at the 'core' of the spheroids – this is consistent with the believed organisation of spheroids with proliferative cells towards the periphery and these apoptotic cells found within the necrotic centre. This suggests that the loss of Hrd1 promotes apoptosis of TNBC cells in a 3D context in a way that is consistent with their proposed structure.



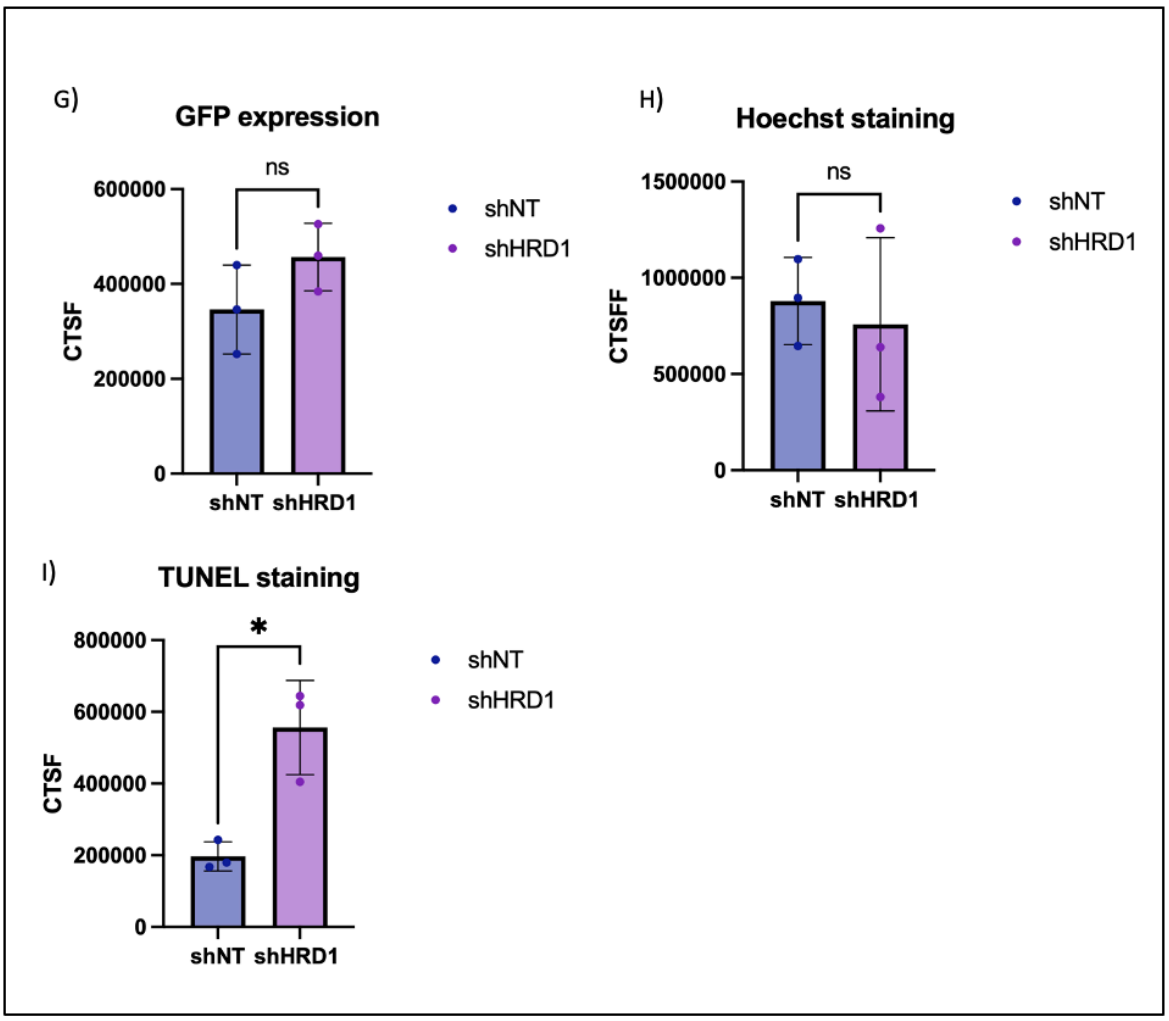


Figure 44: Images were taken from slices believed to be from the middle of the spheroid. Panels A) and B) show TUNEL stained cryosections of an shNT and shHRD1 spheroid respectively. These same spheroids were counterstained with Hoechst C) and D). GFP expression in the cryosections was also visualised E) and F). G), H) and I) Corrected total spheroid fluorescence (CTSF) was calculated for each image as a way of determining intensity of expression.

Discussion

From this work and the studies before it, it is evident that the Hrd1 complex is an important factor required for cell survival and in supporting basic cellular function. This study builds upon our understanding of the Hrd1 complex in the context of cancers hallmarked by ER stress; showing that its presence in TNBC cell lines is required for growth in both 2D and 3D culture contexts and has secondary impact on other interacting proteins. For solid tumour cancer types, such as TNBC, 3D culture systems are seen as a valuable tool as they more representatively recapitulate the *in vivo*

context in ways that 2D systems do not. Phenotypes can be more profound or even uncovered when modelling in 3D systems as opposed to 2D and this has been true to some extent for this research.

The Impact of HRD1 Depletion in TNBC Cells

Of the components involved in ERAD, depleting Hrd1 appeared to have the most profound impact in both 2D and 3D systems. Reduction of Hrd1 levels by 80% and 75% in MDA-MB-436 and MDA-MB-231 cells respectively (Figure 13), caused a decline in short term cell viability (Figures 28 and 30a). Moreover, spheroid sizes for Hrd1 depleted lines were a fraction of those of produced by their non-targeting cells – reduced up to 3.3 and 4.5 fold in MDA-MB-436 and MDA-MB-231 cells respectively (Figures 33B and 36B). Comparable Ki-67 staining indicated however that depleting cellular Hrd1 did not appear to effect proliferation (Figure 41). This could suggest that Hrd1 depletion reduces TNBC viability by favouring a path towards apoptosis rather than attenuating proliferation. This hypothesis is supported by increased TUNEL staining of Hrd1 depleted spheroids compared to those of the non-targeting control (Figure 44), suggesting a shift towards apoptotic outcomes. It is important to note from this that this resulting effect on proliferation and viability of Hrd1 depleted cells could result from the direct loss of Hrd1 or as a result of the indirect loss of one of these other components and the general change in complex composition.

I observed that depleting Hrd1 in TNBC cell lines caused the UPR to upregulate further - marked by increased levels of UPR components: IRE1 and XBP1 splicing (IRE1 branch), ATF4 and phospho-eIF2α (PERK branch) as well as BIP (associated with all 3 branches). Analysis of one branch of the UPR may not be significant enough to draw conclusions on the stress state of a cell as, for example, one branch of the UPR may be upregulated (indicating increasingly stressed conditions) and alternative branch may be showing signs of downregulation. However, the response and upregulation on various branches may occur on different time scales with some

transcriptional machinery being taken advantage of as part of the stress response before others. Regardless, this witnessed upregulation across multiple branches strengthens our conclusions in terms of the effect of Hrd1 depletion on the UPR.

These data support the rational that ER stressed cancers rely on Hrd1 (through non-oncogenic addiction) to maintain protein homeostasis and manage ER stress to a point that prevents apoptosis. When the functioning of Hrd1 and consequently ERAD is disrupted, cells are no longer capable of managing ER stress to the same extent, the threshold for apoptosis is more easily met, in turn impeding cell survival. Consequently, cells may then increasingly rely on other mechanisms, such as autophagy (Figure 42), to ensure survival, but this does not prevent aberrations in growth being detected. Demonstrating that rescue of Hrd1 depleted cells with exogenous Hrd1 mitigated the previously observed phenotypes (reduction in viability, spheroid growth etc) would strengthen these findings.

The Impact of Loss of Other Hrd1 Complex Components on TNBC Cells

Alongside the focus on Hrd1 depletion, several other components in the Hrd1 complex were systematically reduced in TNBC cells. In both cell lines depleting HERPUD1 did not seem to have an effect on cell viability, when using 2D culture systems, for both cell lines despite strong levels of knockdown being achieved both at the transcript and protein level in MDA-MB-231 cells and slightly more so in MDA-MB-436 cells (~50% vs ~75%, Figures 15 and 16). This differed when monitoring viability in 3D spheroids depleted of HERPUD1, which produced significantly smaller MDA-MB-231 spheroids than the non-targeting control but curiously larger spheroids in MDA-MB-436 cells. Time constraints prevented viability data being collected for doxycycline inducible shHERPUD1 cells, which may have provided a clearer picture of the role of HERPUD1 and the difference between cell lines.

Decreased levels of SEL1L also seemed to cause aberrations in growth both in 2D and 3D systems, although to a lesser extent than that caused by depletion of Hrd1. This could be attributable to its loss from the Hrd1 complex and hence disrupting its assembly and structure, also in turn preventing the functioning of the complex in ERAD.

Investigating knockdown of Ube2g2 at the protein level and transcript levels for MDA-MB-436 cells produced conflicting data as to whether this protein was in fact depleted. 2D Alamar Blue data revealed reduced viability (Figure 29C) but another cell line where Ube2g2 knockdown could be confidently confirmed would be preferential to ensure that this was attributable to the loss of Ube2g2. Reducing the other E2 enzyme in the complex, Ube2j1, was achieved but only modestly at the protein level but by around 70% at the transcript level (Figures 15 and 16). Alamar Blue data for these cells exhibited no significant change in viability compared to the non-targeting (Figure 29E), but a reduction of spheroid size was seen relative to the non-targeting (Figure 34A).

Contrastingly, loss of FAM8A1 seemed to cause a short-term increase in cell viability both in an Alamar Blue assay immediately after transduction (pre-selection) and post-selection when treated with an ER stressor (Figures 19 and 29). A possible reason for this effect may be that FAM8A1 performs an inhibitory function within the complex, and upon removal this inhibition is interrupted, increasing the activity of the complex. However, across a longer assay in 3D, spheroids grown with depleted FAM8A1 levels did not display this trend, with a decrease in size being seen when compared to the non-targeting. This may suggest across longer assays these FAM8A1 depleted cells struggle to maintain a normal growth pattern with the effect of any short-term boost in viability being masked. Using the doxycycline inducible system to deplete FAM8A1 may give a clearer image as to immediate versus longer term effect of reduced FAM8A1 in TNBC cells.

Knockdowns vs. Knockouts

One issue with the use of shRNAs is that there is uncertainty as to how many copies are within each cell as each virus integrates independently. This could affect the phenotype seen and create heterogeneity with the population and therefore inconsistency in assays, for example in response to certain treatments. It appears using knockdowns rather than knockouts allows for the cells to survive to monitor what happens when the ERAD system is impaired rather than producing an outcome that results in cell death and therefore not allowing for investigation into parameters such as proliferation rate and relative protein levels. The use of knockouts to study this system proved unfavourable. Lethality as a phenotype increases the difficulty when studying this complex as you cannot monitor changes within a complex if the cells die in the process of doing so.

This study proves the usefulness of temporal control afforded by the DOX-inducible system in producing knockdowns, especially in the monitoring of the immediate aftermath of preventing expression of the gene of interest. The usefulness of this system is only proved true when the adequate precautions are taken in the use of DOX. This includes using a non-targeting control as well as using the minimum required dose of doxycycline to knockdown the component of interest, both of which were done in this study (Figure 18B).

Conclusions From Spheroid Experiments

Spheroid analysis appeared to provide consistent information on the growth of these Hrd1 component depleted cells relative to the non-targeting control (Figures 33, 34 and 36-40). Additionally, spheroids can be analysed compositionally by looking at expression levels of markers of interest (e.g., TUNEL). It is likely some damage to the structure occurs to the spheroids during the harvesting, fixing, freezing and cryosectioning. This also meant the number of spheroids available for analysis decreased by the end of the

assay. In future experiments this should be taken into account with a large quantity of spheroids being produced per condition. Rather than performing the Ki-67 staining assay in 2D, this could have been performed in 3D with spheroids being dual stained for both TUNEL and Ki-67 simultaneously. Using the outlined approach of collecting and fixing cultured breast cancer spheroids, various other molecules could be stained for including proliferation markers as well as substrates of Hrd1 to monitor how a Hrd1 components removal effects the functioning of the complex when looked at in a 3D context. Further analysis could also be done on the internal structure of these spheroids to see if there are any aberrations in composition produced by any of these complex component depletions – for example looking at changes in cell density within these structures.

Although the MDA-MB-231 cells appear to take on a 'fluffy' or 'mass' appearance this did not appear to affect the usefulness of using spheroid area to assess growth. Further work and optimisation on the culturing of MDA-MB-231 cells into spheroids could be performed as these conditions used were with MDA-MB-436 in mind. This difference in shape might be attributed to their shorter doubling time (relative to MDA-MB-436 cells) preferring lower initial seeding density or a shorter assay length to ensure adequate space and media sufficiency for each spheroid containing well.

Treating spheroids with compounds is a useful tool to see how cells depleted of Hrd1 complex components respond to changes in the UPR or through stress upregulation. However, it is important to note that the size of the spheroid may impact how capable drugs are of penetrating the spheroid. Theoretically a positive feedback loop could have been produced, with smaller spheroids being better penetrated by the drug, in turn reducing the size of the spheroid and allowing for the drug to travel further into the spheroid. Nonetheless, as spheroids are structured in such a way that their 'zone of proliferation' is located on the periphery, followed by quiescent cells and lastly necrotic cells working towards the core, the ability of a drug

to penetrate the core of a spheroid becomes somewhat trivial in this kind of growth assay, as long as it is capable of accessing the outer cells that are undergoing proliferation. This same principle applies to the addition of doxycycline and as the half-life of DOX is reported to be around 48 hours, it is important that these spheroids were re-treated throughout the assay.

Options for Expanding this Study

There are many ways to expand this work: to build upon this study further, additional TNBC cell lines could be included in order to see if the same results are recapitulated in different models. This research could also be replicated in other cancers with upregulate ER stress, with prostate cancer being an example of this. As mentioned, this project supplements work performed in the Christianson Lab on the blood cancer multiple myeloma. Multiple myeloma characteristically displays great UPR upregulation and high levels of ER stress (Figure 6B). However due to these being suspension cells and their high level of genetic instability, some of the techniques and strategies employed in this TNBC study would not be suitable in these cells. Further work is required to be done on this complex with a range of other components to investigate as well as a range of other cancer types and cell lines to verify.

As TNBC is described as highly metastatic, with the risk breast tumours metastasising to the lung being well documented, looking at this complex in the context of metastatic potential via co-culture studies could provide greater insight into the usefulness of a potential therapeutic derived from targeting this complex.

To What Extent do TNBC Cells Experience ER Stress?

In our hands both MDA-MB-436 and MDA-MB-231 cells displayed similar levels of splicing but due to the aforementioned literature suggesting MDA-MB-436 were the more stressed out of the two lines (Chen et al., 2014), this line was selected first for performing the initial experiments. These

protocols were then optimised before repeating the same experiments in the MDA-MB-231 cell line. With XBP1 being so highly upregulated in breast cancer, the significance of splicing may be harder to detect if there is a comparatively low quantity of spliced XBP1 compared to what is available.

As these TNBC cell lines do not appear to display the highest levels seen on the spectrum of ER stress (Figures 8A and B) it is likely they are not easily forced into apoptosis via small changes in the UPR (Figure 10) or mild disturbances in the functioning of ERAD. This may mean that large perturbations in these processes are required to affect viability and stress tolerance. This robustness may give an indication as to why the loss of some Hrd1 components seemed to cause little to no change in cell survival. As well as this, an indication is given as to the significance of the loss of the Hrd1 component with this impact on TNBC survival being evident across various of the experiments performed (Figures 28, 30, 31, 33, 36 and 38). This also provides rational for adding additional stress to the system to expose a potentially masked phenotype as well providing an incentive into investigating other cancer cell lines (TNBC cells and beyond) that display higher levels of ER stress.

The Relevance of this Data from a Therapeutic Perspective

As the Hrd1 complex has various components that are upregulated by the UPR during ER stress, it is feasible that these components are also upregulated in cancer cells that experience chronic basal ER stress. This change in complex composition may also change the degree by which the cells rely on certain components with the rational component loss would be more determinantal to a cancer cell than a non-cancerous cell due to the phenomenon of non-oncogenic addiction.

Expanding our understanding of how this complex works and how it adapts to stress provides a stepping stone on the way to uncovering a potential therapeutic modality. Although there is thought to be limited redundancy

within ERAD and the functioning of Hrd1, cancer cells may resort to reducing ER stress via other methods if this system fails to reduce stress to levels that prevent apoptosis. One such method may be an increased reliance on autophagy (Figure 42). The extent as to how much cells do this in Hrd1 deficiency should be further explored; this may reveal that is beneficial to combine two targets (one for Hrd1 and another targeted against how it may mitigate the loss of Hrd1) for a more effective therapeutic and a stronger phenotype.

References:

Alsaadi, M. *et al.* (2021) 'Doxycycline attenuates cancer cell growth by suppressing NLRP3-mediated inflammation', *Pharmaceuticals*, 14(9), p. 852. doi:10.3390/ph14090852.

American Cancer Society (2022) *Treatment of triple-negative breast cancer*, *The American Cancer Society* . Available at: https://www.cancer.org/cancer/types/breast-cancer/treatment/treatment-of-triple-negative.html.

Bakunts, A. *et al.* (2017) 'Ratiometric sensing of BIP-client versus BIP levels by the unfolded protein response determines its signaling amplitude', *eLife*, 6. doi:10.7554/elife.27518.

Bertolotti, A. *et al.* (2000) 'Dynamic interaction of BiP and ER stress transducers in the unfolded-protein response', *Nature Cell Biology*, 2(6), pp. 326–332. doi:10.1038/35014014.

Bernasconi, R. *et al.* (2008) 'A dual task for the XBP1-responsive OS-9 variants in the mammalian endoplasmic reticulum', *Journal of Biological Chemistry*, 283(24), pp. 16446–16454. doi:10.1074/jbc.m802272200.

Bordallo, J. *et al.* (1998) 'Der3p/Hrd1p is required for endoplasmic reticulum-associated degradation of misfolded lumenal and integral membrane proteins', *Molecular Biology of the Cell*, 9(1), pp. 209–222. doi:10.1091/mbc.9.1.209.

Cancer Research UK (2023) *Breast cancer statistics*, *Cancer Research UK*. Available at: https://www.cancerresearchuk.org/health-professional/cancer-statistics/statistics-by-cancer-type/breast-cancer#heading-Zero (Accessed: September 2023).

Carvalho, P., Stanley, A.M. and Rapoport, T.A. (2010) 'Retrotranslocation of a misfolded luminal ER protein by the Ubiquitin-ligase hrd1p', *Cell*, 143(4), pp. 579–591. doi:10.1016/j.cell.2010.10.028.

Chen, H. *et al.* (2018) 'Association between BRCA status and triple-negative breast cancer: A meta-analysis', *Frontiers in Pharmacology*, 9. doi:10.3389/fphar.2018.00909.

Chen, T. *et al.* (2022) 'Multiple myeloma cells depend on the DDI2/NRF1-mediated proteasome stress response for survival', *Blood Advances*, 6(2), pp. 429–440. doi:10.1182/bloodadvances.2020003820.

Chen, X. *et al.* (2014) 'XBP1 promotes triple-negative breast cancer by controlling the hif1α pathway', *Nature*, 508(7494), pp. 103–107. doi:10.1038/nature13119.

Chen, X. and Cubillos-Ruiz, J.R. (2020) 'Endoplasmic reticulum stress signals in the tumour and its microenvironment', *Nature Reviews Cancer*, 21(2), pp. 71–88. doi:10.1038/s41568-020-00312-2.

Chipurupalli, S. *et al.* (2019) 'Hypoxia induced ER stress response as an adaptive mechanism in cancer', *International Journal of Molecular Sciences*, 20(3), p. 749. doi:10.3390/ijms20030749.

Christianson, J.C. *et al.* (2008) 'OS-9 and GRP94 deliver mutant α1-antitrypsin to the HRD1–SEL1L Ubiquitin Ligase Complex for Erad', *Nature Cell Biology*, 10(3), pp. 272–282. doi:10.1038/ncb1689.

Christianson, J.C. *et al.* (2011) 'Defining human ERAD networks through an integrative mapping strategy', *Nature Cell Biology*, 14(1), pp. 93–105. doi:10.1038/ncb2383.

Christianson, J.C., Jarosch, E. and Sommer, T. (2023) 'Mechanisms of substrate processing during ER-associated protein degradation', *Nature Reviews Molecular Cell Biology* [Preprint]. doi:10.1038/s41580-023-00633-8.

Cojocari, D. *et al.* (2013) 'New small molecule inhibitors of UPR activation demonstrate that perk, but not ire1α signaling is essential for promoting adaptation and survival to hypoxia', *Radiotherapy and Oncology*, 108(3), pp. 541–547. doi:10.1016/j.radonc.2013.06.005.

Davey, M.G. *et al.* (2021a) 'Ki-67 as a prognostic biomarker in invasive breast cancer', *Cancers*, 13(17), p. 4455. doi:10.3390/cancers13174455.

Doroudgar, S. *et al.* (2015) 'HRD1 and ER-associated protein degradation, Erad, are critical elements of the adaptive ER stress response in cardiac myocytes', *Circulation Research*, 117(6), pp. 536–546. doi:10.1161/circresaha.115.306993.

Eura, Y., Miyata, T. and Kokame, K. (2020) *Derlin-3 is required for changes in Erad Complex Formation under ER stress*, *MDPI*. Available at: https://doi.org/10.3390/ijms21176146 (Accessed: 11 September 2023).

Fenech, E. *et al.* (2020) 'Interaction mapping of endoplasmic reticulum ubiquitin ligases identifies modulators of innate immune signalling', *eLife*, 9. doi:10.7554/elife.57306.

Friedlander, R. *et al.* (2000) 'A regulatory link between ER-associated protein degradation and the unfolded-protein response.', *Nature Cell Biology*, 2(7), pp. 379–384. doi:10.1038/35017001.

Fukao, Y. (2015) 'Discordance between protein and transcript levels detected by selected reaction monitoring', *Plant Signaling & Behavior*, 10(5). doi:10.1080/15592324.2015.1017697.

Gallagher, C.M. *et al.* (2016) 'Ceapins are a new class of unfolded protein response inhibitors, selectively targeting the atf6α branch', *eLife*, 5. doi:10.7554/elife.11878.

Guerriero, C.J. and Brodsky, J.L. (2012) 'The delicate balance between secreted protein folding and endoplasmic reticulum-associated degradation in human physiology', *Physiological Reviews*, 92(2), pp. 537–576. doi:10.1152/physrev.00027.2011.

Hampton, R.Y., Gardner, R.G. and Rine, J. (1996) 'Role of 26S Proteasome and HRD genes in the degradation of 3-hydroxy-3-methylglutaryl-coa reductase, an integral endoplasmic reticulum membrane protein.', *Molecular Biology of the Cell*, 7(12), pp. 2029–2044. doi:10.1091/mbc.7.12.2029.

Harnoss, J.M. *et al.* (2020) 'IRE1α disruption in triple-negative breast cancer cooperates with antiangiogenic therapy by reversing ER stress adaptation and remodeling the tumor microenvironment', *Cancer Research*, 80(11), pp. 2368–2379. doi:10.1158/0008-5472.can-19-3108.

Hiramatsu, N., Joseph, V. and Lin, J. (2011) 'Monitoring and manipulating mammalian unfolded protein response', Methods Enzymol. (491)1, pp. 183–98. doi: 10.1016/B978-0-12-385928-0.00011-0.

Holohan, C. *et al.* (2013) 'Cancer drug resistance: An evolving paradigm', *Nature Reviews Cancer*, 13(10), pp. 714–726. doi:10.1038/nrc3599.

Hu, H. *et al.* (2019) 'The C/EBP homologous protein (CHOP) transcription factor functions in endoplasmic reticulum stress-induced apoptosis and microbial infection', *Frontiers in Immunology*, 9. doi:10.3389/fimmu.2018.03083.

Huang, C.-H. *et al.* (2014) 'Role of Herp and a HERP-related protein in HRD1-dependent protein degradation at the endoplasmic reticulum', *Journal of Biological Chemistry*, 289(7), pp. 4444–4454. doi:10.1074/jbc.m113.519561.

Hwang, J. *et al.* (2017) 'Characterization of protein complexes of the endoplasmic reticulum-associated degradation E3 ubiquitin ligase HRD1', *Journal of Biological Chemistry*, 292(22), pp. 9104–9116. doi:10.1074/jbc.m117.785055.

Kanehara, K., Xie, W. and Ng, D.T.W. (2010) 'Modularity of the hrd1 erad complex underlies its diverse client range', *Journal of Cell Biology*, 188(5), pp. 707–716. doi:10.1083/jcb.200907055.

Kang, J. *et al.* (2019) 'Prediction of tumor response of rectal cancer cells via 3D cell culture and in vitro cytotoxicity assay before initiating preoperative chemoradiotherapy', *Oncology Letters*, 18(4), pp. 3863–3872. doi:10.3892/ol.2019.10702.

Knop, M. *et al.* (1996) 'DER1, a novel protein specifically required for endoplasmic reticulum degradation in yeast.', *The EMBO Journal*, 15(4), pp. 753–763. doi:10.1002/j.1460-2075.1996.tb00411.x.

Lari, F. (2016) *Resolution of Proteotoxic Stress in the Endoplasmic Reticulum by Ubiquitin Ligase Complexes*. thesis.

Lee, K. *et al.* (2002) 'IRE1-mediated unconventional mrna splicing and S2P-mediated ATF6 cleavage merge to regulate XBP1 in signaling the unfolded protein response', *Genes & Development*, 16(4), pp. 452–466. doi:10.1101/gad.964702.

Lilley, B.N. and Ploegh, H.L. (2004) 'A membrane protein required for dislocation of misfolded proteins from the ER', *Nature*, 429(6994), pp. 834–840. doi:10.1038/nature02592.

Luo, J., Solimini, N.L. and Elledge, S.J. (2009a) 'Principles of cancer therapy: Oncogene and non-oncogene addiction', *Cell*, 136(5), pp. 823–837. doi:10.1016/j.cell.2009.02.024.

Metcalf, M.G. *et al.* (2020) 'Beyond the cell factory: Homeostatic Regulation of and by the UPR ', *Science Advances*, 6(29). doi:10.1126/sciadv.abb9614

McCracken, A.A. and Brodsky, J.L. (1996) 'Assembly of ER-associated protein degradation in vitro: Dependence on cytosol, calnexin, and ATP.', *The Journal of cell biology*, 132(3), pp. 291–298. doi:10.1083/jcb.132.3.291.

Nagaraj, N.S., Singh, O.V. and Merchant, N.B. (2010) 'Proteomics: A strategy to understand the novel targets in protein misfolding and cancer therapy', *Expert Review of Proteomics*, 7(4), pp. 613–623. doi:10.1586/epr.10.70.

Nagel, R., Semenova, E.A. and Berns, A. (2016a) 'Drugging the addict: Non-oncogene addiction as a target for cancer therapy', *EMBO reports*, 17(11), pp. 1516–1531. doi:10.15252/embr.201643030.

Oakes, S.A. (2020) 'Endoplasmic reticulum stress signaling in cancer cells', *The American Journal of Pathology*, 190(5), pp. 934–946. doi:10.1016/j.ajpath.2020.01.010.

Oda, Y. *et al.* (2006) 'Derlin-2 and derlin-3 are regulated by the mammalian unfolded protein response and are required for ER-associated degradation', *The Journal of Cell Biology*, 172(3), pp. 383–393. doi:10.1083/jcb.200507057.

Pirsko, V. *et al.* (2018) 'An effect of culture media on epithelial differentiation markers in breast cancer cell lines MCF7, MDA-MB-436 and SKBR3', *Medicina*, 54(2), p. 11. doi:10.3390/medicina54020011.

Rashid, H.-O. *et al.* (2015) 'Er stress: Autophagy induction, inhibition and selection', *Autophagy*, 11(11), pp. 1956–1977. doi:10.1080/15548627.2015.1091141.

Romero-Ramirez, L. *et al.* (2004) 'XBP1 is essential for survival under hypoxic conditions and is required for tumor growth', *Cancer Research*, 64(17), pp. 5943–5947. doi:10.1158/0008-5472.can-04-1606.

Ruan, J. *et al.* (2019) 'A small molecule inhibitor of ER-to-cytosol protein dislocation exhibits anti-dengue and anti-zika virus activity', *Scientific Reports*, 9(1). doi:10.1038/s41598-019-47532-7.

Sannino, S. *et al.* (2021) 'Unique integrated stress response sensors regulate cancer cell susceptibility when HSP70 activity is compromised', *eLife*, 10. doi:10.7554/elife.64977.

Sheridan, C. *et al.* (2006) 'CD44+/CD24-breast cancer cells exhibit enhanced invasive properties: An early step necessary for metastasis', *Breast Cancer Research*, 8(5). doi:10.1186/bcr1610.

Schulz, J. *et al.* (2017) 'Conserved cytoplasmic domains promote HRD1 ubiquitin ligase complex formation for ER-associated degradation (ERAD)', *Journal of Cell Science* [Preprint]. doi:10.1242/jcs.206847.

Spandl, J. *et al.* (2011) 'Ancient ubiquitous protein 1 (AUP1) localizes to lipid droplets and binds the E2 ubiquitin Conjugase G2 (UBE2G2) via its G2 binding region', *Journal of Biological Chemistry*, 286(7), pp. 5599–5606. doi:10.1074/jbc.m110.190785.

Sun, S. *et al.* (2014) 'Sel1L is indispensable for mammalian endoplasmic reticulum-associated degradation, endoplasmic reticulum homeostasis, and survival', *Proceedings of the National Academy of Sciences*, 111(5). doi:10.1073/pnas.1318114111.

Sun, S. *et al.* (2015) 'IRE1α is an endogenous substrate of endoplasmic-reticulum-associated degradation', *Nature Cell Biology*, 17(12), pp. 1546–1555. doi:10.1038/ncb3266.

Tang, H.-Y. *et al.* (2014) 'Edem2 and OS-9 are required for ER-associated degradation of non-glycosylated sonic hedgehog', *PLoS ONE*, 9(6). doi:10.1371/journal.pone.0092164.

Tyler, R.E. *et al.* (2012) 'Unassembled CD147 is an endogenous endoplasmic reticulum–associated degradation substrate', *Molecular Biology of the Cell*, 23(24), pp. 4668–4678. doi:10.1091/mbc.e12-06-0428.

van der Goot, A.T. *et al.* (2018) 'Redundant and antagonistic roles of XTP3B and OS9 in decoding glycan and non-glycan degrons in ER-associated degradation', *Molecular Cell*, 70(3). doi:10.1016/j.molcel.2018.03.026.

Walter, P. and Ron, D. (2011) 'The unfolded protein response: From stress pathway to homeostatic regulation', Science, 334(6059), pp. 1081–1086. doi:10.1126/science.1209038.

Wu, S.A. *et al.* (2023) 'The mechanisms to dispose of misfolded proteins in the endoplasmic reticulum of adipocytes', *Nature Communications*, 14(1). doi:10.1038/s41467-023-38690-4.

Ye, Y. *et al.* (2005) 'Recruitment of the P97 atpase and ubiquitin ligases to the site of retrotranslocation at the endoplasmic reticulum membrane', *Proceedings of the National Academy of Sciences*, 102(40), pp. 14132–14138. doi:10.1073/pnas.0505006102.

Yamarnoto, N. *et al.* (1995) 'A study on Thapsigargin-induced calcium ion and cation influx pathways in vascular endothelial cells', *Biochimica et Biophysica Acta (BBA) - Molecular Cell Research*, 1266(2), pp. 157–162. doi:10.1016/0167-4889(95)00011-g.

Yang, B. *et al.* (2015) 'Doxycycline induces apoptosis and inhibits proliferation and invasion of human cervical carcinoma stem cells', *PLOS ONE*, 10(6). doi:10.1371/journal.pone.0129138.

Yang, C. *et al.* (2006) 'Bortezomib (velcade®) in metastatic breast cancer: Pharmacodynamics, biological effects, and prediction of clinical benefits', *Annals of Oncology*, 17(5), pp. 813–817. doi:10.1093/annonc/mdj131.

Zaal, E.A. *et al.* (2017) 'Bortezomib resistance in multiple myeloma is associated with increased serine synthesis', *Cancer & Metabolism*, 5(1). doi:10.1186/s40170-017-0169-9.

Zhang, K. *et al.* (2020) 'The UPR transducer IRE1 promotes breast cancer malignancy by degrading tumor suppressor micrornas', *iScience*, 23(9), p. 101503. doi:10.1016/j.isci.2020.101503.

Zhang, L., Zhang, C. and Wang, A. (2016) *Divergence and conservation of the major UPR branch IRE1-bzip signaling pathway across eukaryotes*, *Nature News*. Available at: https://www.nature.com/articles/srep27362.